Optimization of particle detachment by collapse-pulsing during air scour
by Margaret Mary Regan

A thesis submitted in partial fulfillment of the requirements for the degree of Master of Science in Environmental Health Engineering
Montana State University

Abstract:
The effectiveness of backwashing of granular media filters is directly related to the ability of the backwash system to provide abrasion and/or collisions between individual media grains. During these interactions the grain surfaces may slip and slide at their contact points actively removing attached particles. Two-phase, water fluidized, backwash systems provide only hydrodynamic shear mechanisms for particle removal. Alternately, three-phase systems utilizing simultaneous air scour and subfluidization water backwash provide the abrasion mechanism for aggressive particle detachment. Cleaning is significantly improved over particulate fluidization.

A condition can be induced in a fixed bed subjected to specific backwash flow combinations of simultaneous air and water in which the bed behavior is characterized by the formation and collapse of air cavities throughout its depth. This phenomenon, termed Collapse-Pulsing, maximizes the probability of abrasion/collisions between the grains implying optimum particle detachment. An original equation has been developed to predict Collapse-Pulsing behavior by equating the air pressure inside the cavity with the soil stresses in an active Rankine state plus the pore water pressure. Hence, the objectives of this research were: (1) to determine the combination(s) of air and simultaneous sub fluidization water flows which optimize particle detachment in a granular media filter, (2) to experimentally validate or nullify the implication that Collapse-Pulsing behavior is accompanied by optimized particle detachment, and (3) to establish design guidelines for filter backwashing which can be applied to improve filter performance.

Fifty pilot-scale studies were conducted on a small-scale filtration plant. Alum sol suspensions composed of uniformly distributed 1.0-µm particles were prepared by hydrothermal aging. A predetermined quantity of particles in one liter of influent were attached to glass beads of d90 size equal to 0.78-mm during gravity filtration. Subsequently, the filter was backwashed utilizing water flows from 20 to 225 percent of minimum fluidization with simultaneous air flows ranging from 3.44 to 7.39 scfm/ft^2. The three-phase backwash was followed by fluidization at 30-percent expansion with water alone. The backwash water was collected and analyzed to determine particle removal. Particles were sized and counted using a Bausch and Lomb Omnimet Image Analyzer and a Each Turbidimeter.

The results of the experimental investigation indicate: (1) Flow combinations promoting Collapse-Pulsing behavior in a granular media filter provide the optimum condition for particle detachment by abrasion. (2) The fundamental theoretical equation developed to predict Collapse-Pulsing is also valid in predicting optimum particle detachment, i.e., optimum cleaning in a granular media filter. It can, therefore, be applied during design to improve filter performance. (3) The theory is applicable for air flowrates greater than approximately 4.0 scfm/ft2 and seems to have a lower boundary of application.

OPTIMIZATION OF PARTICLE DETACHMENT BY COLLAPSE-PULSING DURING AIR SCOUR

by

Margaret Mary Regan

A thesis submitted in partial fulfillment
of the requirements for the degree

of

Master of Science

in

Environmental Health Engineering

MONTANA STATE UNIVERSITY
Bozeman, Montana

September 1984

APPROVAL

of a thesis submitted by

Margaret Mary Regan

This thesis has been read by each member of the thesis committee and has been found to be satisfactory regarding content, English usage, format, citation, bibliographic style, and consistency, and is ready for submission to the College of Graduate Studies.

Sept 20, 1984 — A. Amirthanayagam by Howard St Deary
Date — Chairperson, Graduate Committee

Approved for the Major Department

Sept 20, 1984 — Fred T Wilder
Date — Head, Major Department

Approved for the College of Graduate Studies

9-25-84 — Michael D. Wallace
Date — Graduate Dean

STATEMENT OF PERMISSION TO USE

In presenting this thesis in partial fulfillment of the requirements for a master's degree at Montana State University, I agree that the Library shall make it available to borrowers under rules of the Library. Brief quotations from this thesis are allowable without special permission, provided that accurate acknowledgment of source is made.

Permission for extensive quotation from or reproduction of this thesis may be granted by my major professor, or in his absence, by the Dean of Libraries when, in the opinion of either, the proposed use of the material is for scholarly purposes. Any copying or use of the material in this thesis for financial gain shall not be allowed without my permission.

Signature Margaret M. Regan

Date 9/20/84

TABLE OF CONTENTS

LIST OF TABLES

LIST OF FIGURES

Figures

Figures Page

NOTATION

(The following is a list of symbols which appear in the thesis.)

b = coefficient corresponding to the y-intercept of the $\%V/V_{mf}$ versus Q_a^2 line

d = media grain diameter

d_{10} = 10 percent finer size of media grains from a probability plot

d_{60} = 60 percent finer size of media grains from a probability plot

d_{90} = 90 percent finer size of media grains from a probability plot

$\frac{dh}{dZ}$ = head loss gradient over the bed depth

D = diameter of filtration column

F_D = fluid drag force

g = acceleration due to gravity

$Ga = \frac{(d_{90})^3 \rho_w(\rho_d - \rho_w)g}{\mu^2}$ = Galileo number

h = head loss over the media

H_1 = height of the column of water above the media

k = coefficient relative to Q_a

l = length of column of air in the closed U-tube manometer

m = coefficient corresponding to the slope of the $\%V/V_{mf}$ versus Q_a^2 line

N_o = horizontal force normal to contact area of grains

P_1 = pressure below the air inlet orifice in psig

P_A = pressure at point A in the closed manometer

P_B = pressure at point B in the closed manometer

Q_a = air flowater in $scfm/ft^2$

r = radius of the menisci of the pores

Rmf	=	Reynolds number at minimum fluidization velocity
Sg	=	specific gravity of the media
T	=	surface tension due to the menisci in the pores
u	=	pore water pressure
U.C.	=	Uniformity Coefficient = ratio of d_{60} to d_{10} grain sizes
V	=	water flowrate in gpm/ft^2
V_{mf}	=	minimum fluidization velocity in gpm/ft^2
$\frac{\%V}{V_{mf}}$	=	the relationship in percent between the applied backwash flowrate and the calculated minimum fluidization velocity
Vb	=	Volume of the bulb on the closed end manometer
Wa	=	mass of flask plus water in Sg test
Wb	=	mass of flash plus water plus sample in Sg test
Ws	=	mass of media sample in Sg test
Z	=	depth of the media
Δy	=	difference between water levels in the legs of the closed end manometer
ϵ_o	=	static bed porosity
γ_b	=	buoyant unit weight of media
γ_d	=	unit weight of dry media
γ_s	=	saturated unit weight of media
γ_w	=	unit weight of water
μ	=	viscosity of water
ϕ	=	friction angle of the media
ρ_d	=	density of dry media
ρ_w	=	density of water
σ_h	=	horizontal intergranular stress

σ_v = vertical intergranular stress

τ_f = shear strength of media at failure

ABSTRACT

The effectiveness of backwashing of granular media filters is directly related to the ability of the backwash system to provide abrasion and/or collisions between individual media grains. During these interactions the grain surfaces may slip and slide at their contact points actively removing attached particles. Two-phase, water fluidized, backwash systems provide only hydrodynamic shear mechanisms for particle removal. Alternately, three-phase systems utilizing simultaneous air scour and subfluidization water backwash provide the abrasion mechanism for aggressive particle detachment. Cleaning is significantly improved over particulate fluidization.

A condition can be induced in a fixed bed subjected to specific backwash flow combinations of simultaneous air and water in which the bed behavior is characterized by the formation and collapse of air cavities throughout its depth. This phenomenon, termed Collapse-Pulsing, maximizes the probability of abrasion/collisions between the grains implying optimum particle detachment. An original equation has been developed to predict Collapse-Pulsing behavior by equating the air pressure inside the cavity with the soil stresses in an active Rankine state plus the pore water pressure. Hence, the objectives of this research were: (1) to determine the combination(s) of air and simultaneous subfluidization water flows which optimize particle detachment in a granular media filter, (2) to experimentally validate or nullify the implication that Collapse-Pulsing behavior is accompanied by optimized particle detachment, and (3) to establish design guidelines for filter backwashing which can be applied to improve filter performance.

Fifty pilot-scale studies were conducted on a small-scale filtration plant. Alum sol suspensions composed of uniformly distributed 1.0-μm particles were prepared by hydrothermal aging. A predetermined quantity of particles in one liter of influent were attached to glass beads of d_{90} size equal to 0.78-mm during gravity filtration. Subsequently, the filter was backwashed utilizing water flows from 20 to 225 percent of minimum fluidization with simultaneous air flows ranging from 3.44 to 7.39 scfm/ft^2. The three-phase backwash was followed by fluidization at 30-percent expansion with water alone. The backwash water was collected and analyzed to determine particle removal. Particles were sized and counted using a Bausch and Lomb Omnimet Image Analyzer and a Hach Turbidimeter.

The results of the experimental investigation indicate: (1) Flow combinations promoting Collapse-Pulsing behavior in a granular media filter provide the optimum condition for particle detachment by abrasion. (2) The fundamental theoretical equation developed to predict Collapse-Pulsing is also valid in predicting optimum particle detachment, i.e., optimum cleaning in a granular media filter. It can, therefore, be applied during design to improve filter performance. (3) The theory is applicable for air flowrates greater than approximately 4.0 scfm/ft^2 and seems to have a lower boundary of application.

CHAPTER 1

INTRODUCTION

Long term filtration efficiency for turbidity removal is dependent on the effectiveness of the backwash system employed. In order to provide water of consistently acceptable quality to subsequent usage it is necessary to devise an efficient method by which the filter grains can be repeatedly cleaned. In a backwash system, cleaning is most effective when the mechanisms which promote collisions and abrasions between the grains are enhanced, so that attached material is actively removed throughout the depth of the bed. Research has shown that particulate fluidization does not function aggressively to remove attached particles, since it only provides the hydrodynamic shear mechanism in which few, if any, collisions occur [2].

In contrast to particulate fluidization, a condition can be induced in a fixed bed subjected to specific backwash flow combinations of simultaneous air and water in which the bed behavior is characterized by the formation and collapse of air cavities throughout its depth. The surrounding media grains are slipping and sliding against one another at their contact points. This phenomenon, termed Collapse-Pulsing [20,21], is theorized conceptually to provide better cleaning than fluidization mechanisms. In fact, the collapse-pulsing condition is anticipated to provide optimum particle detachment, i.e., cleaning, in a filter subjected to simultaneous air scour plus subfluidization water backwash flows.

A quantitative theory which will predict the condition of collapse-pulsing has been developed by Amirtharajah [3]. The flow combinations which are obtained from the theory are dependent on the components of the filtration system, i.e., column dimensions, media

characteristics, and inlet configuration. The systemic components provide a series of coefficients which are either easily measurable or have characteristic values which can be inserted into the theoretical expression. Subsequently, the simultaneous air/water flow combination to provide collapse-pulsing in the three-phase system can be calculated.

A pilot-scale gravity filtration apparatus was designed with three objective in mind: (1) to determine the combination(s) of air and simultaneous subfluidization water flows which optimize particle detachment in a granular media filter, (2) to experimentally validate or nullify the implication that the Collapse-Pulsing phenomenon optimizes particle detachment during backwash, and (3) to establish design guidelines for filter backwashing which can be applied to improve filter performance.

A total of 50 experimental runs were conducted on the filtration plant. Alum sol suspensions containing uniformly distributed 1.0-micrometer particles were prepared by hydrothermal aging. A predetermined quantity of the particles were attached to the media grains during gravity filtration. During backwash the filter was cleaned utilizing typical air flowrates, from 3.44 to 7.39 scfm/ft^2, and simultaneous water flows varying from 20 to 225 percent of minimum fluidization, V_{mf}, were completed. The backwash water was collected and analyzed to determine the number of particles removed.

In order to address the subject of particle detachment by Collapse-Pulsing behavior in a granular media filter bed the thesis is organized in the following manner: Chapter 2 presents a review of the literature pertinent to the development of the Collapse-Pulsing theory. Chapter 3 summarizes the theoretical development relative to the tri-phasic mechanics of the system. Chapter 4, Experimental Methodology, includes an explanation of the experimental apparatus, experimental procedures, and sample calculations. Finally, Chapters 5 and 6 discuss the results and present the conclusions obtained during the experimental investigation.

CHAPTER 2

LITERATURE REVIEW

Both potable and wastewater treatment facilities can include a filtration step in the treatment process. Granular media filters are used as a final polishing step prior to distribution of potable water or as a means of reducing the concentration of suspended material prior to chemical addition in the wastewater industry. The ability of the filter to provide effluent of suitable quality, i.e., suitable to subsequent processing whether it be distribution standards or a suspended solids concentration which does not interfere with chemical treatment, is a function of the applied design criteria. In order to accurately predict the behavior of an on-line filter, the design must reflect a fundamental knowledge of the mechanics of a granular media filter. It is not only necessary to establish a definition of filtration mechanics, but backwash mechanics as well.

A granular media filter which has been repeatedly loaded and cleaned displays poor initial effluent quality. Amirtharajah and Wetstein [6] have shown that the poor effluent quality occurs as a result of two phenomena: (1) backwash water remnants remaining in the filter system and (2) the initial characteristics of filtration. One means available to improve the initial quality of filter effluent is to improve backwash efficacy.

Backwashing is defined herein as a solid-fluid contact system where the backwash fluid follows a path through the filter bed reverse of the influent water path. Any cleaning system which does not encompass the entire depth of the bed is not considered backwash, rather it is considered auxiliary wash. In backwash the solid-phase, media grains, are contacted by the fluid-phase, backwash liquid, which flows through the pores of the filter bed in an effort to remove attached particles in the fluid stream. Water used alone represents a

two-phase, solid-fluid, system. When air and water flow simultaneously through the pores of the filter bed a three-phase, solid-fluid-fluid, system is present.

Typically, filtration plants in the United States employ water, two-phase backwash, at flowrates well above the minimum fluidization velocity, V_{mf}, with substantial bed expansion (20 to 50%) [13,30,31]. Fluidization alone, however, is an inherently weak cleaning process. Amirtharajah [2] has established that particle abrasion in a fluidized bed is limited; hydrodynamic shear forces represent the principal cleaning mechanism. Recent research [6,11,14,15] has shown that air scour either alone or with subfluidization water velocities, promotes collisions between the media grains which significantly improves cleaning. Air scour provides increased backwash effectiveness both as a backwash fluid and as an auxiliary wash. While auxiliary air wash provides limited improvement in particle detachment, the most effective particle detachment is obtained through simultaneous air and subfluidization water backwash [6,11,14,15]. All future references to simultaneous air and subfluidization water flows will be denoted as air/water backwash.

Although the air/water backwash system has been recommended, there is little fundamental understanding of the mechanics of particle detachment in a three-phase system composed of air and water flowing up through the pores of a fixed bed. Design parameters have not been based on established theory. Filter failure due to blowup of undergrain systems and media loss cause engineers to be wary of air scour designs. In fact, filters employing air scour disappeared from U.S. water treatment circa 1900 as a result of these problems. Some resurgence of an air/water backwash system has been generated in the wastewater industry [16]. The application of an air/water backwash system, however, was primarily focused on developing a means of destratifying the bed in preparation for a filter run, rather than as a particle detachment mechanism.

The use of small media in high level suspended solids removal in the wastewater industry results in undesirably short filter runs. Head loss builds up rapidly in the filter bed due

to clogging of the pores. The use of larger diameter grain sizes, 2-4-mm, provides increased filter run-time [11]. The large diameter grains, however, would require prohibitive backwash flows to provide even minimum fluidization of the filter bed. Dahab and Young [16] applied simultaneous air scour and subfluidization water flows as the backwash mechanism in a wastewater filter having an effective size in the 1.0-mm range. The application of air/water backwash destratifies the bed. Smaller grains are not preferentially distributed to the top of the filter bed. High surface capture of suspended solids is no longer a problem. Filter run-time is increased. The air/water combinations which were applied, however, resulted in large amounts of media loss prompting design of an air-water baffle used to reduce media loss.

Most studies concerning particle behavior in a granular media filter have dealt with conditions leading to their adhesion on various substrates [1,8,25,27]. By comparison, only a few investigations [10,29] involve the detachment of attached particles. As a rule, these measurements were restricted to determining the amount of removed solids as a function of chemically varied parameters, i.e., solution chemistry is altered to cause particle detachment. In certain cases [1,8,10,23,25,27] attached particles could be released once the composition of the solution surrounding the particles was altered to the point where the system favored particle detachment. Matijevic and coworkers [23,25] conducted investigations where they simulated a fixed bed system with laminar flow, i.e., low Reynolds number, and the desorption phenomena were interpreted in terms of classical Double-Layer Theory.

Recent particle detachment studies at Montana State University have shifted the focus from solution chemistry to the mechanics of fluidized and fixed beds [29]. The results show that even under optimal conditions, complete removal of attached particles by fluidization is not possible. A preliminary study conducted by Morrison [28] deals with

the formation and motion of air bubbles throughout the filter media. These findings prompted development of a modified mathematical theory predicting bubble motion.

Further investigations [20] dealing with simultaneous air and water flow through granular media resulted in an empirical equation to predict the combination of air/water flows which causes the media to display circular and downward motion:

$$\%(V/V_{mf}) + 3.64Q_a = 49.0 \quad (1)$$

Where $\%(V/V_{mf})$ represents backwash water flowrates as the percentage of minimum fluidization velocity, and Q_a equals the air flowrate in standard cubic feet per minute per foot squared. The downward and circular behavior exemplified by a granular media filter which is subjected to simultaneous air and subfluidization water flow combination predicted by the above empirical formula was termed Collapse-Pulsing [20,21].

A parallel study [5] addressed the problem of media loss in a system using simultaneous air scour and subfluidization water flows. Prior work by Holnbeck [22] indicated that the primary mechanism by which media is carried above the static surface of the bed is a result of the media grains being caught in the turbulent wake of an air bubble. Larger bubbles and co-current air and water flows both tend toward higher media losses. Test results [5] showed that the optimum combination of bubble size and water flow to minimize media loss are present during collapse-pulsing conditions. Media loss is minimized since bubble size is favorable, i.e., air bubble motion during collapse-pulsing does not result in turbulent wake formation.

Visual studies [20] indicated that air movement through the fixed bed, and hence, media movement, occurs in four distinct patterns depending on the air/water flow combination. It was also evident by studies of three separate sand sizes (d_{60} = 0.62-mm, 0.86-mm, 1.54-mm) that the characteristics of air motion change at water flows very close to the same percentage of the V_{mf}. Independent investigations conducted by Cleasby and

Lorence [14] utilizing a much larger sand size (d_{60} = 3.20-mm) also showed similar patterns of media behavior. Figures 1-8 illustrate the typical air and media movement patterns described by Hewitt [20].

Air scour alone. At zero water flow and low air flow rates (1-3 scfm/ft^2) the air moves up through the bed without any motion of the media. Air travels up through the pores of the bed as small bubbles which are completely surrounded by water. Small bubbles are characterized by a high surface to volume ratio. The radius of the bubble is small; therefore, the surface tension pressures are high. As the bubbles rise in the column, the static water pressure, ρ gh, decreases. As a result of the reduction in external pressure, the bubble expands, increasing the radius, effectively reducing the surface tension pressure. When the bubble diameter becomes much greater than the pore size, air flow converts from flow as bubbles to flow through a tubular channel. Figure 1 depicts a filter bed characterized by channel formation in the top layers of the media. A small section of the bed has been enlarged to show both forms of air flow.

At shallow depths, i.e., just below the media surface, the effective stresses between the media grains tend toward zero. Consequently, the uppermost portion of the channel displays a noticeable enlargement. The media grains are pushed apart. At the surface of the bed where the intergranular stresses are zero, the media behaves like a liquid. The air flow is no longer constricted by the presence of the media grains into characteristic tubular formation. Hence, the bubble will regain spherical shape to maintain minimum surface energy. Albeit, the bubble size at exit is much greater than the pore size (see Figure 1).

Given an inlet configuration which supplies multiple small bubbles, it may seem reasonable to assume that the random movement of the air bubbles through the filter bed

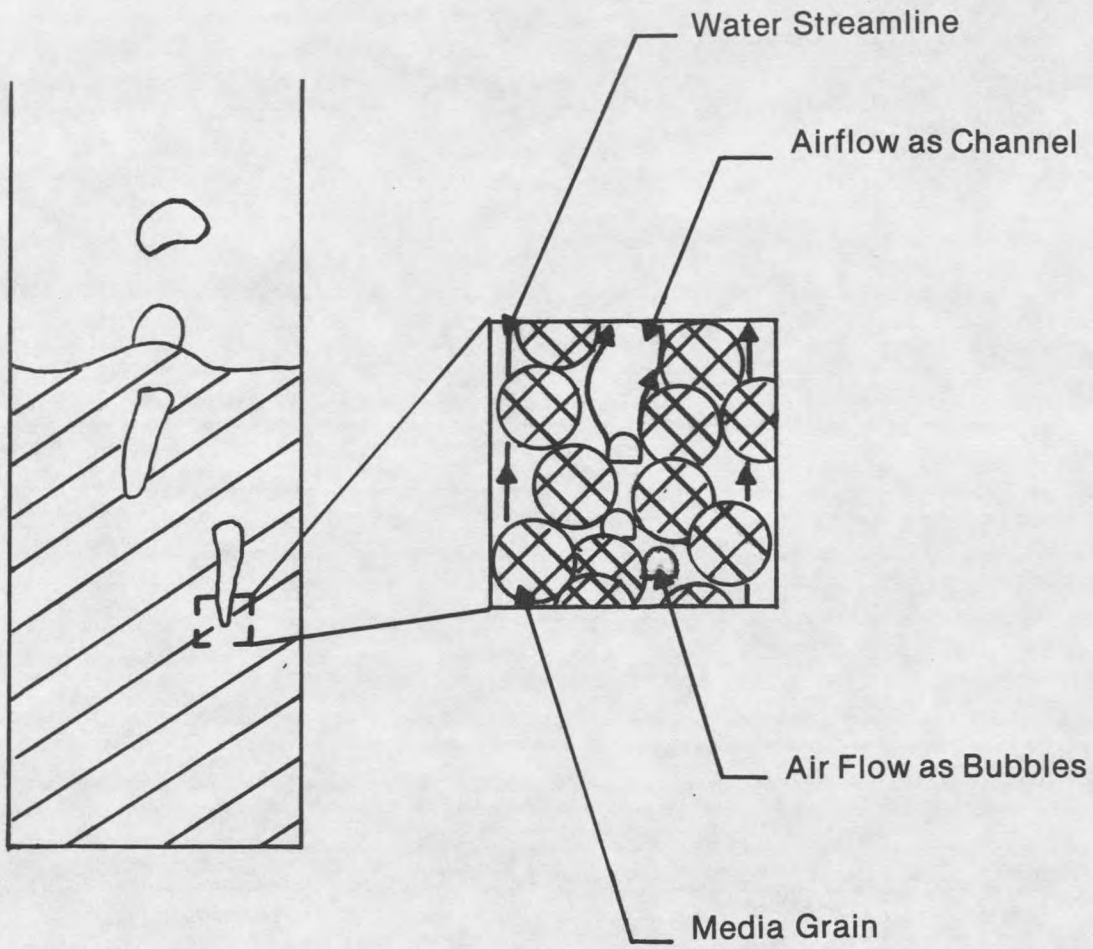

Figure 1. Channel formation in top layers of media.

would cause a sufficient number of collisions between the grains to provide effective cleaning. Cleaning, however, is not significant since the bubbles are smaller than the voids in the pores. The media grains are not actively abrading, i.e., the media grains are not forced into contact. The only apparent cleaning is limited to the top layer of the media where the channels form and collapse. In this region, the air flow is larger than the void spaces in the pores. The grains, however, are merely pushed out of their original position while air flows through the channel. The grains regain their original position once the air flow exits the channel through the surface of the media. Some turbulence develops in the wake of the bubbles above the bed where they exit the media surface. Media is carried above the bed surface in the turbulent wakes. Cleasby and his coworkers [11,15] have shown that the combined turbulence and minimal media movement may be enough to alleviate mudball formation, but air scour alone does little else.

As water flow is increased to low subfluidization flows: the pore water pressure is increased due to the head loss gradient in a flowing system. As water flow is increased the effective stresses decrease throughout the depth of the bed. The head loss increases to a maximum, and the effective stress between the grains reduce to a limit of zero where the media grains are suspended in the liquid stream. This point is defined as the minimum fluidization velocity, V_{mf}.

For fixed bed phenomena the limiting water flowrate of the system is the V_{mf}. In an ideal case where the bed is composed of unisize, spherical grains, the effective stresses would change uniformly over the depth of the bed as the water flow approaches V_{mf}. Channel formation does not occur at the same instant at every depth within the bed. Rather, as the flow increases from zero to low subfluidization water flows, the air channels which initially formed in the surface layers of the media subjected to air scour alone begin to extend deeper into the bed. Consider that a reference line or datum is established at the media surface as in Figure 2. As the distance, y, from the datum increases the pressure

exerted by the media above y also increases. Hence, channels 'grow' from the surface to the base of the bed as the water flowrate is increased. At a specific air/water combination channels will extend from the surface to the base of the bed. Additionally, once channels form, they maintain a fixed position in the bed.

Less abrasion occurs between the media grains in a bed which displays channelling throughout its depth than the case where air scour is used alone. Bear in mind that the air/water flow combination defines the behavior of the bed. Backwash cycles which utilize a constant combination of air and water flowrates will maintain channels which extend from the surface to the base of the bed for the duration of the cycle. Air flow is no longer random. The grains are not moving into and out of position by the formation and collapse of channels. Air channelling behavior in a three-phase fixed bed system resembles that of water flow through channels in a two-phase, water fluidized system described by Leva [26]. Air travels preferentially through an existing channel rather than expend the energy to form a new one. Once a channel extends from the surface to the base of the bed it maintains a fixed position throughout the simultaneous air/subfluidization water backwash cycle.

As water flow is increased to the transition phase from channelling to collapse-pulsing: channelling is still evident in the top layer of media while air cavities begin forming in the bottom layer of media. Figure 3 shows the transition phase. The air cavities form when a favorable quantitative relationship between the air pressure and the soil stresses is reached.

Since the intergranular stresses are greater in the vertical direction than in the horizontal direction the air cavities tend to grow horizontally first, forming a lens shape. Cavity size increases until it reaches a point where the diameter of the cavity is much greater than the diameter of the pores. It causes local rearrangement and compression of the grains. Figure 3 shows a lens-shaped air cavity which is growing in the filter column. Figures 4 and 5 illustrate the isolated section of the filter column outlined in Figure 3 which has been

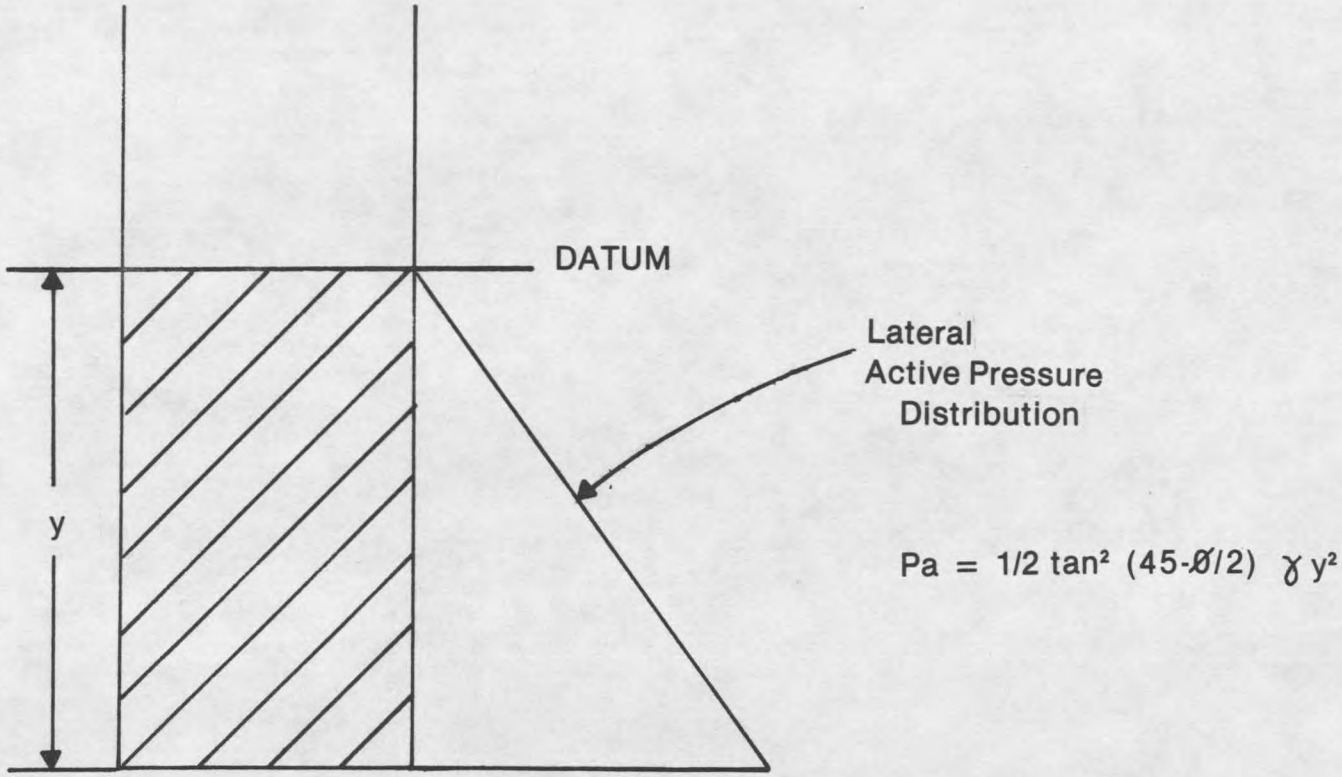

Figure 2. Lateral pressure distribution in a media column.

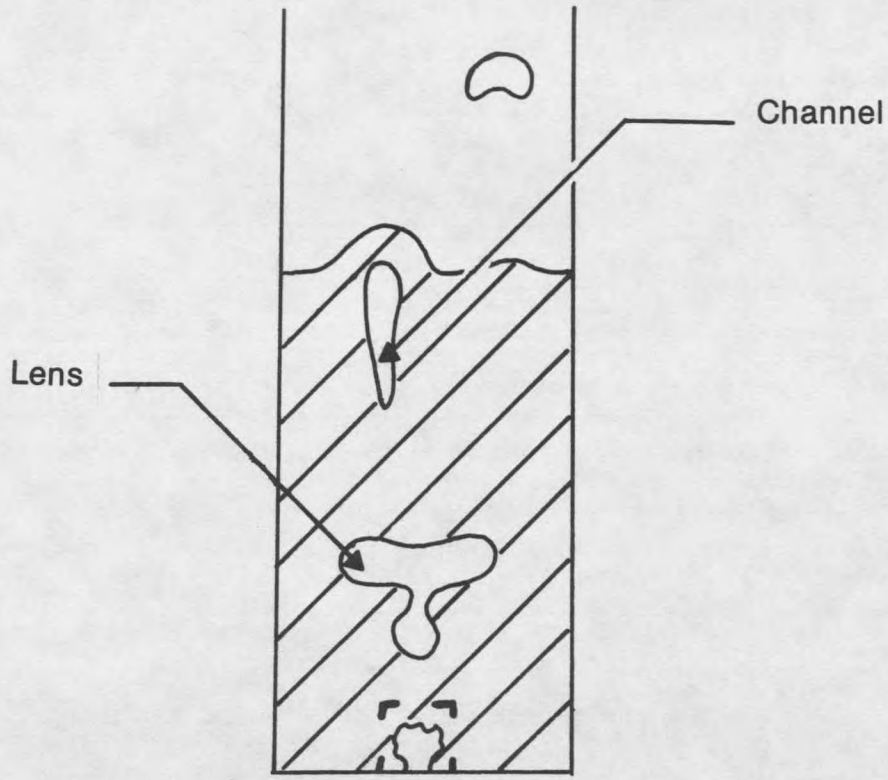

Figure 3. Transition phase from channeling to collapse-pulsing.

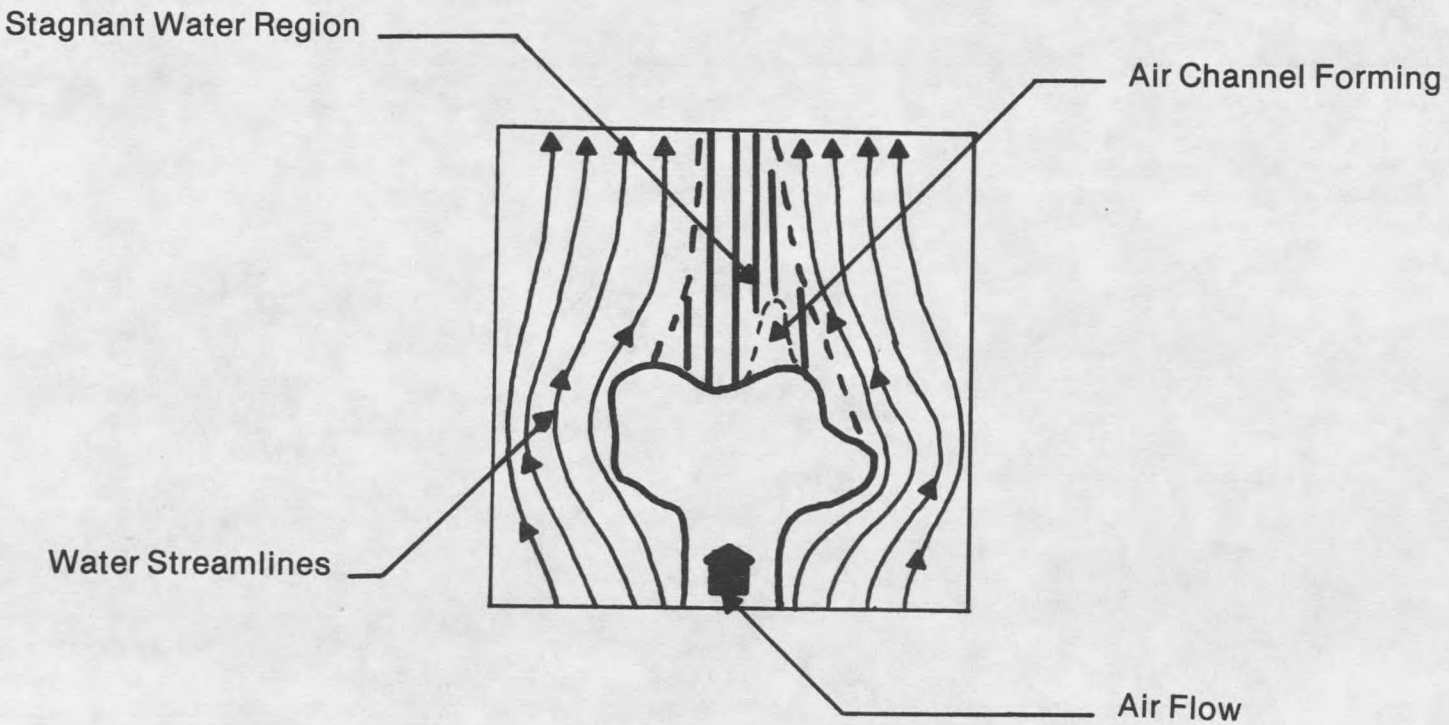

Figure 4. Schematic representation of air/water flows.

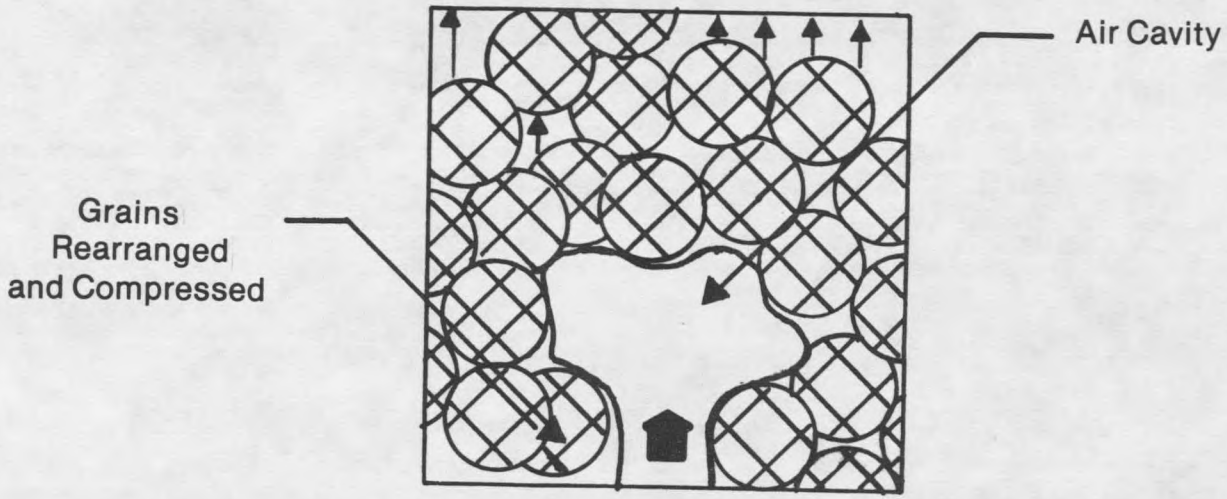

Figure 5. Schematic representation of local grain compression.

enlarged to show, respectively: (1) the air cavity with respect to the surrounding water streamlines and (2) the air cavity with surrounding grains under compression.

Under conditions of simultaneous air and subfluidization water flows, as the cavity grows horizontally (see Figure 4) the water streamlines tend to bend around the cavity resulting in a region of stagnant water, i.e., where the water flow tends toward zero, at the top of the air cavity. The pore water pressure approaches its lower limit, i.e., the effective stresses increase. The horizontal growth of the cavity reaches a limit defined by a pressure equilibrium. Once the internal pressure of the cavity becomes equal to the external pressure exerted by the media grains and the flowing water, horizontal growth stops. A tubular channel begins forming. Figure 4 shows a channel forming near the forward stagnation point of the collapsing cavity.

Air flows rapidly out through the channel and into a newly forming cavity above the first. As the cavity collapses the horizontal stress between the surrounding media grains is reduced. The media grains which are relieved of compressive forces will fail into the space evacuated by the air flow. At the instant of collapse, the shape of the air cavity is indefinite. The stresses cannot be easily quantified in an undefined system. Near the end of collapse, however, the cavity size approaches the grain size and can be quantified. The system resembles an active Rankine failure state. The media grains are slipping into the space once occupied by the air cavity along lines which are assumed to be defined by the Mohr-Coulomb failure law. Figure 6 shows the media circulation pattern during collapse. The grains slip along the lines which are defined by an angle $(45 - \phi/2)^\circ$ and a 90 degree rotation or $(45 + \phi/2)^\circ$ in which ϕ is the friction angle. The media circulation pattern with respect to the friction angle is shown in Figure 7. Note that the media grains follow the slipping planes down and into the center of the collapsing cavity. Following collapse, the cavity will reform and collapse cyclically.

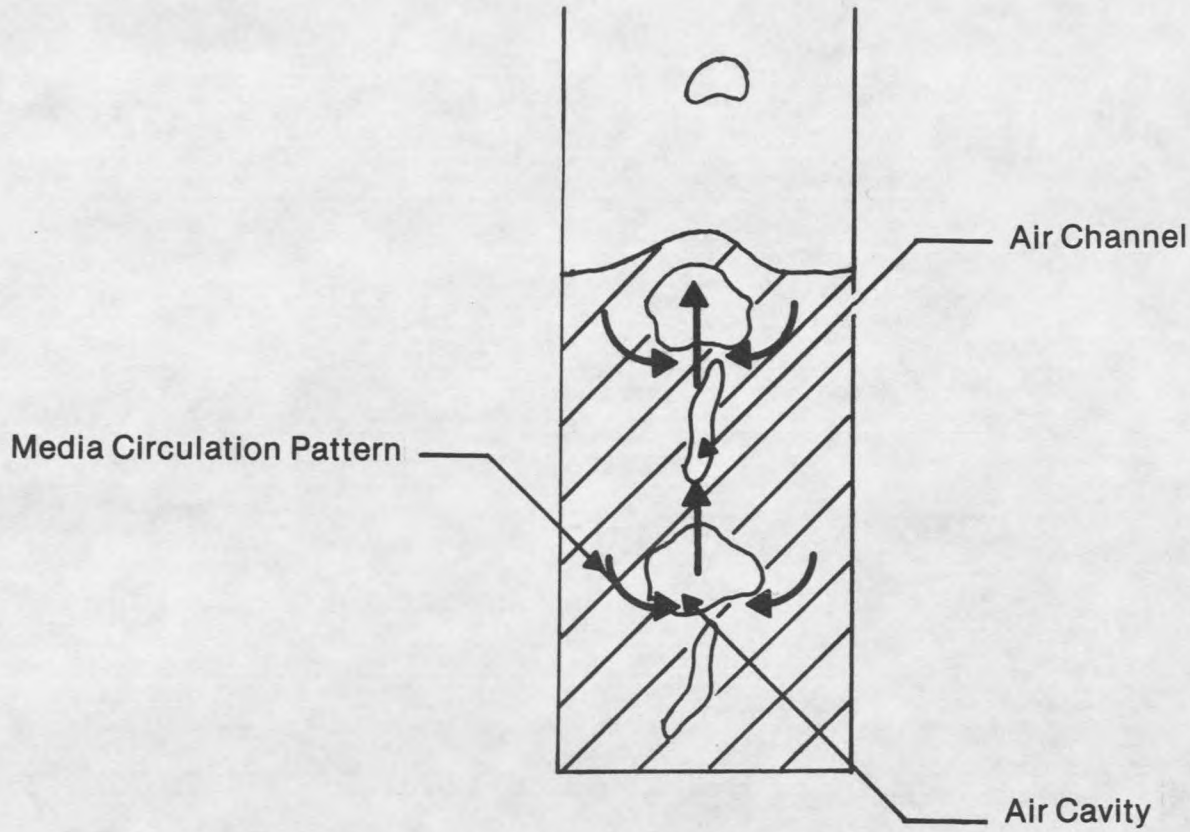

Figure 6. Collapse-pulsing throughout the bed.

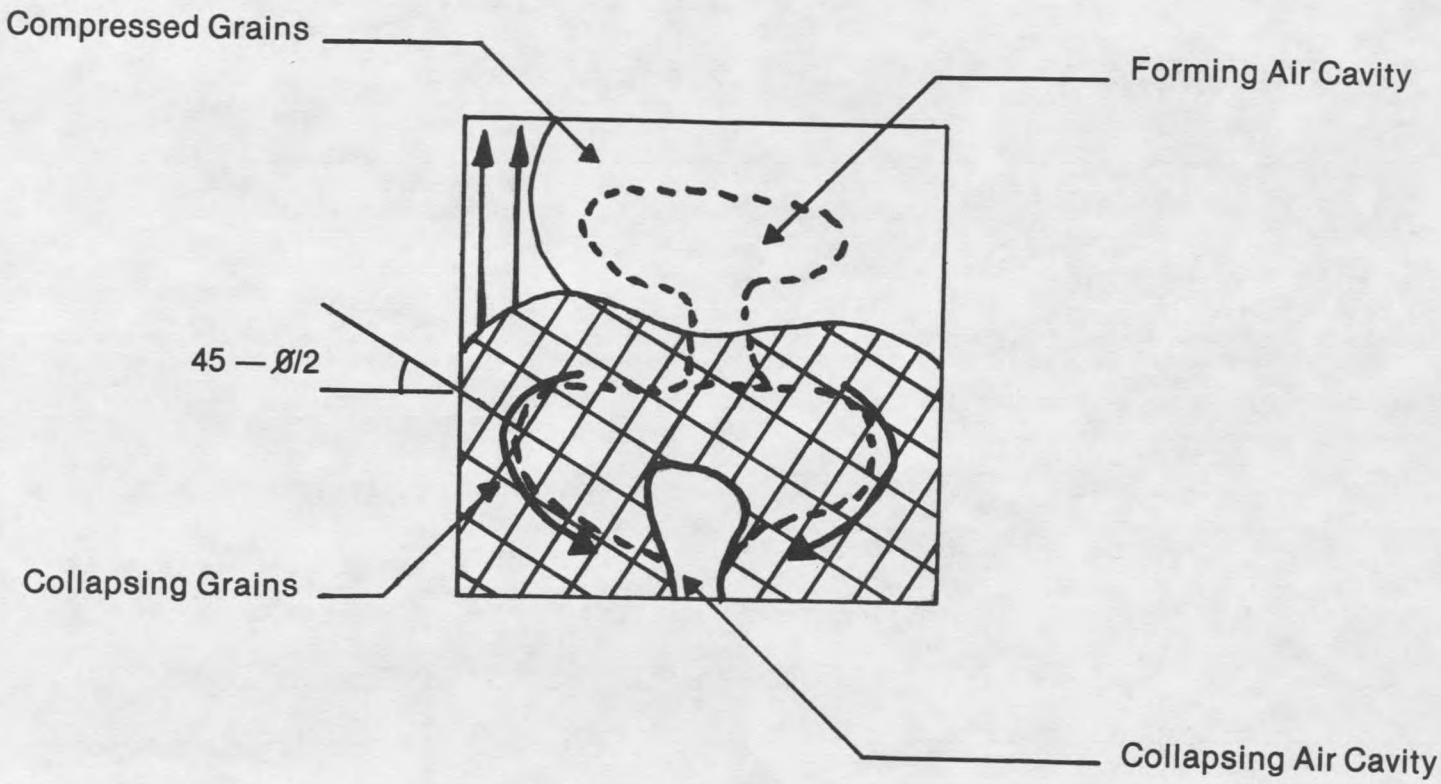

Figure 7. Section collapsing (pulse ended).

In the transition phase from channelling to collapse-pulsing cleaning efficacy should be improved in the bottom layer of media, i.e., particle detachment is probably enhanced over the previous two cases. As collapsing occurs, the media grains are actively sliding against each other causing abrasion. Cleaning is not yet optimum, however, since the top of the bed is still channelling as shown in Figure 3 with limited cleaning.

As water flow increases and collapse-pulsing is evident throughout the bed: the granular media exhibits a circulation pattern as shown in Figure 6. The grains fail down and into the cavity along the slipping lines as shown in Figure 7. Collapsing is followed, instantaneously by pulsing, i.e., it is difficult to isolate the end of collapse from the beginning of the pulse. As the grains are failing into the cavity, they are being forced upward by the subsequent pulsing or cavity reformation.

Conceptually, collapse-pulsing should exhibit the optimum cleaning condition. The grains are actively sliding against one another throughout the depth of the bed. Abrasion may be enhanced by the air flow pushing the media upward as it fills a new cavity. This media circulation pattern evident during collapse-pulsing would seem to favor the occurrence of collisions. Particle detachment should increase over that of the previous cases.

When water flowrates exceed the collapse-pulsing flows: the bed begins to behave like a liquid. The bubbles travel through the bed as if it were fluidized. The media no longer displays a circulation pattern. Abrasion is reduced. Hydrodynamic shear mechanisms, as in fluidization, dominate the particle detachment mechanisms. Cleaning efficacy, i.e., the particle detachment capability, is probably reduced.

Although some assumptions have been made regarding the cleaning efficacy corresponding to each air movement pattern in a granular media filter, exhaustive research has not been performed to date to determine the pattern which provides optimum particle detachment. The research completed by Cleasby and Lorence [14] showed some evidence that an optimum combination of air and water exists for particle detachment near the

collapse-pulsing condition. During actual backwash conditions with flows below the collapse-pulsing combination (Q_a = 7 cfm/ft² and V = 8.0 gpm/ft²) the filters were not cleaned adequately. When the water flow was increased (15.0 gpm/ft²) they found that the media improved and was maintained in good condition for the remainder of the study. Equation 1 would predict that collapse-pulsing occurred in their filter near 12.0 gpm/ft². The correlation between this experimental behavior and the empirical formula lends credence to the basic assumption made by Hewitt and Amirtharajah [21] that collapse-pulsing provides the optimum cleaning condition in a granular media filter subjected to simultaneous air and subfluidization water backwash.

Even though the empirical relationship developed by Hewitt and Amirtharajah [20,21] could be used for design of air scour systems, it was difficult to ascertain whether the equation was applicable in general to the design of granular media filters. The nature of an empirical relationship limits its applicability in design to an ability to predict an adjustable constant for a particular system. A fundamental theoretical equation, however, would provide greater confidence in filters designed to apply the collapse-pulsing phenomenon during backwash. Amirtharajah [3], therefore, has developed an equation to predict collapse-pulsing based on the mechanics of the behavior of a three-phase backwash system.

CHAPTER 3

THEORETICAL CONSIDERATIONS

In order to develop a model which will include all the physical factors contributing to the backwash phenomena in a granular media bed it is necessary to look at every aspect of bed behavior. During simultaneous air scour and subfluidization water backwash a three-phase system is present which consists of air and water flowing through the pores of a fixed bed. A fundamental formulation of the collapse-pulsing phenomenon, therefore, must consist of applicable concepts from each phase of the system. The system can be defined by concepts derived from soil mechanics, fluid mechanics, and bubble mechanics.

Accordingly, some basic assumptions are necessary to simplify the mathematics of the system:

1. Assume that the system is isolated at a point near the end of collapse where the stresses are defined.
2. Assume that the grains behave in an active Rankine state of failure.
3. Assume that surface tension acts at the menisci in the pores of the grains rather than in the air cavity which has an indefinite shape.
4. Assume that the horizontal stress controls the collapse.

With the above assumptions Amirtharajah [3] has developed a fundamental theoretical equation from which the combination of air and water flows for collapse-pulsing can be calculated. The theoretical development is summarized below.

In a saturated granular media filter bed, a collection of forces are present. Where the bed surface is horizontal and the properties of the media do not vary horizontally there are three mutually perpendicular planes in which there exists no shear stress, i.e., the normal

stresses predominate. These stresses are called principal stresses, the maximum stress, the minimum stress, and the intermediate stress. In a system which acts in the confines of these stresses, only the upper and lower limits are relevant. The intermediate stress is not considered. Within a column of granular media the horizontal stress is less than the vertical stress. Consider, then, that the minimum and maximum stresses are in the horizontal and vertical directions, respectively. The pressure against which an air cavity will form in the filter bed is then the total horizontal stress, σ_h.

The intergranular stresses in a column of media act, and are concentrated, at the contact points of the grains. The actual horizontal stress, noted as σ_h, however, which is used in computation is obtained as an average of all the normal forces acting over the entire contact area of the grains.

$$\sigma_h = \frac{\Sigma N_o}{\text{Contact Area}} \tag{2}$$

where N_o is a horizontal force normal to the contact area.

The vertical stress, σ_v, is calculated by considering the weight of the media above the depth at which the stresses are calculated:

$$\sigma_v = Z\gamma_s \tag{3}$$

where γ_s is the saturated unit weight of the media and Z is the depth below the media surface.

The total horizontal and vertical stresses consider the pore water pressure, u. The pore water pressure, however, acts with the same intensity in both the solid and liquid phases. Frictional resistance at the contact points is slightly reduced by wetting the surface of the grains. The effective stress, $\bar{\sigma}$, causing frictional resistance at the grains is, therefore, calculated as the total stress minus the pore water pressure:

$$\bar{\sigma}_h = \sigma_h - u \tag{4}$$

By a similar argument, it can be shown that:

$$\bar{\sigma}_v = Z(\gamma_s - \gamma_w) = Z\gamma_b \tag{5}$$

where γ_w is the unit weight of the water, and γ_b is the buoyant unit weight of the media.

Strain at the contact points can be elastic at static points of contact or it can be due to the sliding of grains against one another at movement, or relative failure, of the grains. A granular mass has a defined strength during failure. The strength is represented by the Mohr-Coulomb failure law:

$$\tau_f = \bar{\sigma}_f \tan \phi \tag{6}$$

where τ is the shear strength of the granular mass, ϕ is the friction angle of the media, and f denotes a failure condition.

When the effective horizontal stress of a soil is decreased to a minimum of $\bar{\sigma}_f$, some movement occurs. The surfaces of the grains are brought into contact, i.e., they are pressed together. The water is squeezed away from the contact points. The full shear strength of the soil is mobilized. The media is said to be in an active Rankine state of stress. The media grains are actively sliding against each other at their contact points, i.e., abrasion/collisions are occurring. Abrasion/collisions promote particle detachment from the media grains [6,11,14,15].

The ratio between the horizontal and vertical stresses can be obtained from a Mohr circle analysis. With standard trigonometric identities the relationship can be expressed:

$$\frac{\bar{\sigma}_h}{\bar{\sigma}_v} = \tan^2 (45 - \frac{\phi}{2}) \tag{7}$$

During backwash the effective stresses are influenced by the fluid drag force, F_D, where the fluid flows past the media grains. The effective stresses are further reduced by the water flowing in the system. The fluid drag force is related to the head loss across the

column of media, i.e., the flow path, and can be expressed as a function of the hydraulic gradient, dh/dZ, in the following equation:

$$F_D = Z\gamma_w \left(\frac{dh}{dZ}\right) \tag{8}$$

The effective vertical stress is then given by:

$$\bar{\sigma}_v = Z\gamma_b - Z\gamma_w \left(\frac{dh}{dZ}\right) \tag{9}$$

Further, the intergranular stresses in a column of media subjected to three-phase backwash must be related to the air flow in the system. In a constant pressure supply system, the rate of gas flow over long times approaches a constant. For constant pressure, Davidson and Schuler [18] have shown that the rate of gas flow is proportional to the square root of the pressure difference across the inlet orifice. Therefore, if the rate of air flow is related to its pressure, P_1, the horizontal stress in the media can be equated to the effective pressure in the air cavity by:

$$\sigma_h = P_1 - \frac{2T}{r} - kQ_a^2 \tag{10}$$

where P_1 is the pressure below the air flow inlet, r is the radius of the menisci within the pores, T is the surface tension acting at r, k is a coefficient related to the air velocity at the orifice, and Q_a is the air flowrate.

Consider that the media is in an active Rankine failure state during the formation and collapse of air cavities in the filter bed. The Mohr-Coulomb failure law can be used to calculate the total horizontal stress due to the grains and the pore water pressure present in a flowing system:

$$\sigma_h = \tan^2\left(45 - \frac{\phi}{2}\right)\left[Z\gamma_b - Z\gamma_w \left(\frac{dh}{dZ}\right)\right] + (Z + H_1)\gamma_w + Z\gamma_w \left(\frac{dh}{dZ}\right) \tag{11}$$

where Z is the depth of the media, H_1 is the height of the column of water above the media, and dh/dZ is the head loss gradient over Z.

An expression for the head loss gradient, dh/dZ, can be calculated using the Carman-Kozeny and Fair and Hatch relationships:

$$\frac{dh}{dZ} = (Sg - 1)(1 - \epsilon_o)\frac{V}{V_{mf}} \tag{12}$$

where Sg is the specific gravity of the grains, ϵ_o is the static bed porosity, and V is the backwash water flowrate.

Consider the instantaneous equilibrium at the point where the cavity just collapses and is in transition to reforming. The total horizontal stresses acting inside the cavity just equal the horizontal stresses acting outside the cavity. Figure 8 shows the location of the stresses acting in the system at collapse-pulsing conditions. Note that only the horizontal and vertical portions of the stresses acting at each location are considered.

Equations 11 and 12 are combined with 10 to give the final form of the equation:

$$P_1 - \frac{2T}{r} - kQ_a = \tan^2(45 - \frac{\phi}{2})\left[Z\gamma_b - Z\gamma_w (Sg - 1)(1 - \epsilon_o)\frac{V}{V_{mf}}\right] + (Z + H_1)\gamma_w + Z\gamma_w (Sg - 1)(1 - \epsilon_o)\frac{V}{V_{mf}} \tag{13}$$

The above expression can be rearranged and simplified to:

$$\% \frac{V}{V_{mf}} + mQ_a^2 = b \tag{14}$$

where m and b are coefficients. The equation can be plotted as a straight line in which m and b correspond to the slope and intercept of the line, respectively.

Equation 14 predicts the collapse-pulsing condition defined by the systemic components of the filter which were presented in Equation 13. The experimental investigation was designed to verify (or nullify) whether the collapse-pulsing phenomenon predicted by these equations will also promote the optimum number of abrasion/collisions between the media grains thus optimizing particle detachment from the media grains, i.e., cleaning of the media.

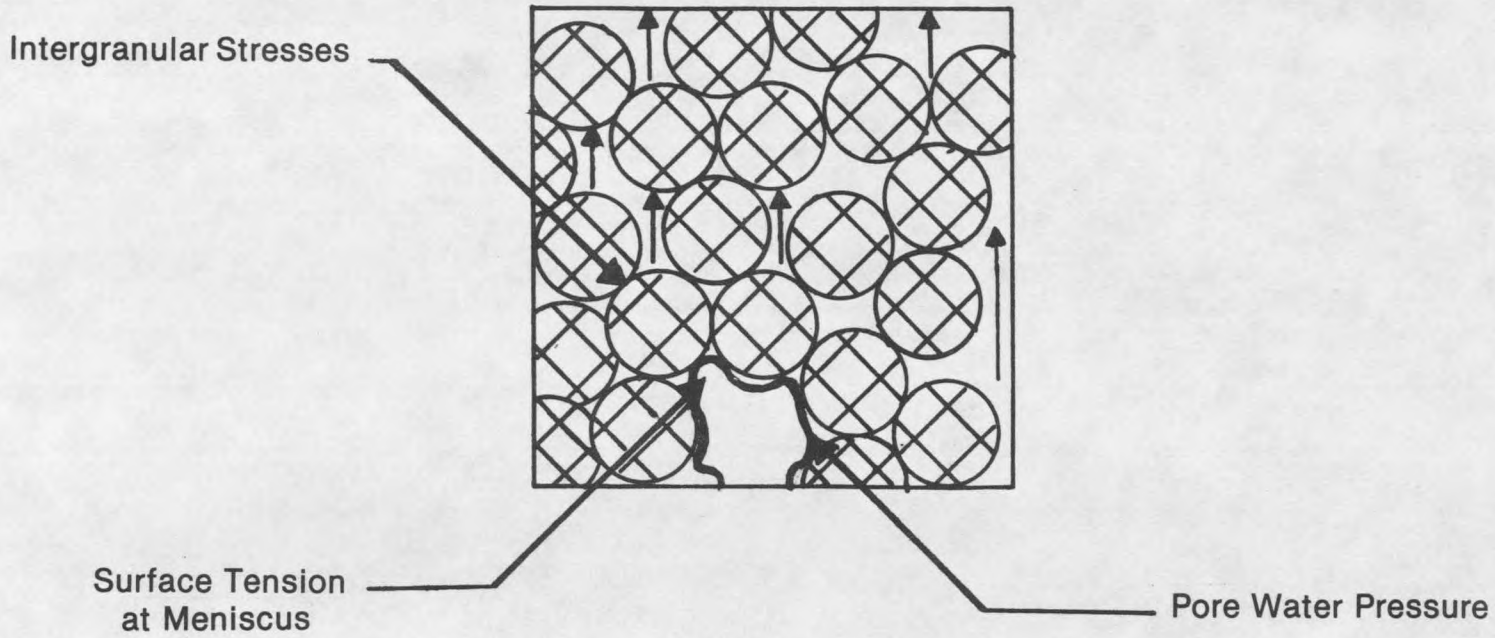

Figure 8. Stress locations at end of collapse.

CHAPTER 4

EXPERIMENTAL METHODOLOGY

Overview

The pilot plant studies were conducted on a small-scale gravity filtration plant. A schematic representation of the apparatus is shown in Figure 9. An alum sol suspension was filtered from a one-liter reservoir, A, through a pyrex column, E, to provide particle attachment on Cataphote Class II microbeads, e. The flow was monitored by meter, C, having influent control at valve B. The effluent was collected at g and recycled during filtration to the reservoir, A, via line G. Valves L, P, and Q were closed during filtration.

The filter was backwashed using simultaneous air and water backwash, i.e., three-phase backwash. Valves D and F were closed during backwash. The clean backwash water from reservoir H was pumped by a Little Giant centrifugal pump, I, through the column, E. The flow was monitored by meter, K, with influent control valve, J. Simultaneously, air was fed from a University tap through flowmeter, N, with influent control valve, M. Air and water travel up through the column, E, and the backwash water remnants were collected in Nalgene bottles at R.

Experimental Apparatus

Nest of Sieves

The nest of sieves used in the grain size analysis consisted of four U.S.A. Standard Testing Sieves, A.S.T.M.E. specification #11, and a pan. The sieve sizes which were used in the grain size analysis are listed in Table 1.

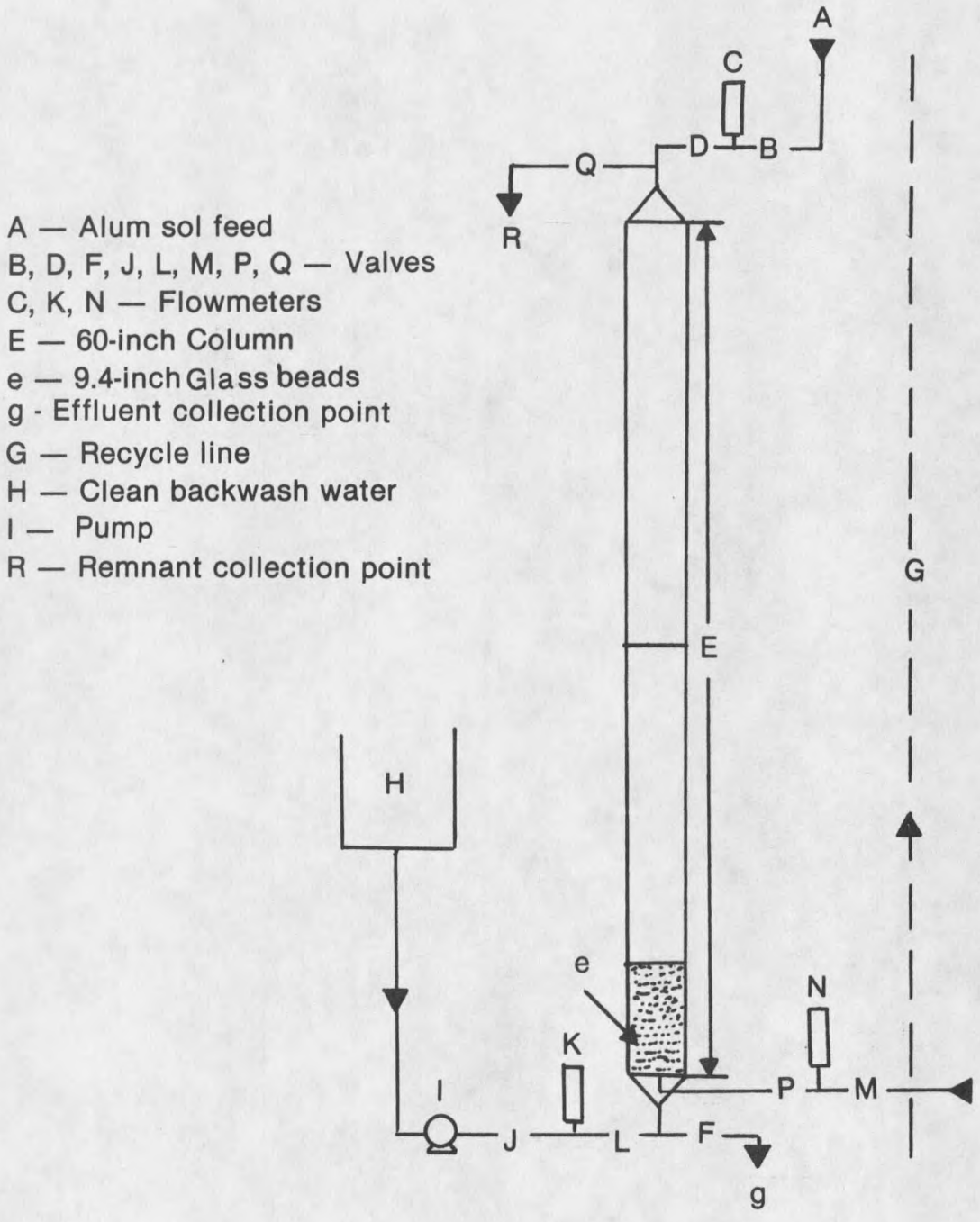

Figure 9. Experimental set-up.

Table 1. Nest of Sieves Used in Grain Size Analysis.

Sieve	Opening Size (mm)
#16	1.18
#30	0.60
#40	0.425
#50	0.300

Friction Angle Box

A 4.5-inch deep plexiglass box equipped with a sliding gate on one end was used to determine the friction angle of the glass beads. The box is shown in Figure 10. The dimensions of the box are shown in Figure 10 as 6-inches wide by 11 3/8-inches long. The gate is not shown in the figure. It has been removed from the front face of the box. The gate rode in grooves in the adjoining walls and could be easily removed without disturbing the media.

Filter Column

The filtration column used in all pilot plant runs was composed of two one-inch diameter thirty-inch long cylindrical pyrex sections joined at the center for a total of sixty inches. Figure 9, part E portrays the filter column. A nylon mesh with 441 openings per square inch was inserted at the junction of the two portions of the column as a baffle to prevent the media from being backwashed into the collection vessels. The mesh was large enough to allow single beads to pass, but not large enough to allow beads which were attached to spheres of air to pass.

The influent and effluent configurations were conical. 'Influent' and 'effluent' are in terms of backwash in the system. The effluent configuration consists, only, of a conical section constricting to an outlet. The dimensions of the effluent cone are, however, the same as those given for the influent section. Figure 11 shows the influent portion of the column which has been enlarged to show detail. The cone was one-inch (2.54-cm) in diameter at its widest, i.e., at the point of juncture to the cylindrical column. Cone diameter

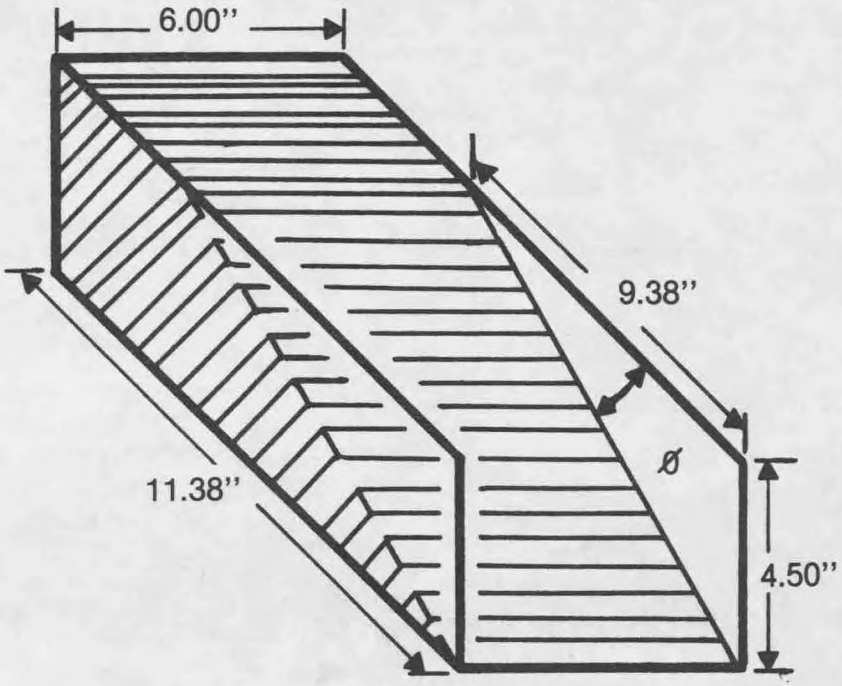

Figure 10. Friction angle box.

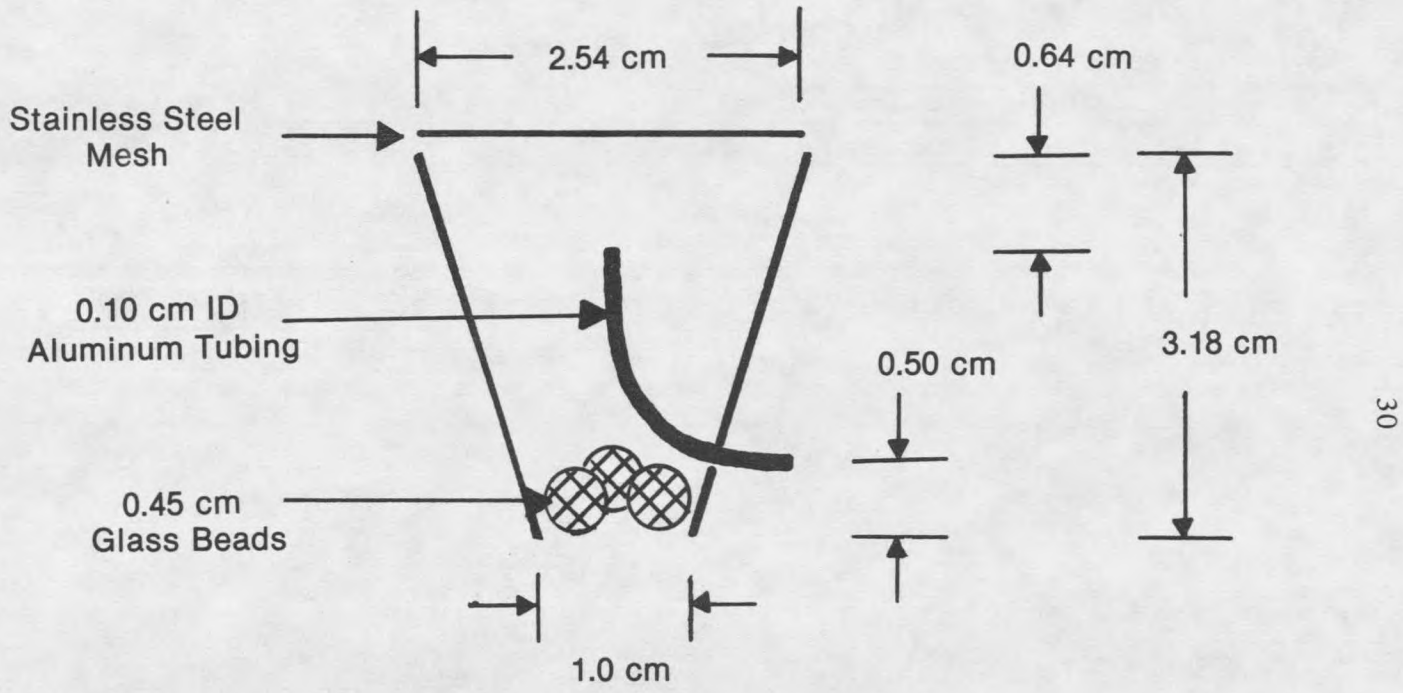

Figure 11. Cross section of influent configuration.

constricts through an angle of 74 degrees to 3/8-inch (1.0-cm) at the water inlet. The air inlet was a 1.0-mm ID aluminum tube which entered the cone 0.196-inch (0.50-cm) above the water influent. The tube bent gradually into the center of the water path, and terminated, i.e., air was fed to the system 0.25-inch (0.64-cm) below the media. A stainless steel mesh with 2070 openings per square inch supported the media. In order to prevent spouting of the bed, three 4.50-mm glass beads were placed in the influent cone. Figure 11 shows the placement of the air inlet tube, the stainless steel mesh, and the glass beads, as well as the dimensions of the inlet.

The influent, effluent, and recycle lines were 0.25-inch (0.64-cm) ID flexible Tygon tubing.

Flowmeters

The filter influent was monitored using a size 12 Gilmont Flowmeter with a black glass float. The flowmeter was calibrated volumetrically using deionized water.

The backwash water flows were monitored using a Sargent Welch Flowmeter. Tube number 448-324 with either a black glass or a stainless steel float was used to measure the applied flows. The flowmeter was calibrated volumetrically using deionized water at 20 ± 1°C. The calibration curves are shown in Figures 12 and 13.

The air flow was monitored by means of a size 12 Gilmont flowmeter with a black glass float. The meter was calibrated using a Precision Wet Test Meter to standard cubic feet per minute. The calibration curve is shown in Figure 14. Figure 14 also shows the air flow for the test column in $scfm/ft^2$.

Heat Exchanger

A schematic diagram of the heat exchanger used to maintain backwash water temperature is shown in Figure 15. The heat exchanger consisted of a 13-inch deep open plastic container. The plan area was 9.25-inches square. The influent line was one half-inch ID

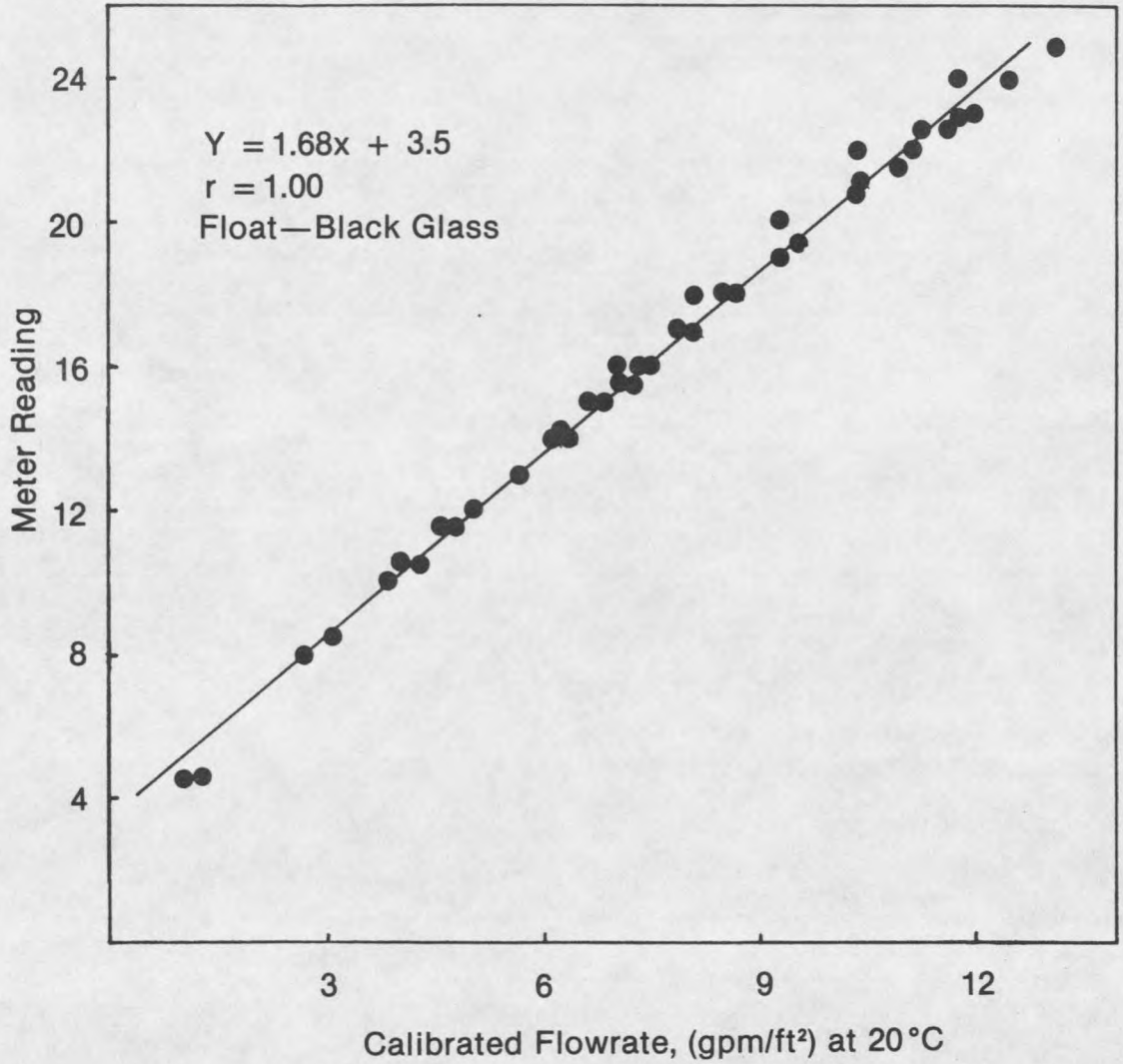

Figure 12. Backwash flowmeter calibration curve, black glass float.

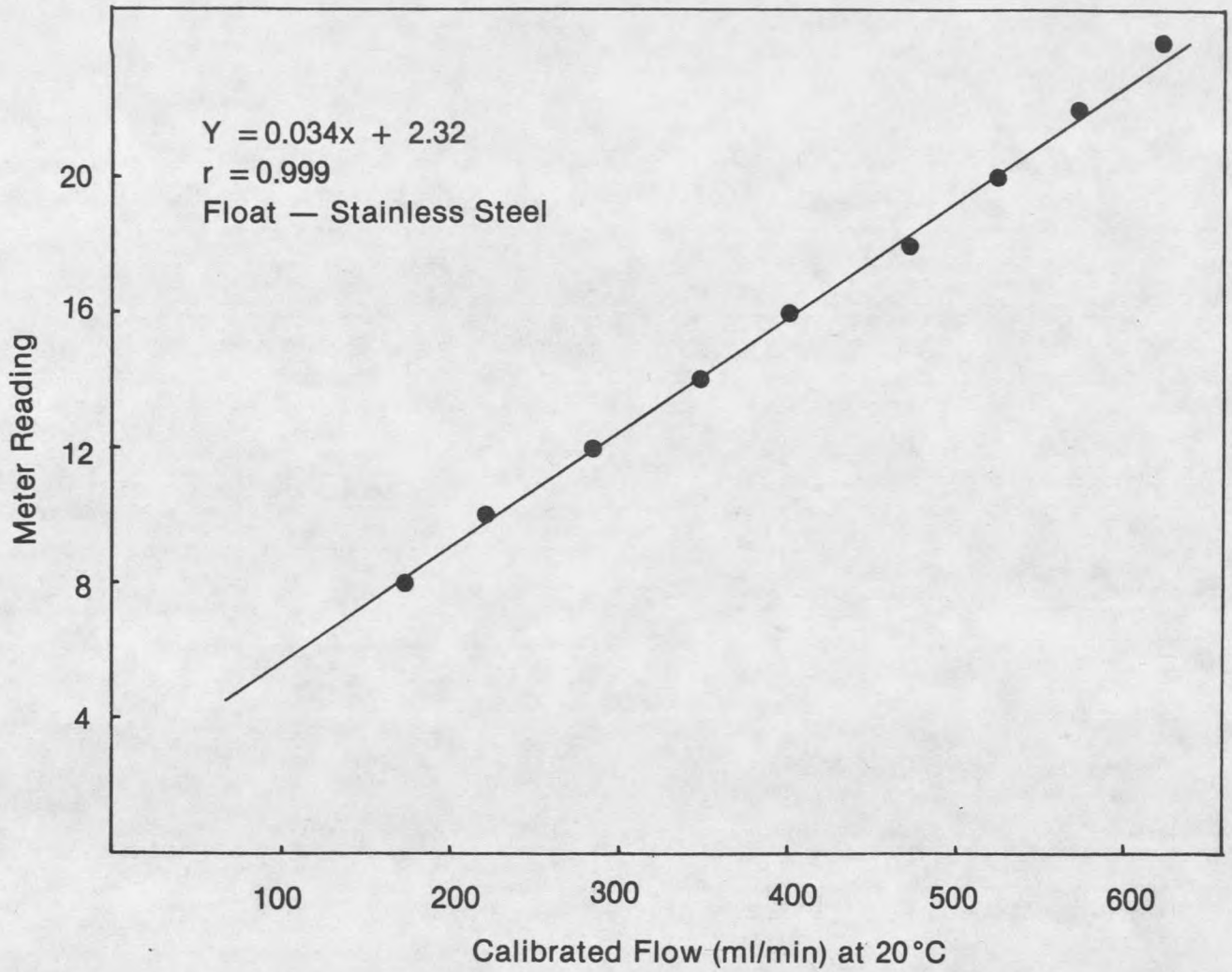

Figure 13. Backwash flowmeter calibration curve, stainless steel float.

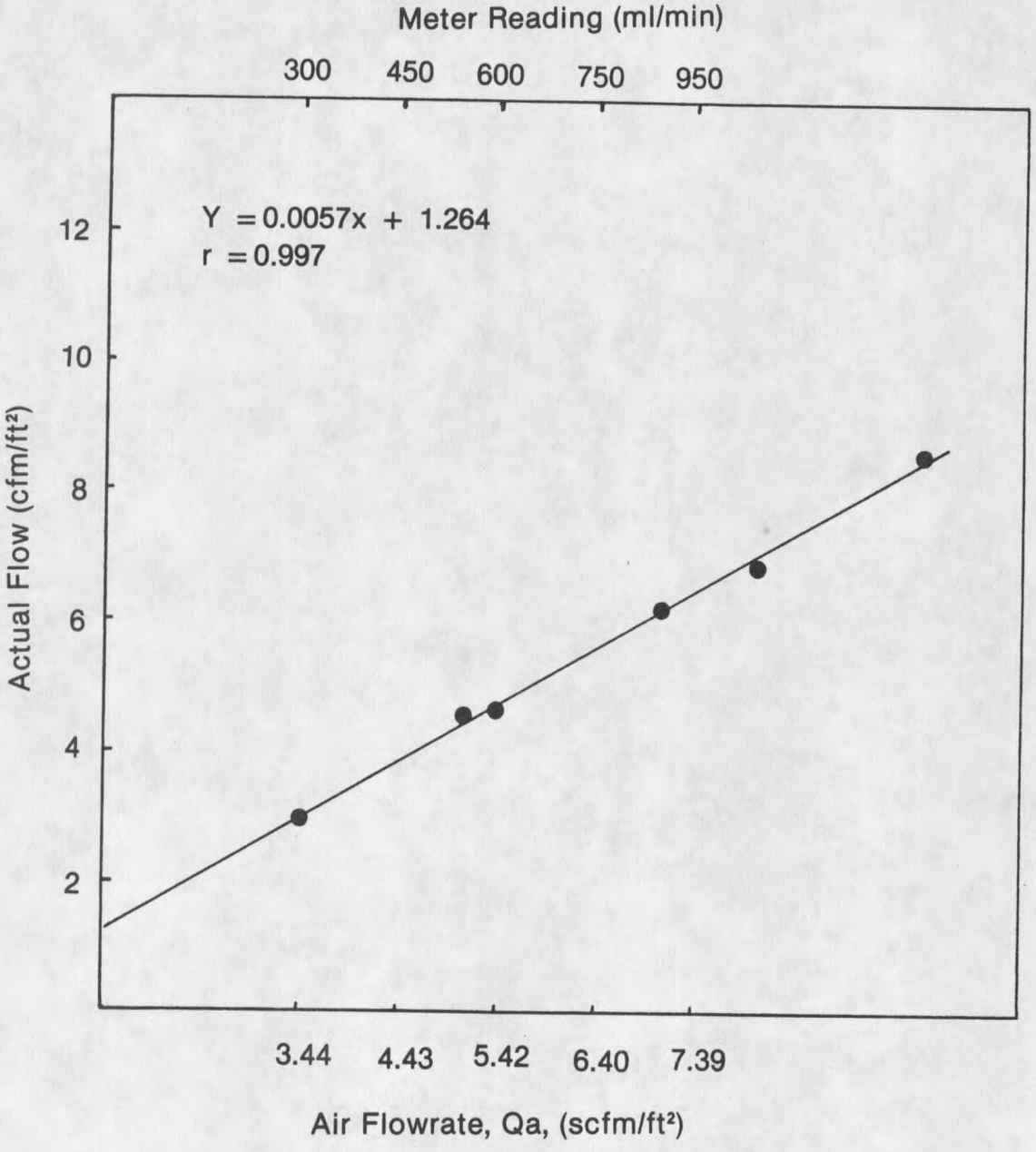

Figure 14. Air flowmeter calibration curve.

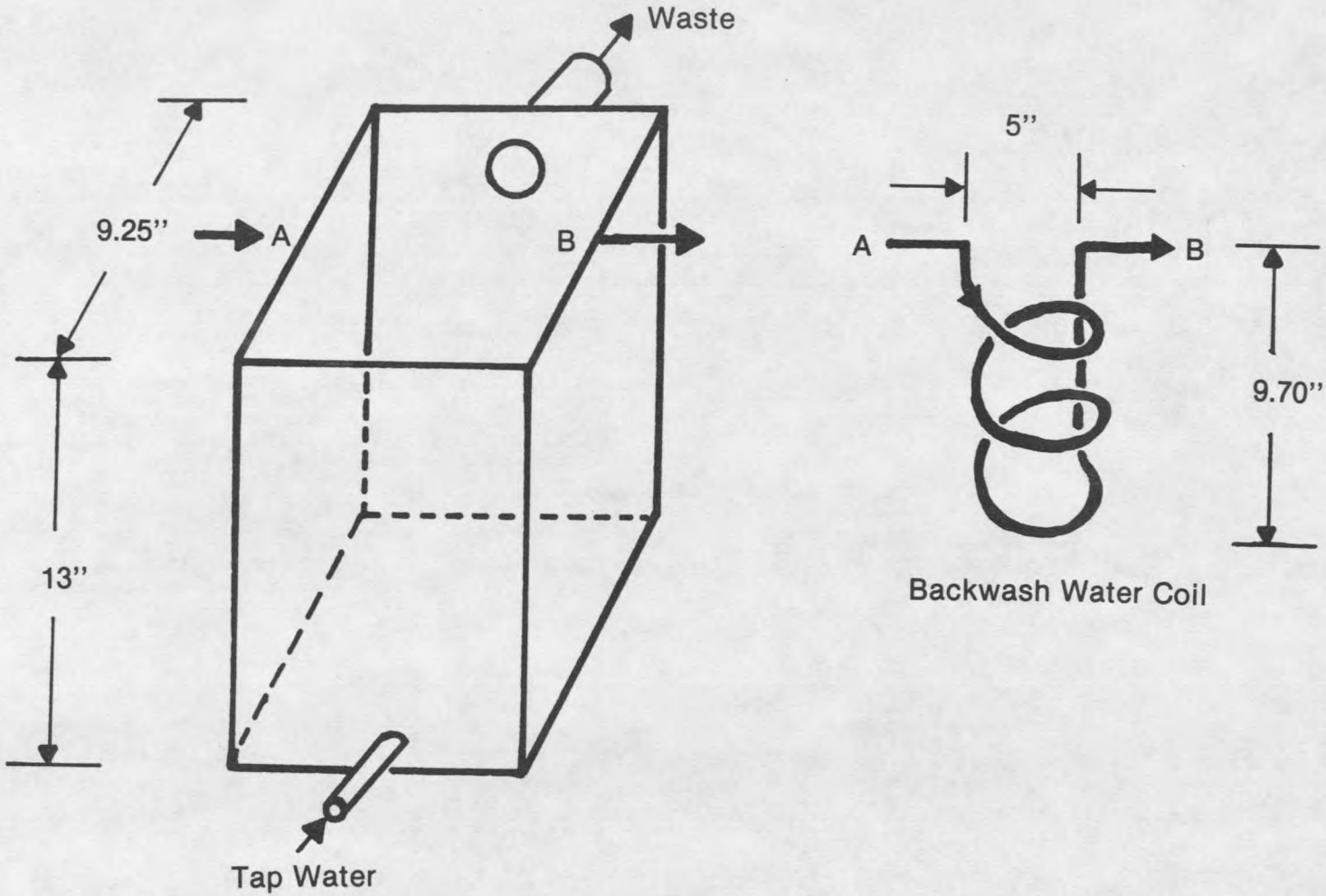

Figure 15. Schematic representation of heat exchanger.

flexible Tygon tubing. The effluent line was one and one half-inch flexible Tygon tubing. The backwash water flowed through three rounds of coil which had a 2.5-inch center. The coil was 0.45-cm ID aluminum tubing. The coil is shown in Figure 15. The system applied the concept of countercurrent heat exchange. The backwash water flowed down through the coil and out into the column; University tap water flowed up through the reservoir and out. The water in the reservoir was maintained at 18.0 ± 0.5°C by mixing hot and cold tap water.

Manometers

A set of two open water manometers were used to determine the pressure drop across the filter bed. One manometer was connected with flexible tubing below the bed. The other was connected via flexible tubing below the nylon mesh at the junction between the two cylindrical portions of the column.

A closed end air water manometer was used to determine the pressure drop below the air inlet orifice. A schematic representation of the closed end manometer is shown in Figure 16. The manometer consisted of a 94-ml volume glass bulb, Vb, connected to one end of a U-tube manometer. The U-tube was 5.74-mm ID glass tubing. The other end of the manometer was connected at a T to the air inlet tube. The manometer was calibrated using a Meriam Instruments, Type W Mercury Manometer. The mercury manometer was factory calibrated, dry, and read in inches of water pressure.

Drying Oven

A GCA Precision Scientific Drying Oven was used to age the alum sol particles. A 230°C maximum mercury bulb thermometer was used to monitor the temperature inside the oven. In order to maintain the inside temperature at a constant 98 ± 2°C, it was necessary to stabilize the ambient temperature. Accordingly, the oven was placed in a fume hood with air continuously flowing during the particle aging period.

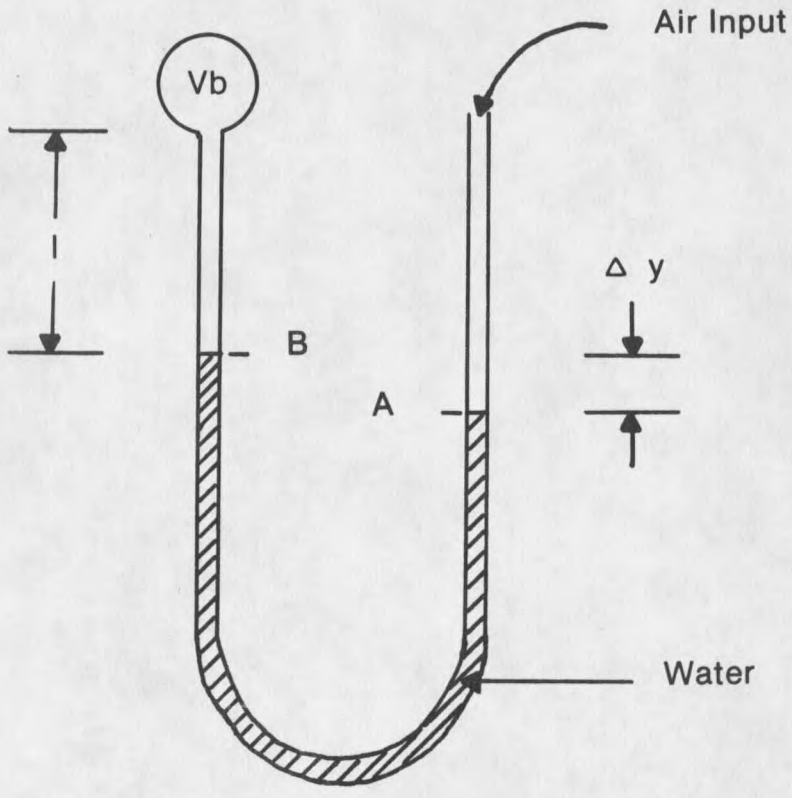

Figure 16. Schematic representation of closed end manometer.

Omnimet Image Analyzer

A Bausch and Lomb Omnimet Image Analyzer attached to a Nikon Microscope was used to determine particle size and count. A 40x objective lens with a 10x ocular were used which provided 400x magnification. A grided Brightline Hemacytometer was used as a sample holder on the microscope stage. The image analyzer provided a black and white screen image of the samples to provide easy viewing. The Image Analyzer provided computerized results of both particle size and count for each sample.

Experimental Procedures

Media Characteristics

Sieve Analysis. To determine the grain size distribution of the glass bead media the procedure given as the standard method for sieve analysis of fine and coarse aggregates, AASHTO designation: T 27-77-I, was followed [7].

A representative sample of glass beads was obtained in the following manner. A large quantity of the glass beads (25-lb of the manufacturer's 50-lb sack) was mixed well. Approximately 1000-grams of beads were removed using a 100-ml beaker as a scoop. The beads were dried at 100°C in a drying oven and cooled in a desiccator. Cooled glass beads totaling 440.35-grams were weighed for sieving.

The dried and cooled sample of glass beads was placed in the nest of sieves. The sieves were mechanically shaken using a Tyler Ro-Tap Testing Sieve Shaker for a five minute interval. The weight retained on each sieve as well as that collected in the (terminal) pan was determined using a top-loading Metler balance accurate to ±0.05-grams.

Specific Gravity. The specific gravity of the glass beads was determined using a 500-ml volumetric flask and a small sample of glass beads. The specific gravity test followed the AASHTO T 100-74 test procedure [7]. Three samples of glass beads, along with three

flasks were dried, cooled in a desiccator, and weighed. Then each sample of media, 114.80-g, 117.20-g, and 116.51-g, was poured into a flask. For comparison, the flask plus sample weights were also determined. If these measurements varied by more than the accuracy of the scale a new sample was prepared.

Enough deionized water was poured onto the glass beads to cover them. Subsequently, in order to remove all of the air, the sample was heated and subjected to a vacuum. While still subjected to a vacuum, the slurry was mechanically stirred to further insure that all of the air would be removed. Water was added in 100-ml, 50-ml, and finally, 10-ml increments until the sample was saturated. Each addition of water was followed by heating and stirring under vacuum. Once the sample was saturated, it was cooled to room temperature prior to adjustment in 5.0-ml and 1.0-ml increments to the final 500-ml volume. The weight of the flask plus sample plus water was determined.

Next each of the sample flasks was filled to the 500-ml mark with deionized water. The water was allowed to stabilize to room temperature. The weight of the water plus the flask was then determined. The specific gravity of the media could then be calculated.

Porosity Determination. The porosity of the glass bead media was determined as the average of three measurements. The method used to determine porosity was similar to the specific gravity determination. In this instance, however, three samples of dried glass bead were measured using volumetric flasks, two 100-ml volumes and one 150-ml volume. Each sample volume was then placed in a dried 500-ml flask. The water required to fully saturate the beads was accurately measured using volumetric flasks and pipettes. Although each addition of water was followed by heating and stirring under a vacuum, the temperature of the sample was kept well below the boiling point of water in order to minimize evaporation. Once a final volume of 500-ml was reached, the porosity was calculated.

Friction Angle Determination. The cleaned and dried plexiglass friction angle box was levelled and completely filled with dried and cooled (to room temperature) glass beads. The beads were loosely packed into the box. The gate was removed without disturbing the media. The beads were allowed to spill into a plastic bucket. The resulting angle of inclination with the horizontal, ϕ, was characteristic of the failing plane of the media. The friction angle was measured as shown in Figure 10. This procedure was repeated three times. Each try resulted in a friction angle of 25.63°.

Filter Column Preparation

The filtration and subsequent backwash cycle behavior was directly dependent on the effectiveness of the column preparation. Any minor misbehavior of the filter bed during backwash, e.g., channelling, nullified the data obtained. The following procedure was developed and followed to prevent such frustrations:

The heat exchanger was turned on and brought to the operating temperature of 18.0 ± 0.5°C. To insure that the temperature in the heat exchanger would remain stable over the column preparation period, it was allowed to flow for a minimum of 45-minutes prior to column preparation. During this time, the temperature was closely monitored. Once operating temperature was established and stable for 15-minutes actual column preparation began.

The bottom portion of the column consisting of the inlet section plus one attached 30-inch length of pyrex tube was first anchored to the support frame. A check was made to assure that the section was on a vertical line.

Eight point six inches of dried and cooled media were poured into the column. Since the media was not easily wetted, it was necessary to force water into the voids between the media grains. If any air were allowed to remain in the system, i.e., prior to filtration in the void spaces, or as a result of leaks in the plumbing, channelling occurred.

While the bottom portion of the column remained open to the atmosphere, backwash water was pumped through the media at low subfluidization rates. The backwash water flow was set so that the flowmeter read in the 9 to 11 range, i.e., 3.3 to 4.5 gpm/ft^2. Dahab and Young [16] have shown in wastewater filtration studies that low subfluidization rates could be utilized to aid in forcing air out of the void spaces between the media grains.

The water was allowed to flow undisturbed until the media began to be lifted by the flowing water. At this point, a damper, a 35-inch length of 1.0-mm ID aluminum tubing with a loop fashioned on the end, was pushed down and through the glass beads. Damping was continued for as long as the filter bed was being pushed up the filter column by the backwash water. Subsequently, damping was discontinued, and water was allowed to fill the column undisturbed.

Once the water began to overflow the bottom section of the column the backwash water flow was temporarily increased to provide 50-percent expansion. The flow was estimated by observing the column. The flow was maintained near the point where the bed was expanded, but not fluidized, to a fourteen-inch depth. Actual fluidization was not possible until the bed was completely saturated. The media was mixed by passing the damper rapidly through the media several times. In this manner, more air bubbles were eliminated.

The backwash flowrate was reduced to a low subfluidization flow. The aluminum rod was removed. Backwash water was allowed to flow through the system and onto the floor for 10-minutes. The rod was passed through the media one more time, and removed.

With the water still flowing, the upper portion of the column was then joined to the lower portion. The nylon mesh baffle was inserted between the two sections of the column. To make this connection air tight, rubber o-rings were inserted on either side of the nylon mesh. Again, the column was checked to assure it was vertical.

The system was backwashed at the low subfluidization flows until the entire column was filled with water. Once full, the water was allowed to flow until 500-ml were collected at the backwash collection point. The water was then turned off. The column was allowed to stand overnight to insure that all of the void spaces became saturated.

The following day, and just prior to filtration, the heat exchanger was brought to operating temperature. The column was then backwashed at 30 percent expansion for 5-minutes. Backwash was stopped. The bed was allowed to compact slowly, i.e., the backwash water was turned off over a 15-second interval. The column was then ready for particle attachment.

Particle Preparation

The particles used in the detachment studies were uniformly distributed spheres one-micrometer in diameter. The alum sol suspension was prepared using the hydrothermal aging process developed by Brace and Matijevic [9]. To deionized water were added 1.898-g of Potassium Aluminum Sulfate for a total of 4000-ml in an Erlenmeyer flask. An inverted 250-ml beaker was placed over the opening of the flask to prevent contamination during aging and storage of the particles. (Aluminum foil was used temporarily, but it was found to contaminate the solution.) Contamination was defined as any substance which caused nonhomogeneous nucleation of the sol particles. The $KAlSO_4$ crystals were allowed to dissolve at room temperature. The solution was then aged in the drying oven at 98 ± 2°C for exactly 96-hours.

The alum sol suspension was removed from the oven and immediately stabilized with NaOH to a pH of 9.7. Figure 17 depicts an electron micrograph of the particles obtained from the aging process. Subsequently, the sol suspension was cooled to room temperature. The suspension was either used within 40-hours of completion of the aging period or discarded. The particles became irregular in shape if they were allowed to age at room temperature for longer periods.

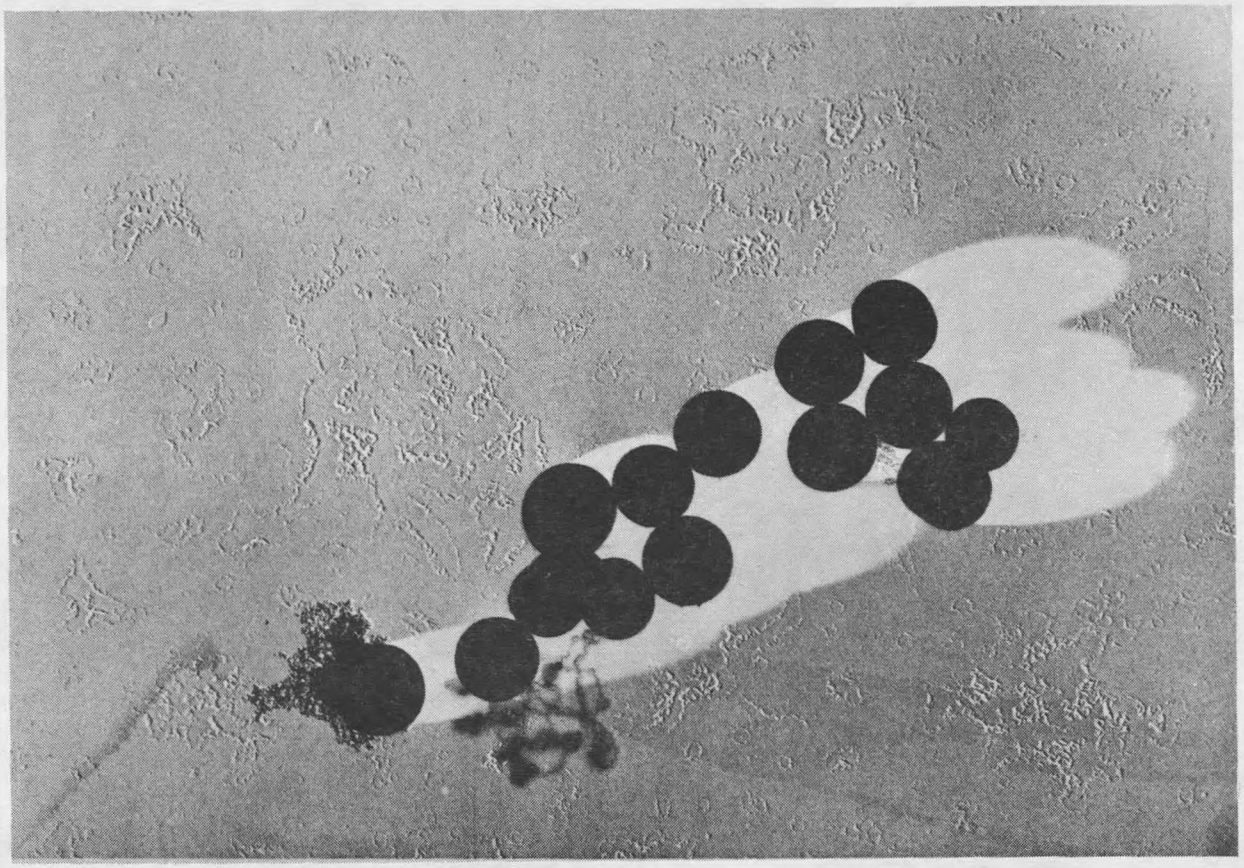

TEM OF ALUM SOL (X13,500)

Figure 17. Alum sol particles (from 29).

Just prior to filtration, the sol suspension was concentrated to a turbidity of 20 NTU. The suspension was concentrated by siphoning the supernatant until approximately 1500-ml of suspension remained in the flask. The siphoned supernatant was reserved and reintroduced to the suspension in the event that the turbidity was found to be greater than 20 NTU. The suspension was placed in a 2000-ml jar. The jar was placed on a magnetic stirring device. While the suspension was gently stirred, the pH was adjusted to 7.37 ± 0.02 using 0.10 Molar solutions of HNO_3 and NaOH. This pH provided an effective, i.e., diluted, filtration pH of 7.25 ± 0.05. A 250-ml volume of the suspension was reserved in order to determine the total dissolved solids of the filter suspension. One-liter of the suspension was then placed in a one-liter Erlenmeyer flask for filtration.

All potassium aluminum sulfate crystals used in the hydrothermal aging process were Baker reagent grade crystals. No further purification was done.

Total Dissolved Solids

The TDS of the filtered suspension as well as the TDS of the backwash water was determined by the following procedure: A 250-ml sample was allowed to stand undisturbed for 30 minutes. A Micro-Mho electrical conductivity meter was then rinsed twice with sample and a third volume was drawn into the bulb for measurement. The TDS was then calculated. The undiluted influent varied in TDS from 250 mg/l to 350 mg/l; the clean backwash water was maintained in a TDS range of 1-5 mg/l.

Filtration/Particle Attachment

A known quantity of particles in one-liter of alum sol suspension was attached onto the media grains during gravity filtration. In order to shorten run-time, the influent was filtered at a very high rate until the particles were within three inches of the top of the filter bed. The filtration rate was then reduced and maintained near 2.0 gpm/ft^2 until breakthrough, defined as a sharp jump in turbidity to a value greater than 0.40 NTU.

Subsequently, the filtration rate was allowed to decline until the effluent was characterized by a low and constant turbidity of 0.12 NTU. This point was defined as the state of maximum particle attachment for a filter run. Figures 18 and 19 show, respectively, an electron micrograph of a glass bead surface prior to particle attachment and after particle attachment.

Effluent turbidity was measured every five minutes during filtration. The filtered effluent was recycled manually, i.e., it was poured back into the one-liter reservoir by the operator until it was characterized by a low and constant turbidity (0.12 NTU).

Pressure Determinations

The pressure below the inlet was measured while the system was subjected at a constant air flowrate to various water flowrates. A closed end air/water manometer as shown in Figure 16 was used to measure the pressures. Each pressure reading was obtained by calculating the difference in water meniscus height measured in the two legs of the manometer. Under conditions of flowing water, the pressure fluctuated. The actual value of P_1 was chosen as the best observed average of the fluctuations in pressure. Independent pressure readings were also obtained using a mercury manometer. The closed end manometer was then calibrated against the mercury manometer. Figures 20 through 24 show plots of air pressure (gage) below the inlet versus water flowrate, V, at constant air flowrate, Q_a. Figure 25 shows the air pressure corresponding to the collapse-pulsing condition for each air flow.

Backwash/Particle Detachment

Particle detachment, i.e., backwash, was carried out using simultaneous air scour and subfluidization water flows. The water was turned on first. Deionized water was pumped into the column at flows from 20 to 225 percent of V_{mf} corresponding to 1.5 and 17.1 gpm/ft^2, respectively. A lag time of 10-seconds was experienced before the air was turned

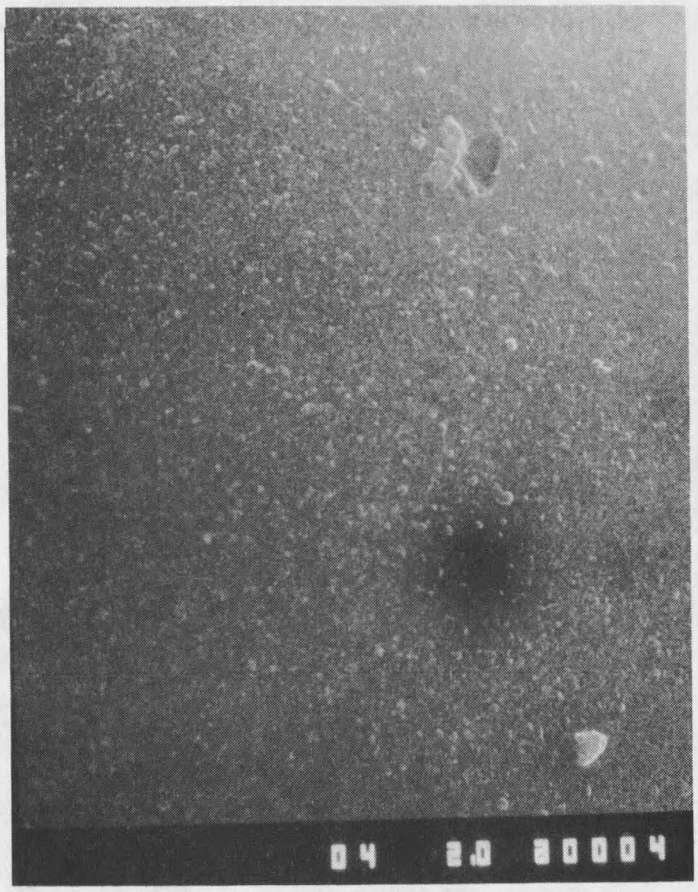

Figure 18. Glass bead surface prior to particle attachment (from 29).

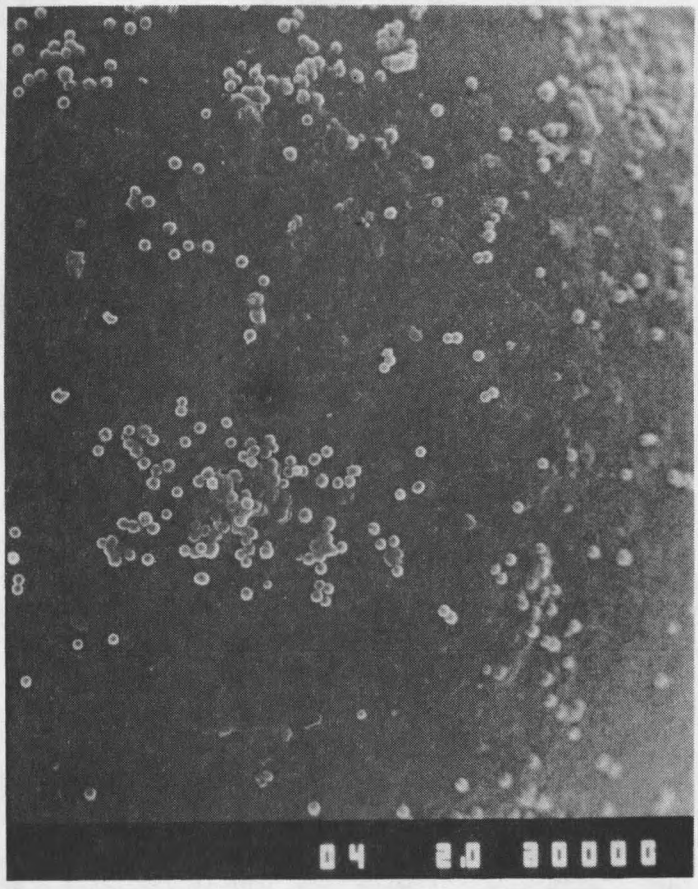

Figure 19. Glass bead surface after particle attachment (from 29).

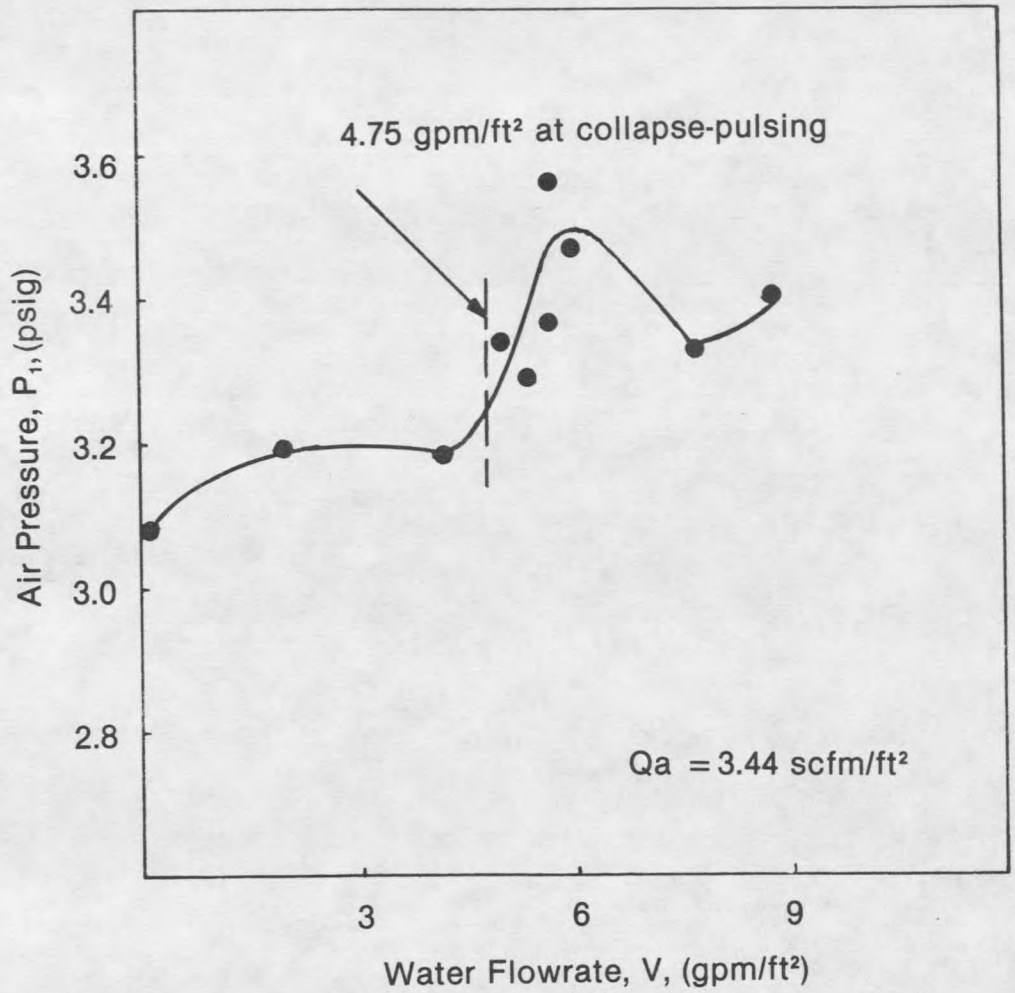

Figure 20. Air pressure below the inlet, 3.44 scfm/ft².

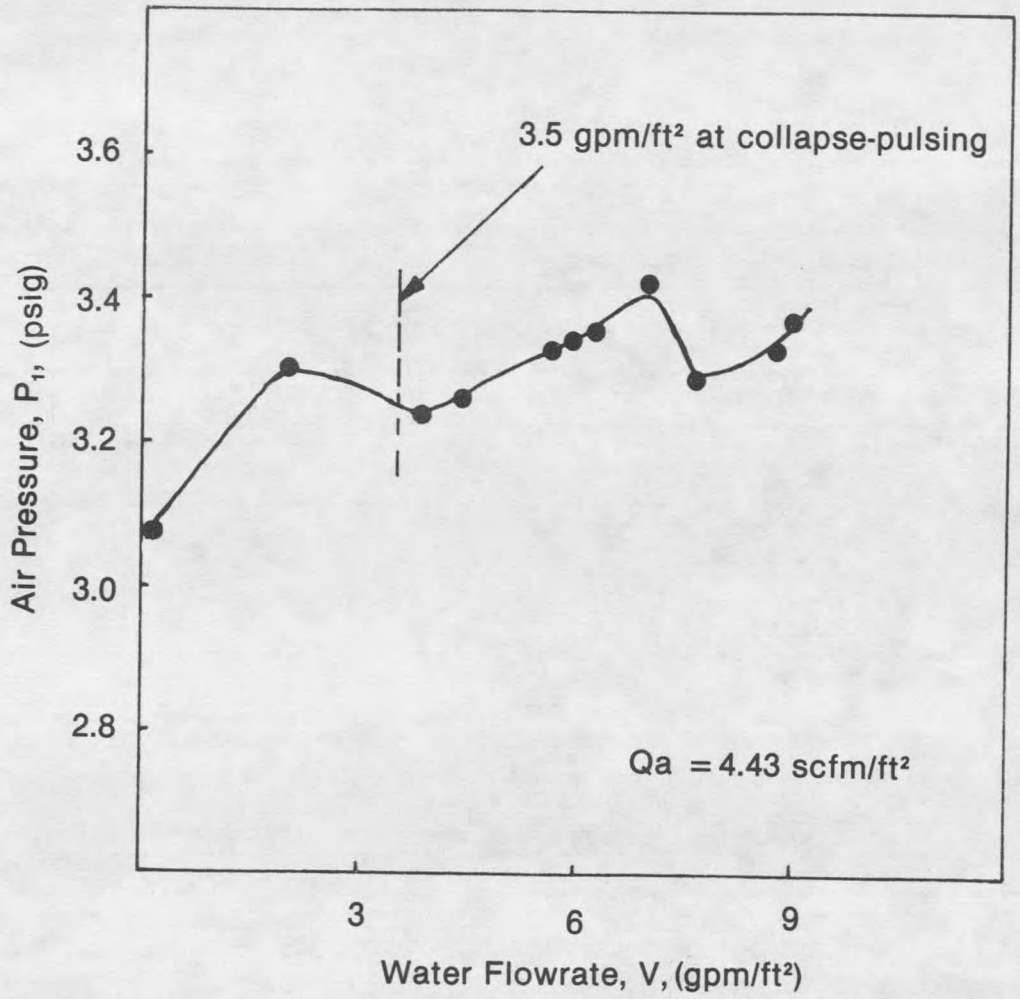

Figure 21. Air pressure below the inlet, 4.43 scfm/ft².

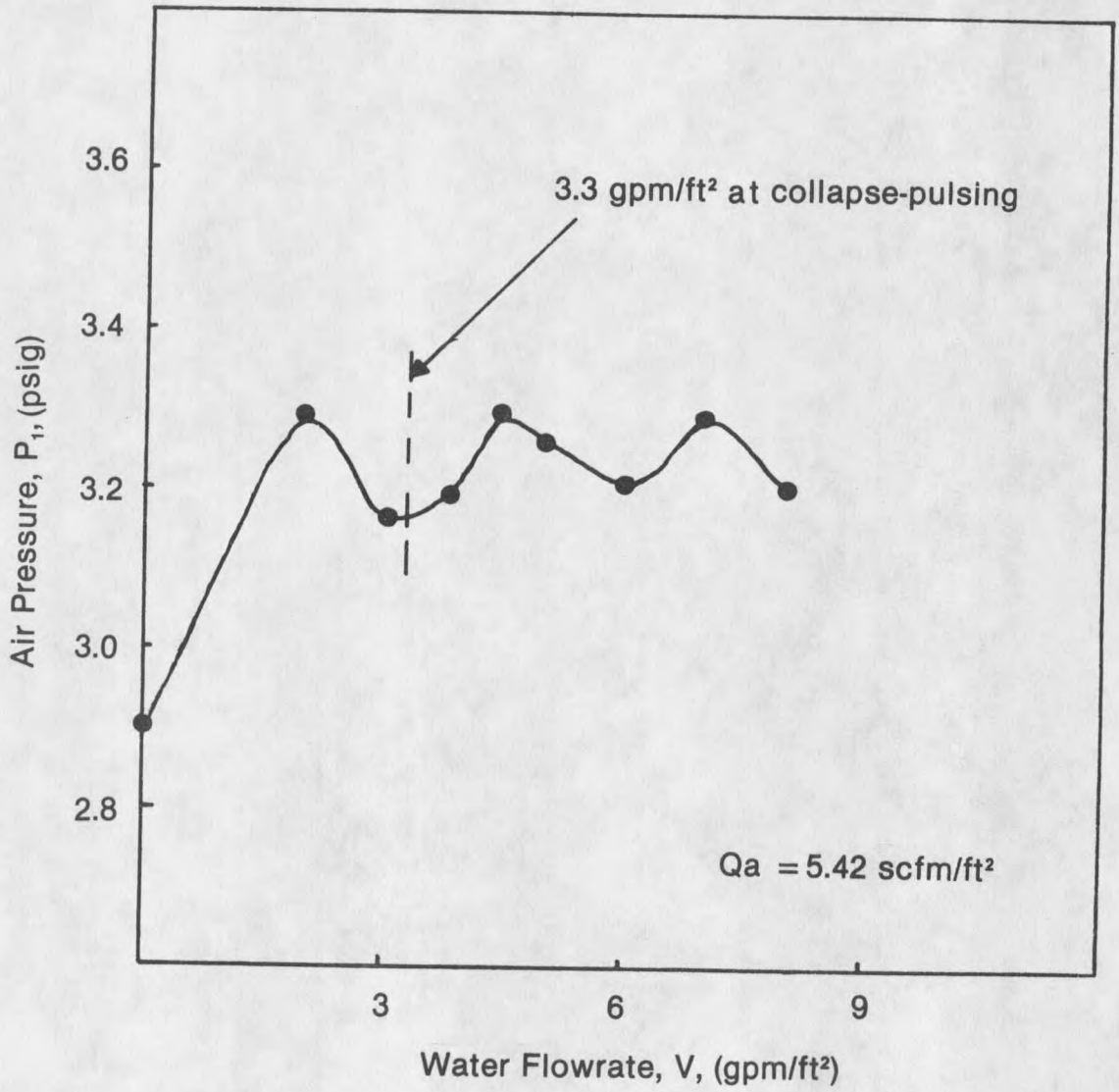

Figure 22. Air pressure below the inlet, 5.42 scfm/ft².

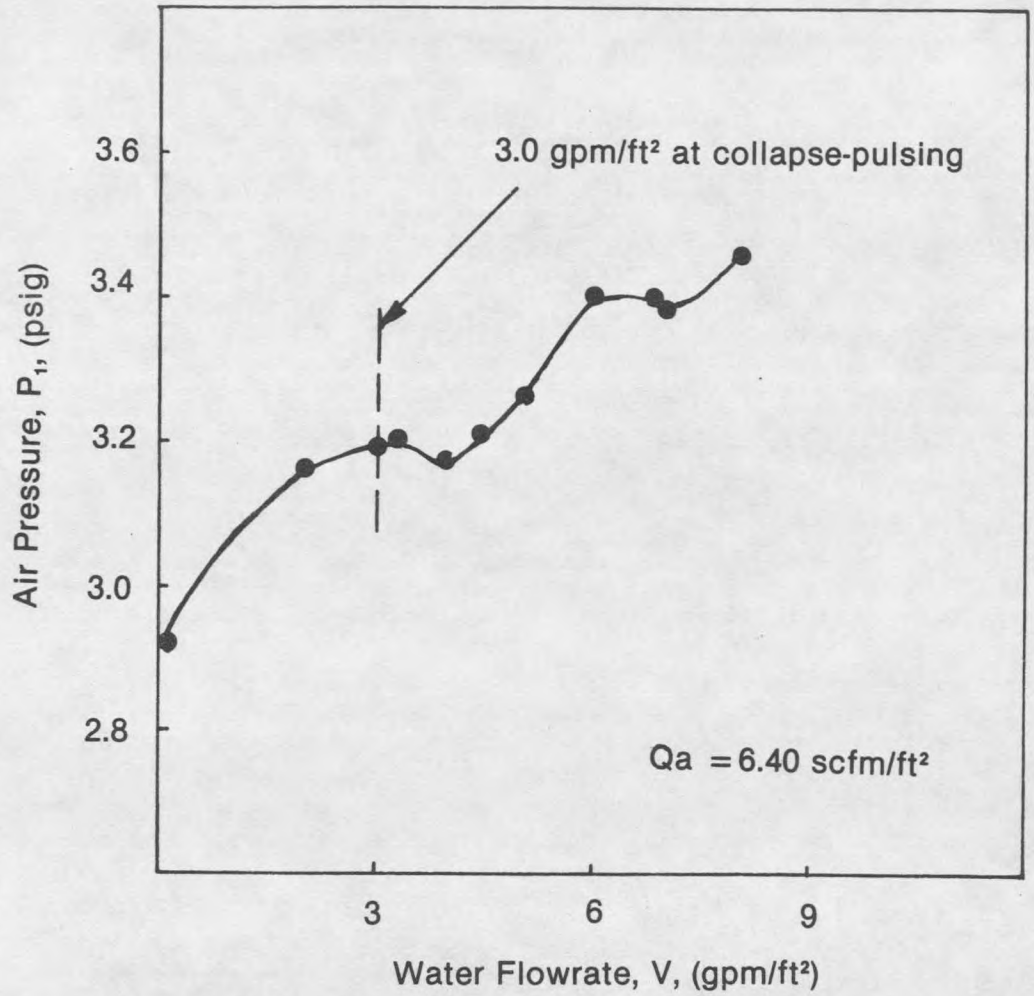

Figure 23. Air pressure below the inlet, 6.40 scfm/ft².

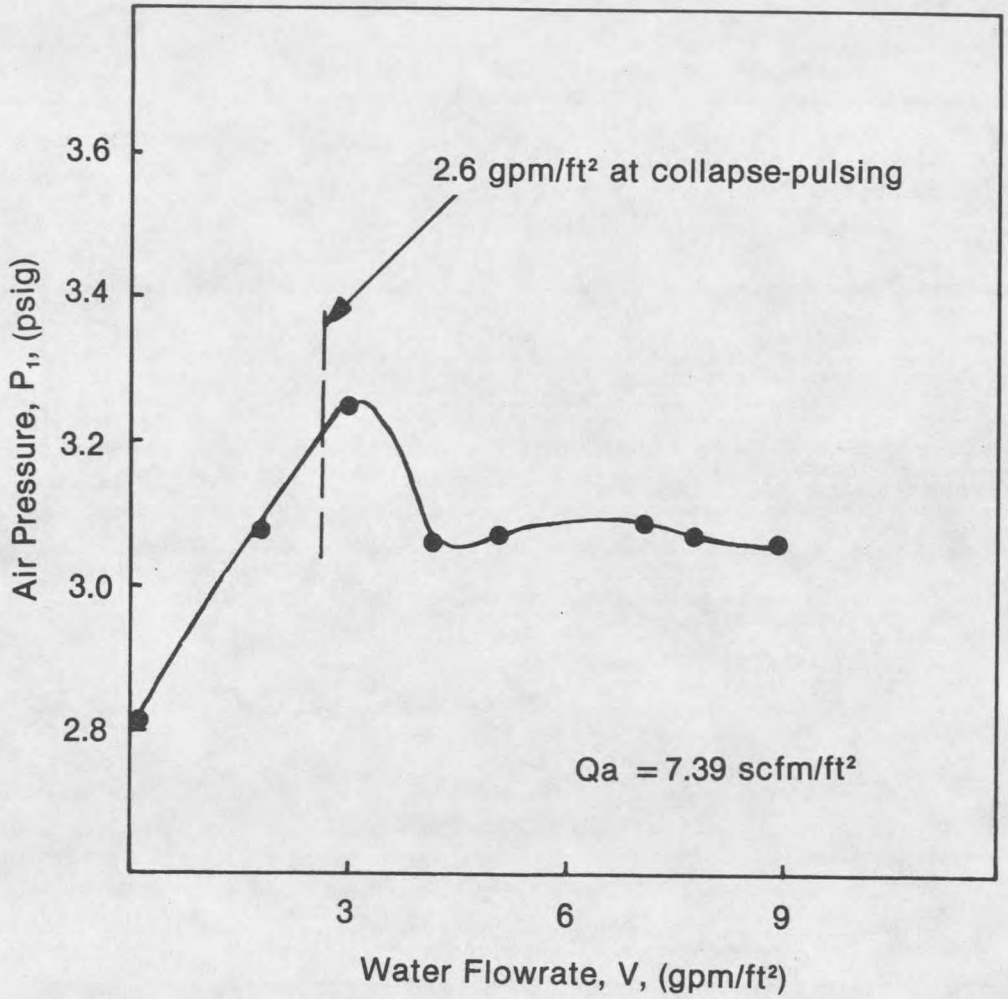

Figure 24. Air pressure below the inlet, 7.39 scfm/ft²

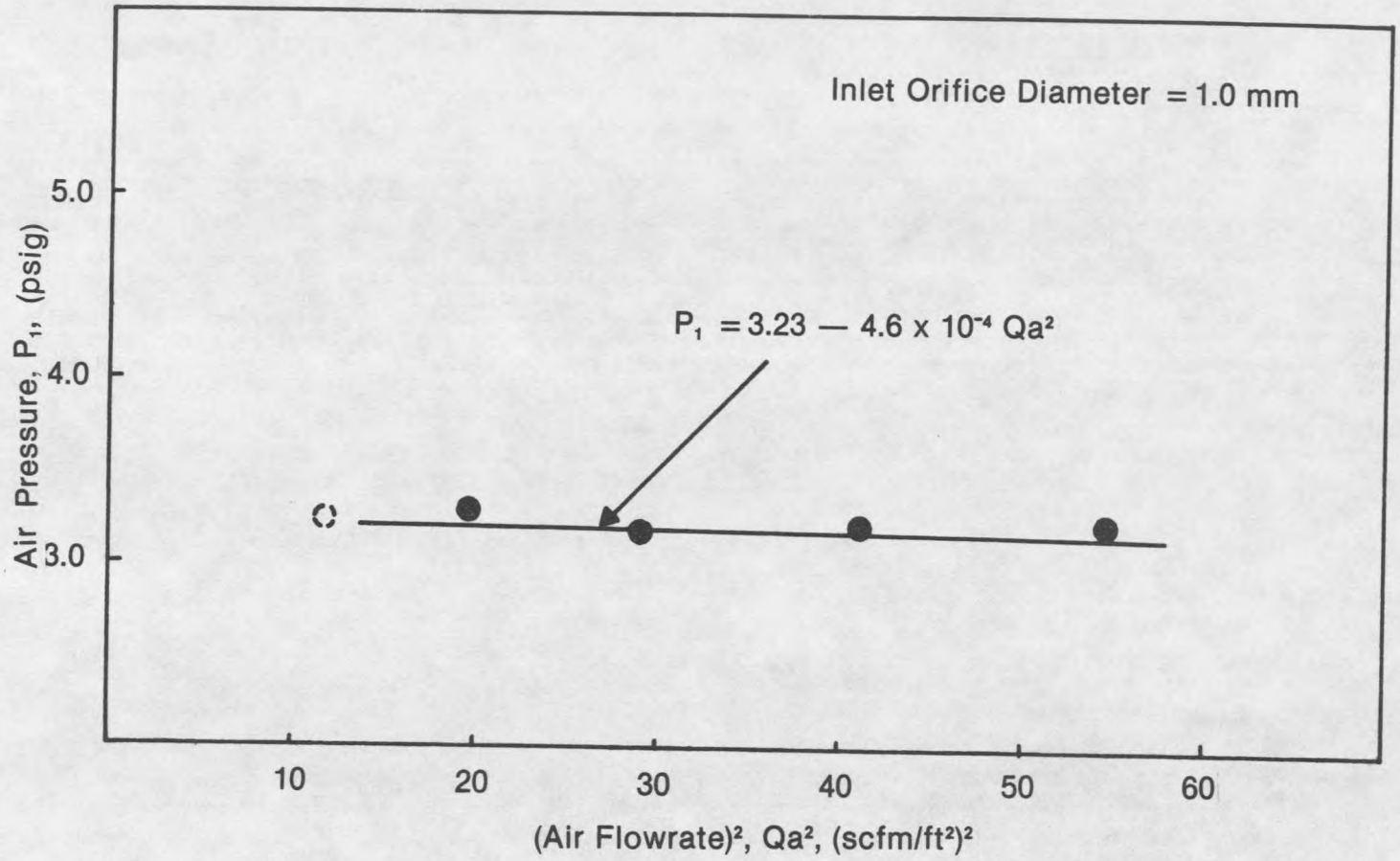

Figure 25. Air pressure at collapse-pulsing.

on. Air was fed into the center of the water path at flowrates of 3.44, 4.43, 5.42, 6.40, and 7.39 scfm/ft^2. Air scour plus subfluidization water flows were maintained for seven minutes. Subsequently, the air scour was turned off and the bed was fluidized for three minutes at 30 percent expansion with water alone. The provision for 30 percent expansion time would provide for restratification in a graded filter bed. The temperature of the backwash water was maintained at 20 ± 1°C.

The backwash water was collected and stored in Nalgene bottles for analysis. For the first seven minutes of backwash time each collected sample represented 15-seconds of backwash time. During the remainder of backwash, the samples represented one-minute of backwash time. The pH was maintained at 7.25 ± 0.05 during backwash. Figure 26 shows an electron micrograph of a media grain after particle detachment.

Particle Counting

The number of particles present in the sol suspension prior to filtration as well as the backwash remnants were counted using a Bausch and Lomb Omnimet Image Analyzer. A small volume of each suspension was obtained using an eye dropper. The sample was placed on a Brightline Hemacytometer and viewed using a Nikon microscope. Particles were sized and counted using the attached Image Analyzer.

A representative particle count was obtained by the following stepwise procedure:

a. The hemacytometer was soaked in warm sudsy water, rinsed with a stream of deionized water from a squirt bottle, and dried with cheesecloth to prevent any foreign matter from being retained in or around the etched grid counting surface.

b. The cover slip was soaked in dilute sulfuric acid in a 10-ml beaker. The sulfuric acid was discarded. While the cover slip remained in the beaker it was filled three times with deionized water. The water was discarded after each filling. The cover slip was then dried with a Kimwipe and placed over the grid surface of the hemacytometer.

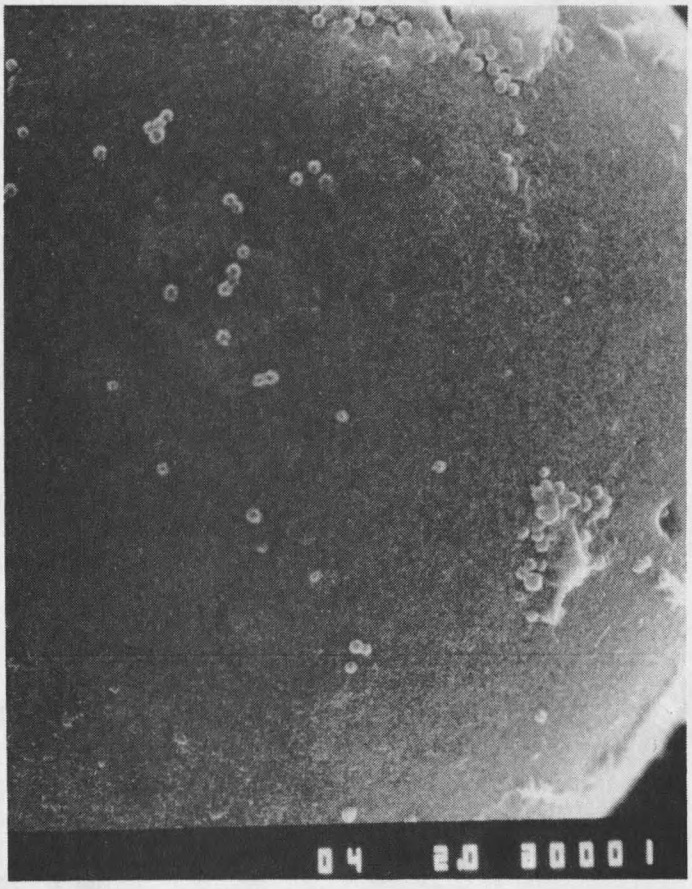

Figure 26. Glass bead after particle detachment (from 29).

c. The eye dropper was thoroughly rinsed with deionized water contained in a squirt bottle reservoir. A 15-ml stream of water was forced through the glass portion of the dropper from the squirt bottle.

d. The dropper was shaken to remove excess water.

e. The sample suspension was inverted five times. Three draws of sample suspension were taken into the dropper and wasted. The dropper was then half filled with sample.

f. One drop of suspension was placed on each side of the Brightline Hemacytometer adjacent to the edge of the cover slip. The sample was drawn under the cover slip by capillary action.

g. The borders of the Variframe of the Image Analyzer were set to correspond to an area of 2.50×10^{-3}-mm^2 on the Brightline Hemacytometer grid. Five such areas were counted randomly over the hemacytometer grid for each sample. The actual particle concentration was calculated as the arithmetic average of the five sample areas.

Serial Dilution

A linear relationship was established between turbidity and particle concentration to facilitate easy data collection. Four serial dilutions were performed. Each sample was prepared in a manner similar to the preparation of the filtration sample. The 4000-ml hydrothermally aged volume was drawn down to a point where the turbidity was equal to 20-NTU. The pH was then adjusted to 7.35 ± 0.01 using 0.10-M solutions of sodium hydroxide and nitric acid.

Four ranges of particle concentrations were studied: 2.7-26 NTU, 3.0-27 NTU, 4.5-19.5 NTU, and 7.2-17 NTU. In the first two ranges the suspensions were further concentrated by siphoning the supernatant to 26 NTU and 27 NTU; in the latter two cases the suspensions were diluted to 19.5 NTU and 17 NTU by adding deionized water. Each sample was then serially diluted as follows:

a. 500-ml of the suspension was placed in a volumetric flask.

b. 50-ml of the suspension was removed by volumetric pipette and placed in a 100-ml Nalgene container. The turbidity of the 50-ml sample was obtained. The sample was retained for particle counting.

c. The 500-ml flask was refilled to the mark on the flask with deionized water. The flask was covered and inverted five times.

d. The procedure was repeated from b until ten samples were obtained for particle counting. The number of particles in each sample were subsequently determined using the procedure in the section entitled Particle Counting.

The graph in Figure 27 shows the data obtained from the serial dilutions plotted as particle concentration (# particles per ml) $\times 10^7$, versus turbidity, NTU's. The plot does not pass through zero due to the instrument correction imposed on the particle counts by the Image Analyzer.

Volume/Turbidity Determinations

Following backwash, the volume and turbidity of each sample were determined. All volumes were measured using volumetric glassware and graduated cylinders.

The turbidity of each sample was determined using a Hach 2100 Turbidimeter. The turbidimeter was standardized prior to each reading. Sample turbidities were acceptable only in the range of the data points obtained in Figure 27. If the turbidity exceeded the plotted maximum, then the sample was diluted 3:1, i.e., three parts sample to one part water for a total volume of 40-ml. If the measured turbidity still exceeded the upper limit, another 3:1 dilution was performed.

Electrophoretic Mobility Determination

The electrophoretic mobility of the particles collected during backwash was measured using a Zeta Meter and found to be $+ 1.1 \pm 0.5$-μm/sec/volt $\cdot$ cm.

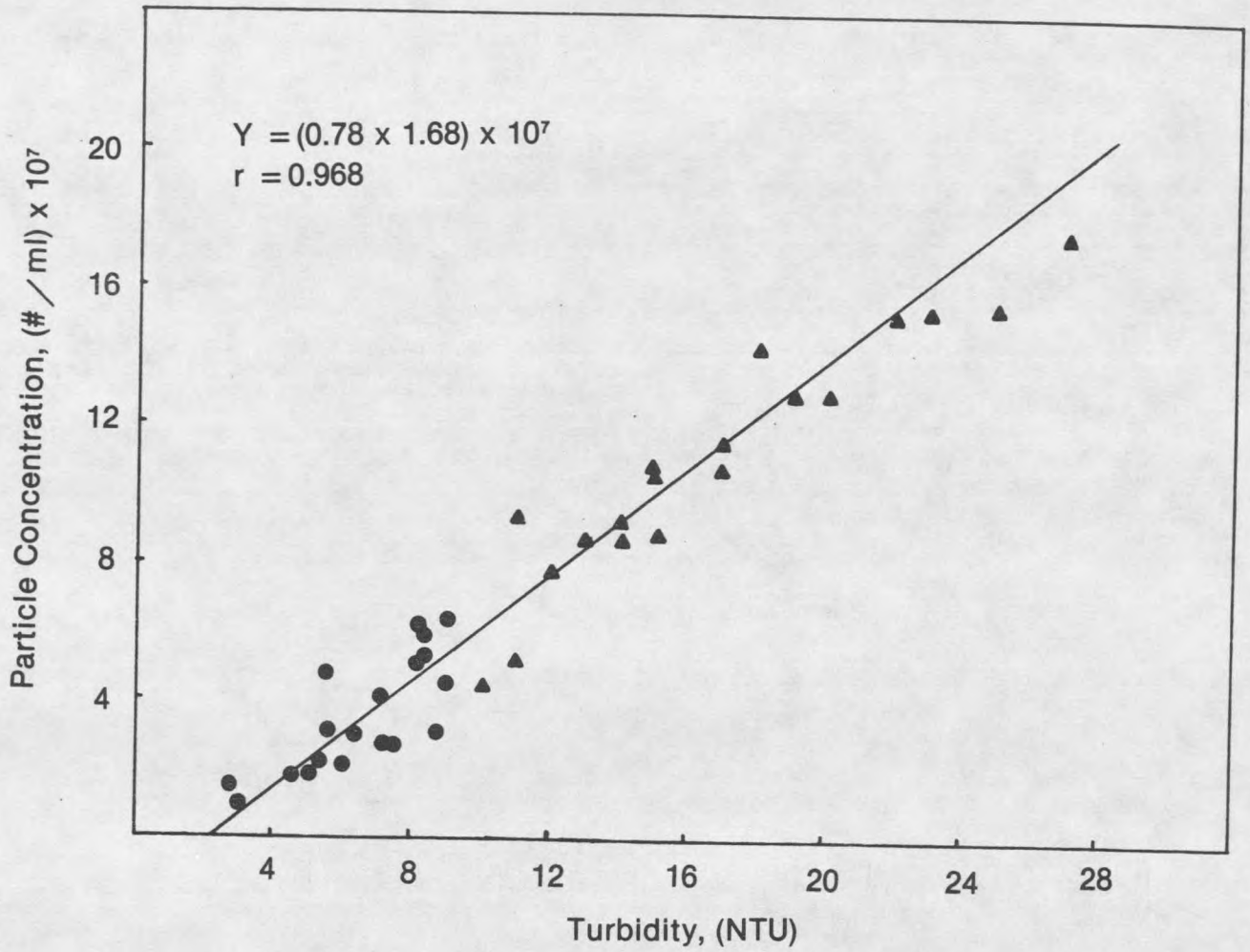

Figure 27. Particle concentration versus turbidity relationship.

Cleaning Glassware

All glassware and pyrex column sections were detergent washed and dried followed by acid washing and drying prior to each use. The Nalgene containers were detergent washed and dried prior to each use and acid washed and dried every second use.

Sample Calculations

Media Characteristics

Sieve Analysis. The results of the sieve analysis are shown in tabular form in Table 2. The tabular results were subsequently plotted on log-probability paper in Figure 28. d_{10}, d_{60} and d_{90} sizes were obtained from the graph. d_{10} is equal to 0.465-mm. d_{60} is equal to 0.635-mm. d_{90} is equal to 0.78-mm. These sizes are marked on the graph.

Table 2. Sieve Analysis of Glass Bead Media.

Sieve #	Diameter Opening (mm)	Mass Retained (gm)	Percent Retained %	Cumulative Percent Retained %	Cumulative Percent Passing %
16	1.18	0	0	0	100
30	0.60	214.95	48.81	48.81	51.19
40	0.425	205.90	46.76	95.57	4.43
50	0.300	18.95	4.30	99.87	0.13
pan		0.55	0.12	99.99	0.01
	total	440.35-gm			

The uniformity coefficient of the media is obtained by:

$$U.C. = \frac{d_{60}}{d_{10}} = 1.37 \qquad (15)$$

Specific Gravity. The specific gravity of the sample was determined at 22°C. The mass of flask plus water, i.e., no sample present, was determined at 23°C. To calculate the mass of the flask plus the water at 22°C the following general equation is applied:

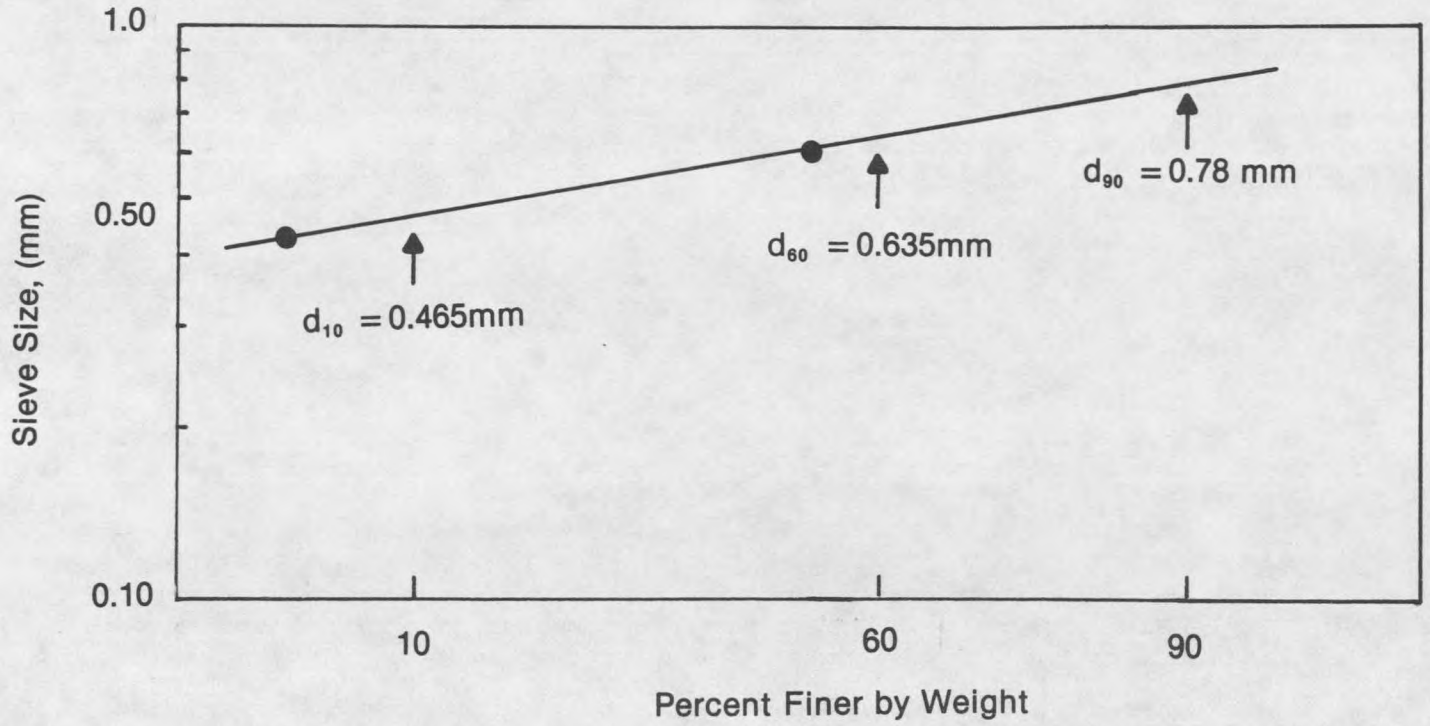

Figure 28. Log-probability plot from sieve analysis.

$$Wa_i = \frac{\rho_{wi}}{\rho_{wx}} \times (Wa_x) \qquad (16)$$

where:

i =	sample temperature	22°C
x =	flask + water temperature	23°C
ρ_{wi} =	water density at i	0.9978 g/cc
ρ_{wx} =	water density at x	0.9976 g/cc
Wa_x =	mass of flask + water at x	696.45 g

therefore:

Wa_i = mass of flask + water at i

$$Wai = \frac{0.9978 g/cc}{0.9976 g/cc} \times (696.45 g) = 696.61 \text{ g}$$

To determine the specific gravity of the glass beads at the sample temperature of 22°C the following general equation was applied:

$$Sg_i = \frac{Ws}{Ws + (Wa_i - Wb)} \qquad (17)$$

where:

Ws =	mass of sample	114.80 g
Wb =	mass of flask + water + sample	765.42 g

therefore:

$$Sg_i = \frac{114.80 g}{114.80 g + (696.61 - 765.42 g)} = 2.50$$

In order to adjust the specific gravity to the operating temperature of 20°C it is necessary to multiply the specific gravity at 22°C by a relative density conversion factor as follows:

$$Sg_{20} = K \times Sg_i \qquad (18)$$

where:

$$K = \frac{\rho_{wi}}{\rho_{w20}} = 0.9996$$

therefore, the specific gravity of the media under operating conditions at 20°C was found to be:

$$Sg_{20} = 0.9996(2.50) = 2.50$$

Three specific gravity calculations were performed similarly. The specific gravity obtained from each calculation was 2.50.

Porosity. The static bed porosity was calculated using the following collected data:

	Sample A	Sample B	Sample C
1. dry sand volume (ml)	100	100	150
2. water volume (ml)	436.95	441.15	408.70
3. sand + water volume (ml)	498	498	498

The sample porosity, ϵ, was calculated by the following general formula:

$$\epsilon = \frac{Vol_2 - [Vol_3 - Vol_1]}{Vol_1} \qquad (19)$$

4. ϵ	0.39	0.43	0.40

The porosity of the media was calculated as an average of the three values obtained above.

$$\epsilon_o = \frac{\Sigma\epsilon}{3} = \frac{1.22}{3} = 0.41$$

The static bed porosity, 0.41, was used in all of the experimental calculations.

Friction Angle. The friction angle was calculated as the angle of inclination to the horizontal which was present after the media was allowed to flow undisturbed from the friction angle box. The friction angle, ϕ, which resulted after each of three tries was 25.63°. The calculation were performed as follows:

$$\tan \phi = \frac{4.50 \text{ inches}}{9.38 \text{ inches}}$$

$$\phi = 25.63°$$

Minimum Fluidization Velocity

The minimum fluidization velocity, V_{mf}, was calculated using two methods:

Leva Method. Leva [26] devised a calculation procedure to determine the required minimum fluidization velocity in a granular filter bed. In this instance the 90 percent finer size of the media was used in the calculation of V_{mf} by Leva's method. The reasoning for the d_{90} substitution into the Leva equation is given in the chapter entitled Results and Discussion. The modified version of the Leva equation is given by the following empirical, nonhomogeneous equation:

$$V_{mf} = \frac{0.00381 (d_{90})^{1.82} \gamma_w (\gamma_d - \gamma_w)^{0.94}}{\mu^{0.88}} \qquad (20)$$

where:

d_{90} = 90% finer size of the media 0.78 mm

at 20°C:

γ_w = unit weight of water 62.29 lb/ft^3

γ_d = unit weight of dry media 155.73 lb/ft^3

μ = viscosity of water 1.002 cp

When all of the above values are inserted into Leva's equation:

$$V_{mf} = \frac{0.00381 (0.78)^{1.82} [62.29(155.73 - 62.29)]^{0.94}}{(1.002)^{0.88}}$$

the V_{mf} value calculated with d_{90} media size was 8.37 gpm/ft^2.

Wen and Yu Method. In order to determine the V_{mf} by the Wen and Yu [12,30] method two dimensionless constants were first calculated, the Reynolds number and the Galileo number. The Galileo number was calculated by:

$$Ga = \frac{(d_{90})^3 \rho_w (\rho_d - \rho_w) g}{\mu^2} \quad (21)$$

where:

d_{90} = 90% finer size of the media 0.078 cm

at 20°C:

ρ_w = density of water 0.9982 g/cc

ρ_d = density of glass beads, dry 2.50 g/cc

g = acceleration due to gravity 981 cm/sec²

μ = viscosity of water 0.01002 g/sec·cm

therefore:

$$Ga = \frac{(0.078)^3 (0.9982)(2.50 - 0.9982)(981)}{(0.01002)^2}$$

$$Ga = 6951.07$$

The Reynolds number at minimum fluidization velocity, Rmf, was then calculated by substituting the Galileo number into the following equation:

$$Rmf = [(33.7)^2 + 0.0408\, Ga]^{0.5} - 33.7 \quad (22)$$

$$Rmf = 3.97$$

At V_{mf} the Reynolds number can be related to the minimum fluidization velocity by:

$$Rmf = \frac{d_{90}\, V_{mf}\, (\rho_w)}{\mu} \quad (23)$$

Rearranging, V_{mf} is calculated by:

$$V_{mf} = \frac{\mu\, Rmf}{d_{90}\, (\rho_w)}$$

therefore:

$$V_{mf} = \frac{(0.01002)(3.97)}{(0.078)(0.9982)}$$

The V_{mf} calculated by the Wen and Yu method was 7.53 gpm/ft^2.

Pressure Below Air Inlet Orifice

Initially, the right leg of the manometer shown in Figure 16 is open and allowed to equilibrate to atmospheric pressure. The data listed below were collected for the initial condition. Figure 16 shows the placement of the following measurements:

at 26°C:

The pressure at A, P_{A1}, is equal to the barometric pressure of the lab:

$$P_{A1} = 606.3 \text{ mm Hg} \times \frac{\text{inch}}{25.4 \text{ mm}} \times \frac{844.52 \text{ lb}}{\text{ft}^3} \times \frac{\text{ft}^3}{1728 \text{ in}^3}$$

P_{A1} = 11.67 psia

l_1 = length of the column of air in the closed end manometer under atmospheric pressure only

= 64.00 inches - 35.25 inches = 28.75 inches

Δy_1 = difference between the heights of water in the legs of the closed end manometer

= 35.25 inches - 33.15 inches = 2.1 inches

The pressure at B, P_{B1}, is calculated as:

$$P_{B1} = P_{A1} + \Delta y_1 (\gamma_w) \qquad (24)$$

where:

γ_w = 62.22 lb/ft^3

therefore:

$\Delta y_1 (\gamma_w)$ = 0.076 psig

and

$$P_{B1} = 11.67 + 0.076 = 11.75 \text{ psia}$$

The pressures obtained while the manometer was attached to the air inlet were obtained by applying Boyle's Law in the following manner:

$$P_{B1}(Vb + l_1) = P_{B2}(Vb + l_2) \quad (25)$$

where:

Vb = volume of the bulb used to close the manometer

= 94.0 ml

When the system is under pressure, the level of water in the left leg of the manometer is higher than that of the right leg of the manometer, therefore, the pressure which the air exerts on the water in the manometer or the pressure at the inlet orifice, P_{A2}, is the pressure at B, P_{B2}, plus Δy_2 times γ_w, for example:

l_2 = length of the column of air in the closed end manometer under pressure from the test column

= 9.20 inches

Δy_2 = 33.3 inches

with 5.74-mm ID manometer legs:

$$P_{A2} = 12.85 \text{ psi} + 1.20 \text{ psi} - 11.67 \text{ psi} = 2.38 \text{ psig}$$

All air inlet pressure calculations were performed similarly.

Mean Turbidity and Particle Concentration

All mean turbidity and particle concentration calculations were obtained via computer programs which can be seen in Appendix A.

CHAPTER 5

RESULTS AND DISCUSSION

Overview

The results of the pilot-scale investigation are presented in Figures 29 through 53. The experimental data were separated as a function of the applied air flowrate, i.e., Q_a is set constant. Five air flowrates were chosen for testing: 3.44, 4.43, 5.42, 6.40, and 7.39 scfm/ ft^2. At constant Q_a the water flowrate, V, varied during three-phase backwash, respectively: from 50.9 to 183.7, from 44.0 to 113.1, from 20.5 to 226.6, from 34.8 to 111.8, and from 24.8 to 114.6 percent of the calculated minimum fluidization velocity [12,32], V_{mf} equal to 7.53 gpm/ft^2. Following three-phase backwash, the two-phase, 30 percent expansion water flowrate was constant for all experimental runs.

The experimental results were graphically interpreted as a function of the number of particles detached during backwash. The parameter designated to represent the quantity of particles detached during backwash is either average or instantaneous turbidity. Average turbidity is a measure of the average backwash water quality over either a constant time or a constant volume. Alternately, instantaneous turbidity represents backwash water quality at a point in time. In both cases, the turbidity value given on the y-axis depended on the water flowrate supplied during three-phase backwash, V, given as the x-axis variable.

To prevent any bias in favor of the proposed theory which predicts Collapse-Pulsing [3] behavior, the simultaneous air/water flow combinations which provided optimum particle detachment were determined prior to any theoretical application. Subsequently,

these flow combinations were analyzed to determine whether Collapse-Pulsing behavior in the filter bed promoted optimum particle detachment from the media grains.

Experimental Results

A series of five graphs corresponds to each air flowrate. Eight, ten, sixteen, nine, and seven runs were performed at 3.44, 4.43, 5.42, 6.40, and 7.39 scfm/ft^2, respectively, for a total of fifty runs. Each experimental run is depicted as one data point per set of graphs. (An additional six runs were performed. They were not, however, included in the analysis since the bed displayed channelling during backwash due to either improper saturation of the filter bed or plumbing leaks.)

In order to verify that the described experimental method provided reliable results, the water flowrate, V, was extended over the wide range given for the constant air flowrate, Q_a equal to 5.42 scfm/ft^2. Figures 29 through 33 show the results of the 16 runs completed at this air flowrate. In Figures 29 through 32 a peak is evident at a water flowrate equal to 14.5 gpm/ft^2. This water flowrate corresponds to a calculated expanded bed porosity of 0.60, a value close to the optimum porosity range [2] 0.65-0.70 for fluidized beds. This phenomenon implies that the experimental method employed provided reliable results.

Test Case: Q_a equal 5.42 scfm/ft^2

Due to the bulk of the data, the results obtained at the air flowrate equal to 5.42 scfm/ft^2 will be presented as a test case to simplify interpretation of the results. This air flowrate was chosen as the test case for two reasons. It provided a wide range of data with respect to water flowrates. Additionally, the trends present in this set of data are characteristic of the balance of the data. Hence, the test case will be utilized: (1) to present the rationale by which each set of graphs was developed, (2) to distinguish the trends present

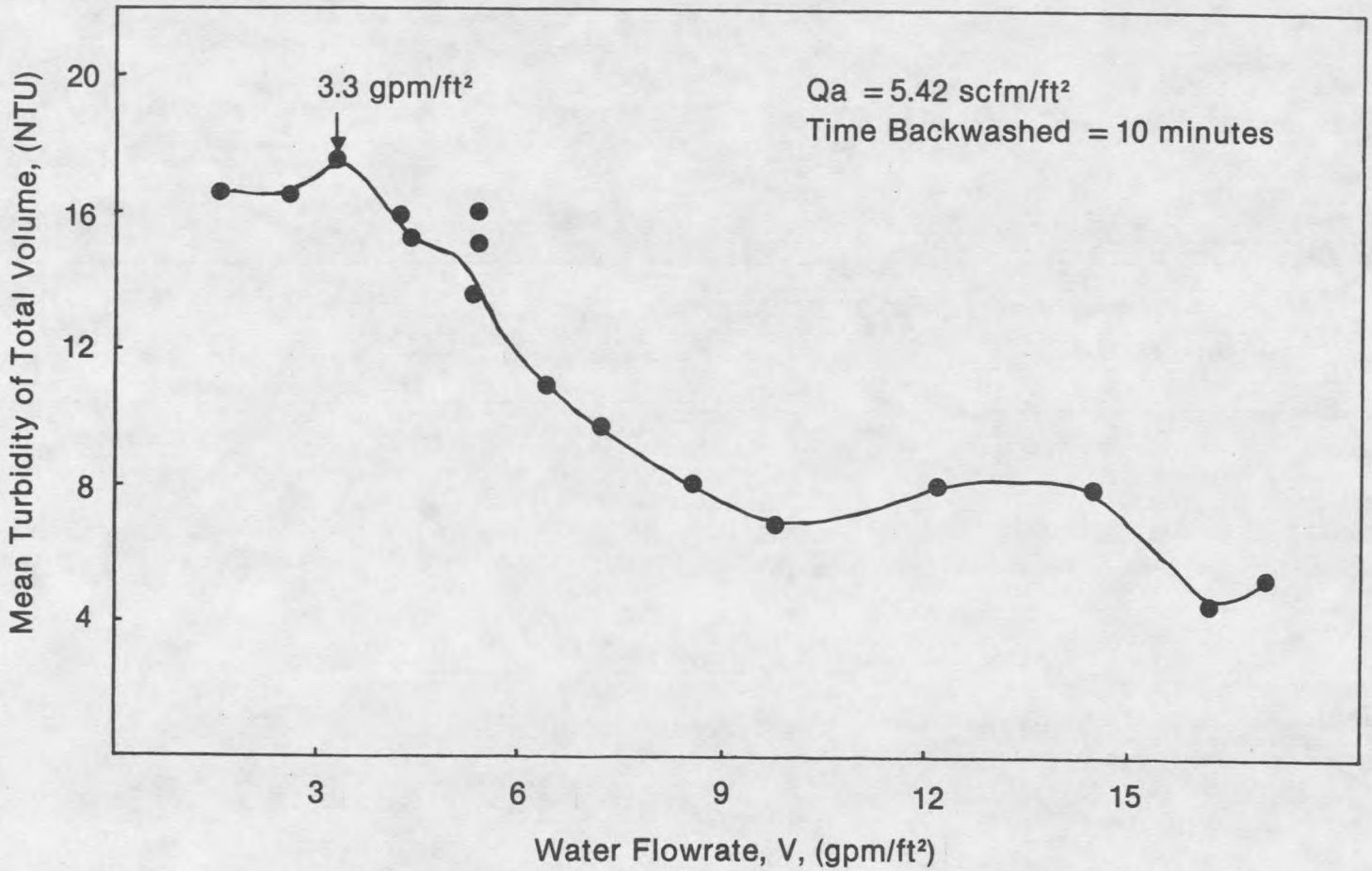

Figure 29. Average water quality, 5.42 scfm/ft² in 10 minutes.

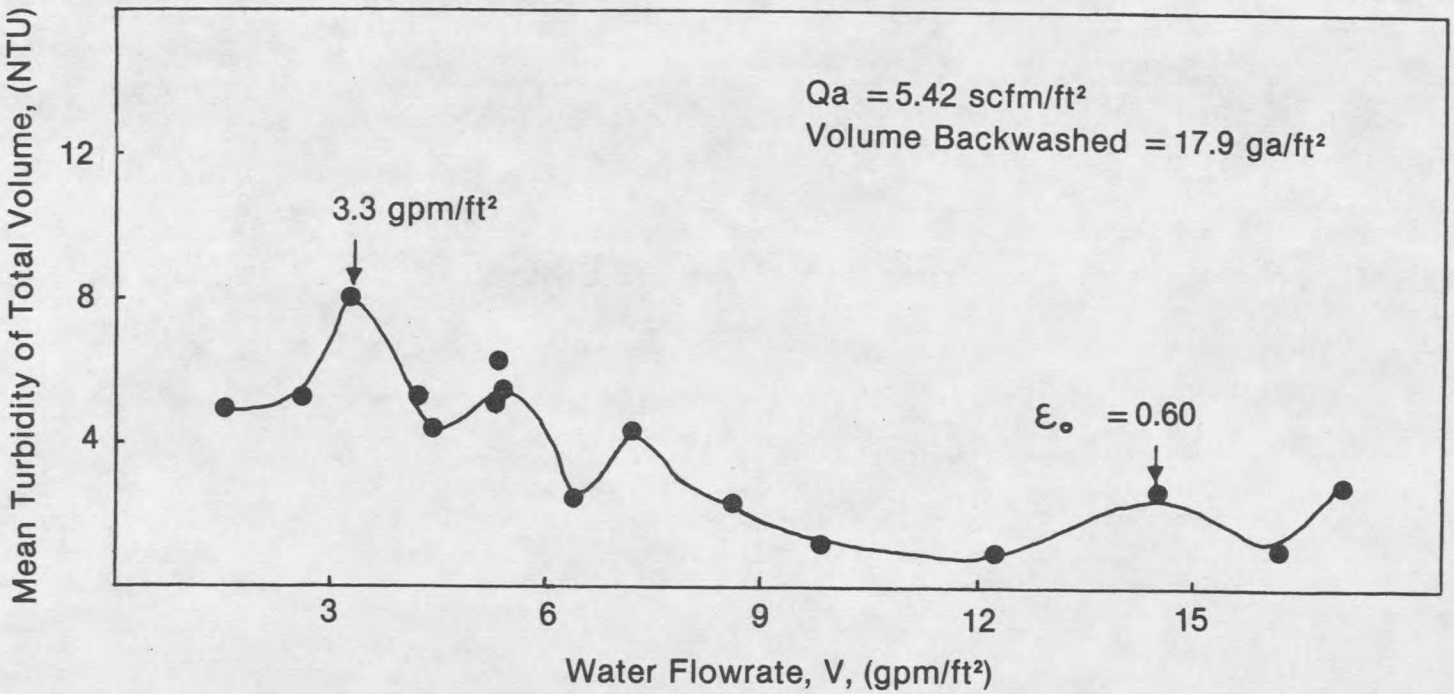

Figure 30. Average water quality, 5.42 scfm/ft² in 17.9 ga/ft².

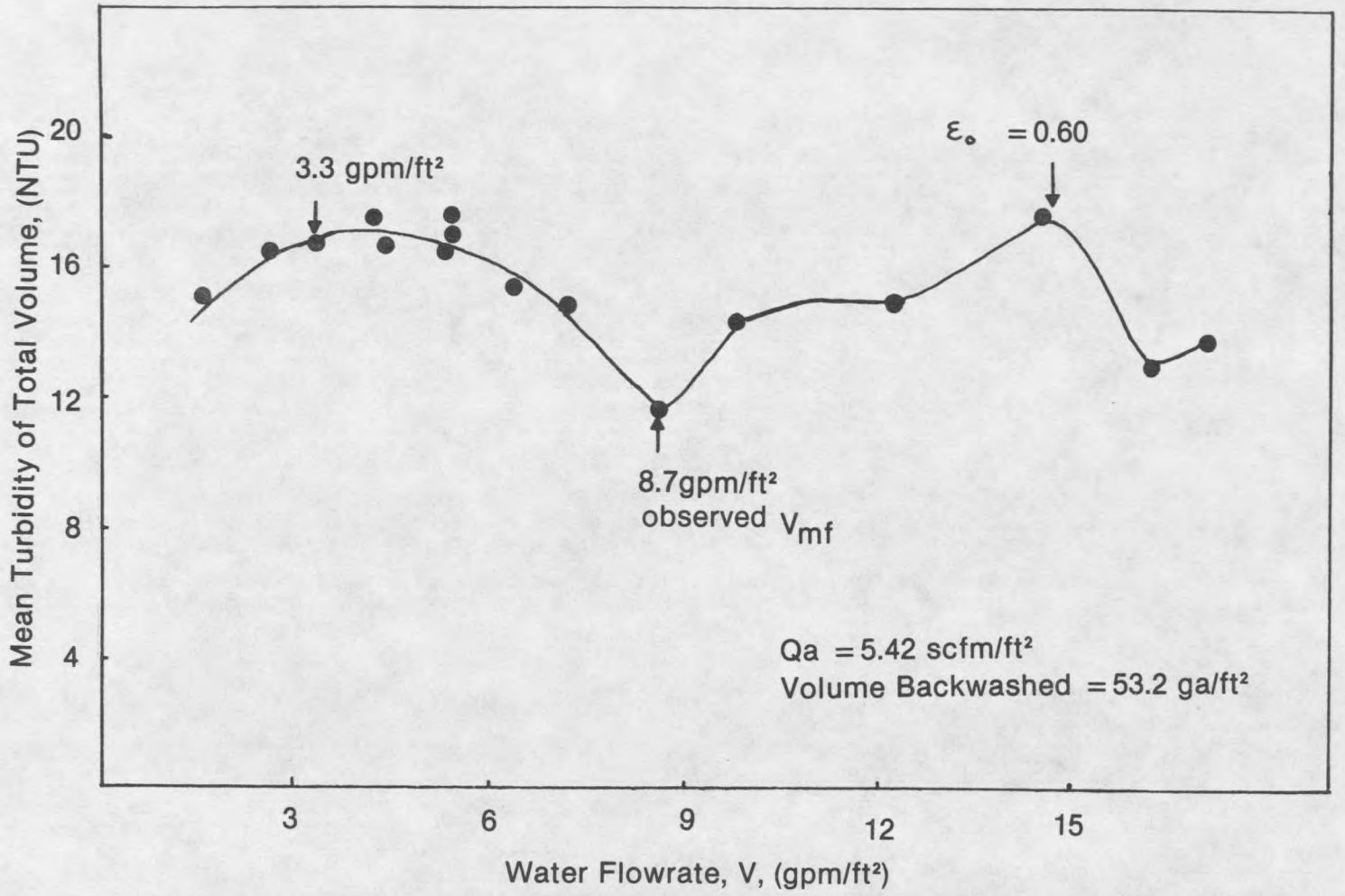

Figure 31. Average water quality, 5.42 scfm/ft² in 53.2 ga/ft².

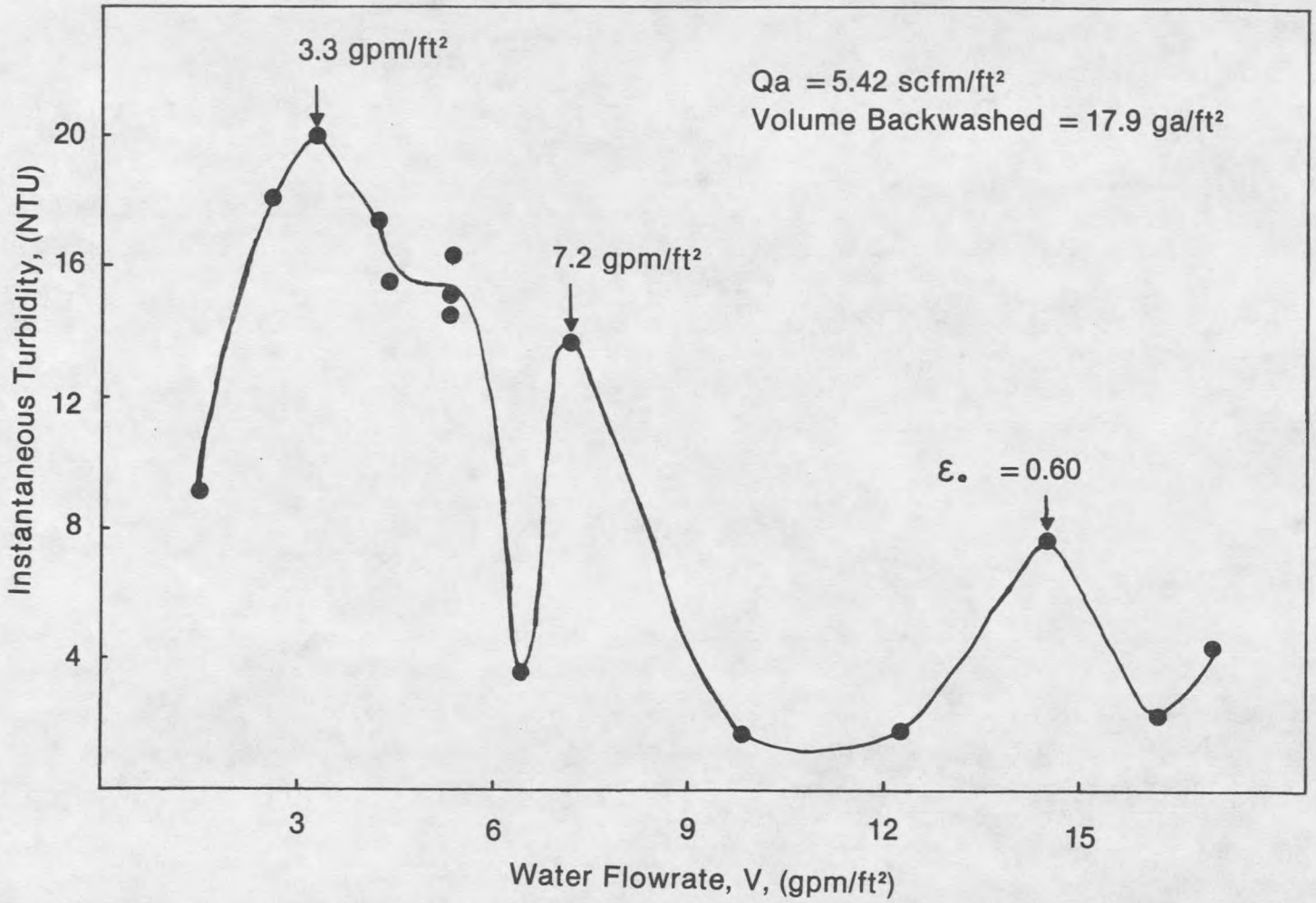

Figure 32. Instantaneous water quality, 5.42 scfm/ft² at 17.9 ga/ft².

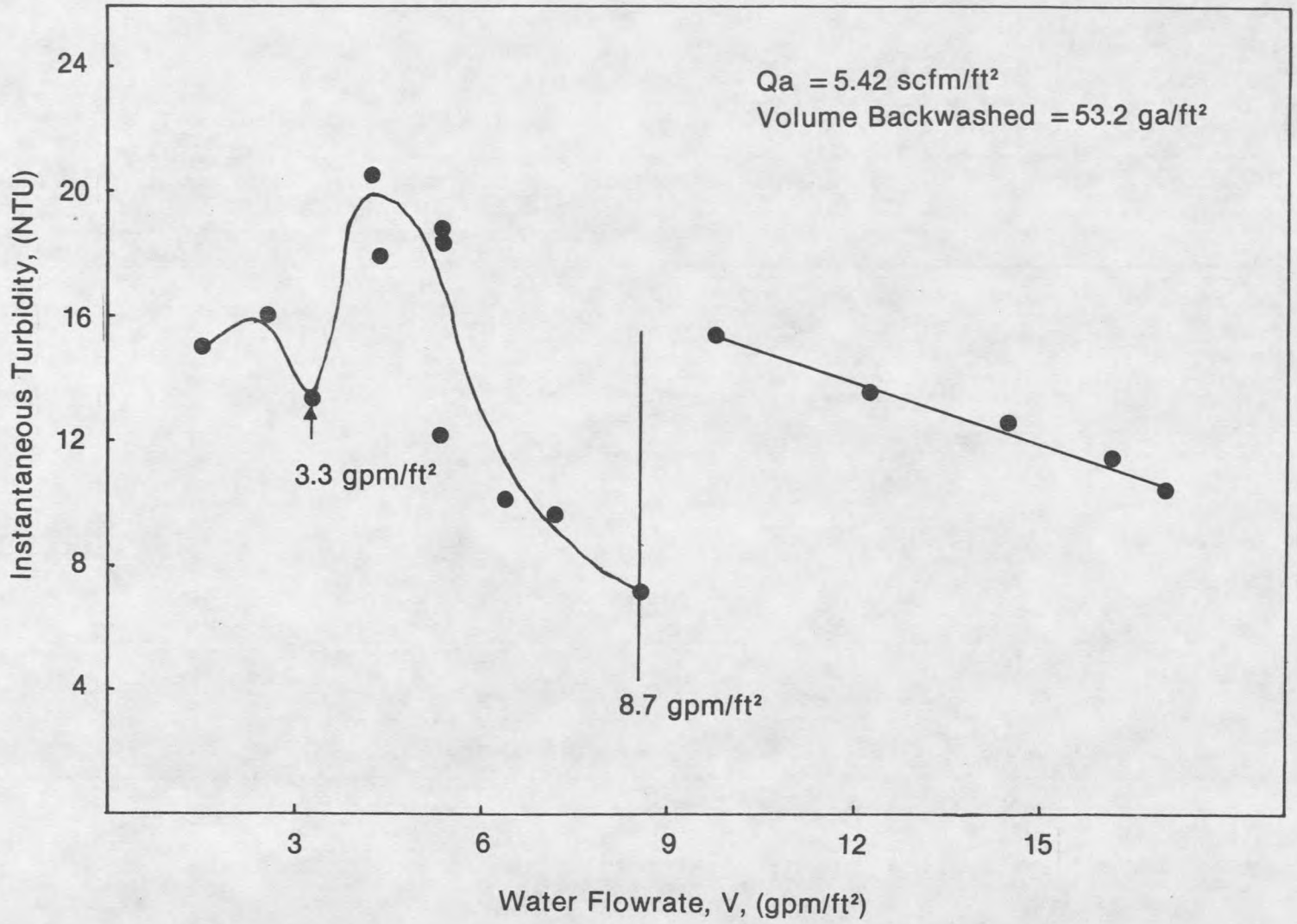

Figure 33. Instantaneous water quality, 5.42 scfm/ft² at 53.2 ga/ft².

in this set of data, and finally, (3) to describe the pattern used to determine the subfluidization water flow which provided optimum particle detachment at a particular air flowrate. Following the test case presentation, the remaining sets of data corresponding to air flowrates of 7.39, 6.40, 4.43, and 3.44 scfm/ft^2 will be presented individually. Each set of graphs will be accompanied by a synopsis of the data interpreted according to the methods outlined in the test case.

The data plotted in Figure 29 represents the mean quantity of particles detached over the total backwash water volume at constant time equal to 10 minutes. Although the plotted water flowrates represent the flowrates during simultaneous air/subfluidization water, three-phrase, backwash the 30 percent expansion water volume collected during two-phase fluidization is also included in these data. The total water volume corresponding to each data point, i.e., the volume for which each mean turbidity was calculated, varies by data point. The water volumes in Figure 29 range from 44.7 ga/ft^2 at V equal to 1.5 gpm/ft^2 to 171.5 ga/ft^2 at V equal to 17.1 gpm/ft^2. Optimum particle detachment was noted as the peak at water flowrate, V equal to 3.3 gpm/ft^2.

Although an optimum was detected in the constant time plot of Figure 29, it was necessary to determine the effect that adding the water collected during fluidization had on the position of the optimum. In addition, by convention [2,11,13,30,31], backwash is noted as a function of the water volume backwashed rather than as a function of time. Therefore, the results were plotted at two volumes, a volume collected early in backwash, 17.9 ga/ft^2, and a volume collected later in backwash, 53.2 ga/ft^2. The smaller volume represents the smallest volume obtained during three-phase backwash only. The larger volume represents the smallest volume of backwash water during two-phase backwash in addition to three-phase backwash.

Figure 30 represents the average turbidity, i.e., average particle detachment, in a volume of backwash water equal to 17.9 ga/ft^2. This plot of mean turbidity versus water flowrate displays the same peak as that evident in the constant time plot.

Figure 31 shows a plot of the average water quality at the larger volume, 53.2 ga/ft^2. This plot, however, would seem to indicate that particle detachment is most favorably obtained at a water flowrate greater than the 3.3 gpm/ft^2 previously noted in Figures 29 and 30. In fact, Figure 31 would seem to indicate that the conditions of air and water flow which provide optimum porosity where $V > V_{mf}$ also provides for optimum particle detachment. This phenomenon is a result of two factors: (1) the existence of an upper limit of particles available to detach during backwash and (2) the dilution effect.

The pilot-plant systems was designed to provide a mass balance on alum sol particles. A known quantity of particles was attached to the media grains during filtration. A one-liter solution with a measured 20-NTU turbidity contained 15.6×10^7 particles. The number of particles remaining in the influent after filtration plus the number attached to the nylon mesh were subtracted from the original influent solution to give the number of particles attached to the media grains. The maximum number of particles which could be detached was, therefore, limited by the number of particles collected by the grains.

As for the dilution phenomenon, consider that the flows below the observed V_{mf} value of 8.7 gpm/ft^2 resulted in small backwash volumes with high turbidity (particle concentration) during the simultaneous air scour and subfluidization water backwash time. When the balance, low turbidity, high volume expansion water was averaged with the subfluidization water, the result was to mask, by dilution, the peak which was evident in both the constant time graph as well as the 17.9 ga/ft^2 constant volume graph.

In order to assure the proper interpretation of the experimental data, instantaneous effluent quality was also plotted as a function of water flowrate at the two volumes, 17.9 ga/ft^2 and 53.2 ga/ft^2, for which the average turbidity was plotted. In this manner, the dilution effect was eliminated. Figures 32 and 33 represent the number of particles detaching from the media grains at 17.9 ga/ft^2 and 53.2 ga/ft^2, respectively.

Simply stated, the set of graphs represents particle removal at two points in the backwash cycle. Since the system was operated to provide a mass balance on alum sol particles, the instantaneous turbidity can be interpreted as either the number of particles removed from the grains or the number remaining on the grains at a particular point in time during backwash. When a large number of particles was removed early in backwash during the air plus subfluidization portion of the backwash cycle the first graph, Figure 32, shows a peak. Given a mass balance, the remainder of the backwash cycle could only provide lesser removal. Therefore, if a peak were evident in the first graph, a corresponding valley, or low removal is evident in its companion. As a set, then, the graphs acted as verification of each other for defining the optimum particle detachment flow combination. The optimum water flowrate at an air flowrate equal to 5.42 scfm/ft^2 was chosen as that water flowrate which provided the highest measured turbidity in Figure 32 which corresponded to a minimum measured turbidity in Figure 33. The water flowrate providing optimum particle detachment obtained by this method was 3.3 gpm/ft^2.

In addition to the optimum particle detachment peak, a lesser peak is also evident in Figure 32 at a 7.2 gpm/ft^2 water flowrate. This value corresponds to 83 percent of the observed V_{mf}. The data show a gradual decline in particle detachment from the optimum followed by this sharp peak. Two plausible explanations for the occurrence of this peak are: (1) a rearrangement of the smaller-sized grains may be taking place which causes collisions and subsequent detachment of particles or (2) it may be due to the slugging feature of the experimental system used.

Slugging occurs in granular media beds [17,24] with a high ratio of bed depth to bed diameter. The 9.4:1 ratio is much higher than values suggested by Davidson [17] and Kehoe [24]. Slugging was observed in the experimental setup, but the effect can be considered constant for the system.

The plot in Figure 33 exhibits a discontinuity at the observed value of V_{mf}. Possibly this discontinuity is an indication of the two separate removal mechanisms: (1) at $V < V_{mf}$ in a three-phase system the grains collide to promote particle detachment by abrasion mechanisms, and (2) at $V > V_{mf}$ in a three-phase system the grains are no longer in contact and removal is a result of hydrodynamic shear mechanisms similar to a particulate fluidized bed.

The remaining data were interpreted in a manner similar to that used for the results obtained at Q_a equal to 5.42 scfm/ft^2. The data corresponding to the remaining air flowrates, 7.39, 6.40, 4.43, and 3.44 scfm/ft^2 are presented in Figures 34-38, 39-43, 44-48, and 49-53, respectively. Each set of five graphs will be compared and contrasted to the test case individually. All similarities to the test case will be briefly stated. Arguments stated for the test case can be applied in these instances. Any digression from the test case will be so noted and explained. To simplify comparison only the chosen optimum water flowrate for each constant Q_a is shown in each graph of the series.

Q_a equal 7.39 scfm/ft^2

Each average water quality graph, the constant time graph as well as both constant volume graphs, at constant Q_a equal to 7.39 scfm/ft^2 shown in Figures 34-36 displays the same optimum water flowrate, at V equal to 2.6 gpm/ft^2. The 53.2 ga/ft^2 constant volume graph in Figure 36 digresses from the test case in that the water flowrate necessary to provide the peak associated with optimum porosity was not applied at this air flowrate. The set of instantaneous water quality graphs presented in Figures 37 and 38 provide further verification of optimum particle detachment occurring at water flowrate, V equal to 2.6 gpm/ft^2.

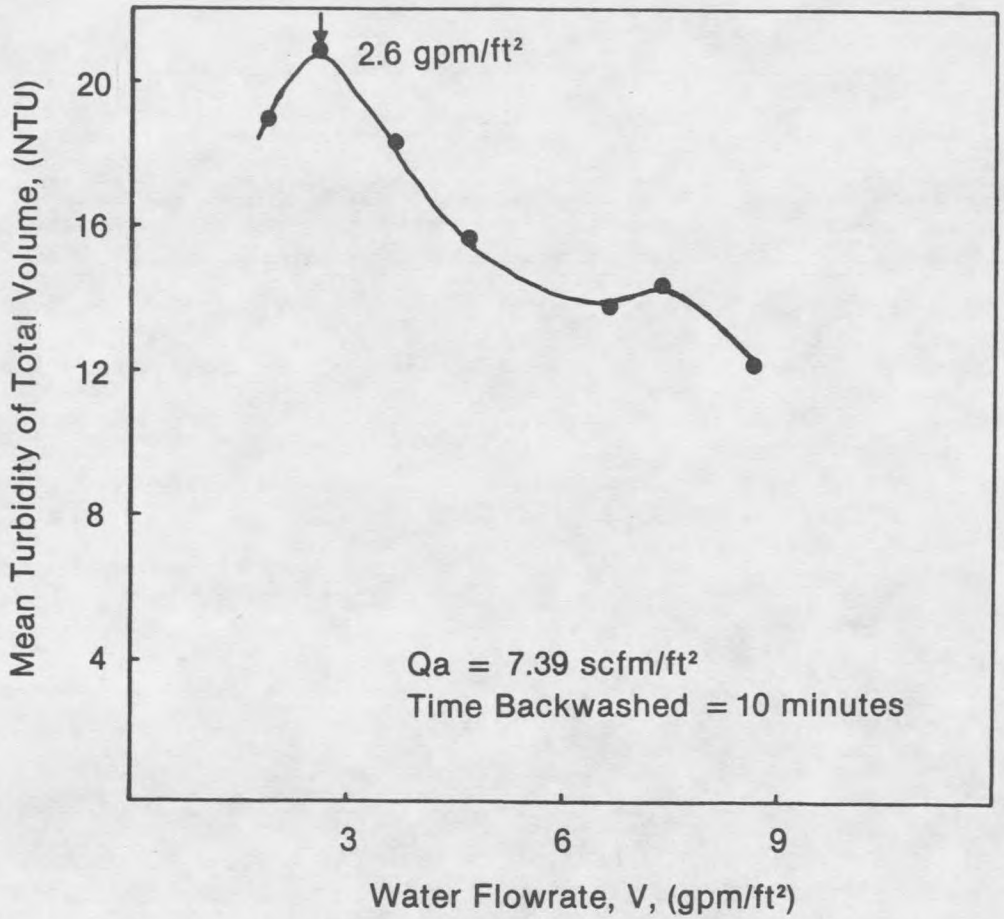

Figure 34. Average water quality, 7.39 scfm/ft² in 10 minutes.

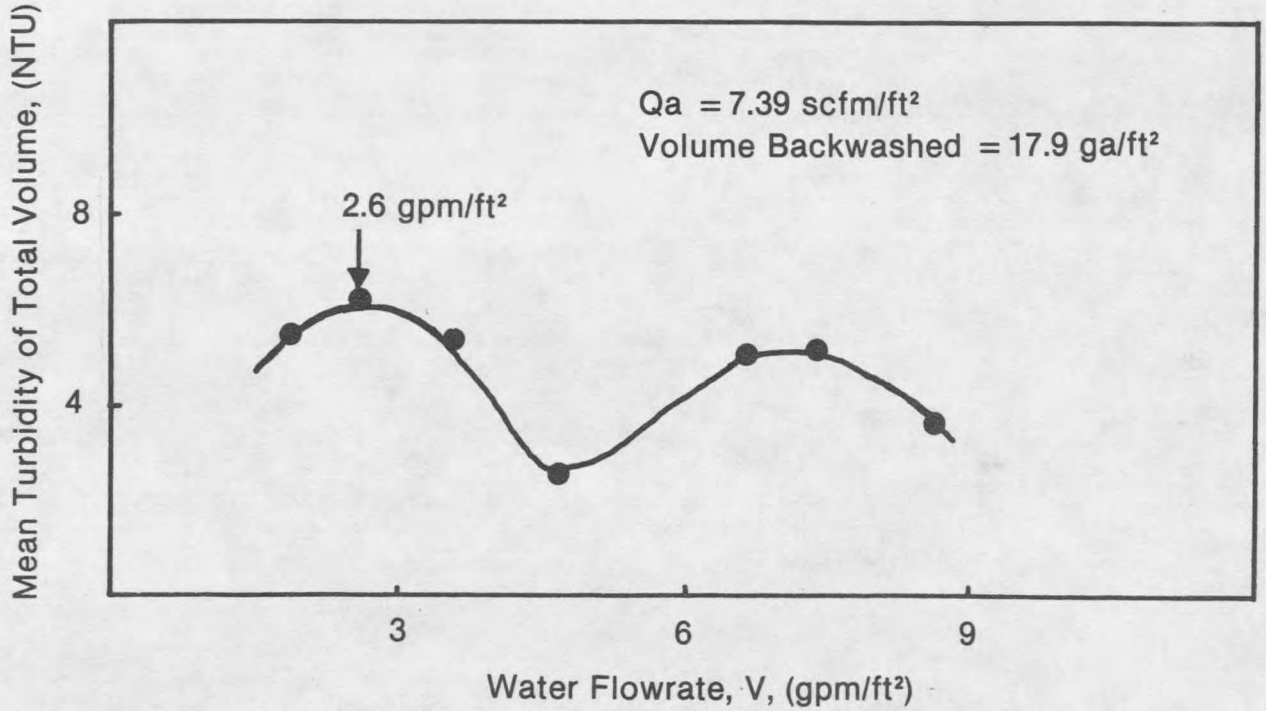

Figure 35. Average water quality, 7.39 scfm/ft² in 17.9 ga/ft².

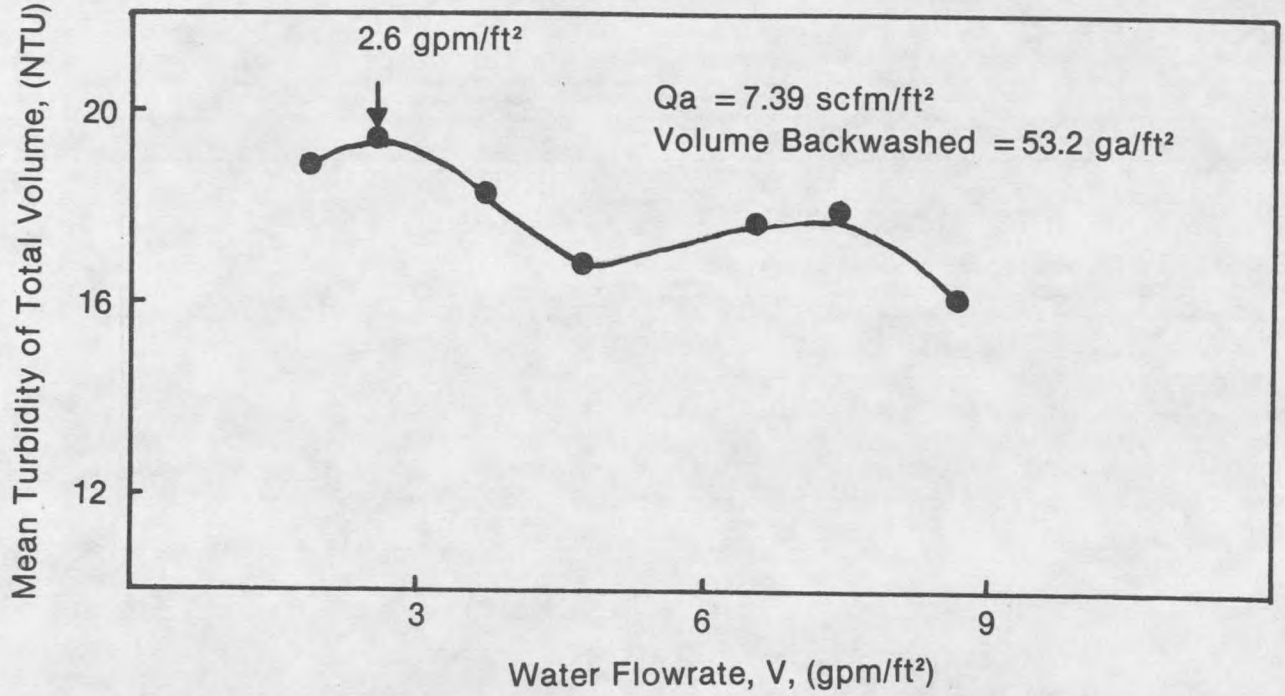

Figure 36. Average water quality, 7.39 scfm/ft² in 53.2 ga/ft².

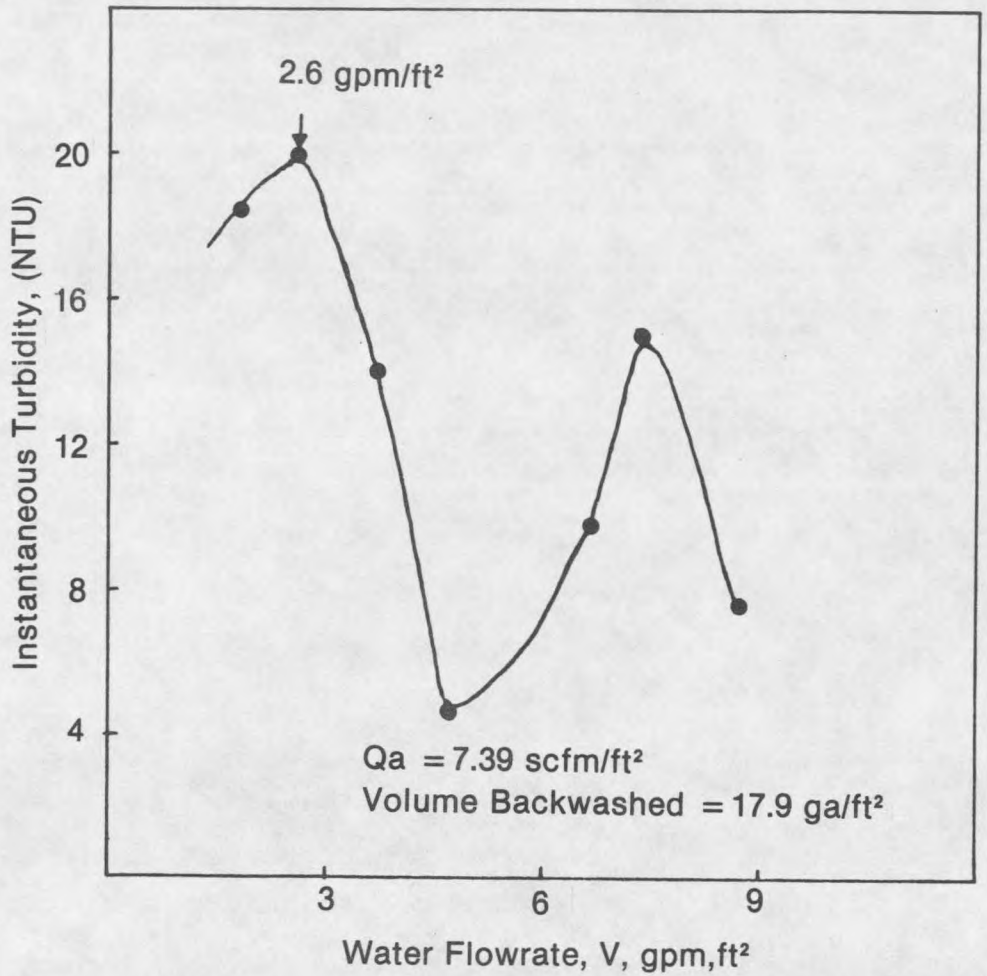

Figure 37. Instantaneous water quality, 7.39 scfm/ft² at 17.9 ga/ft².

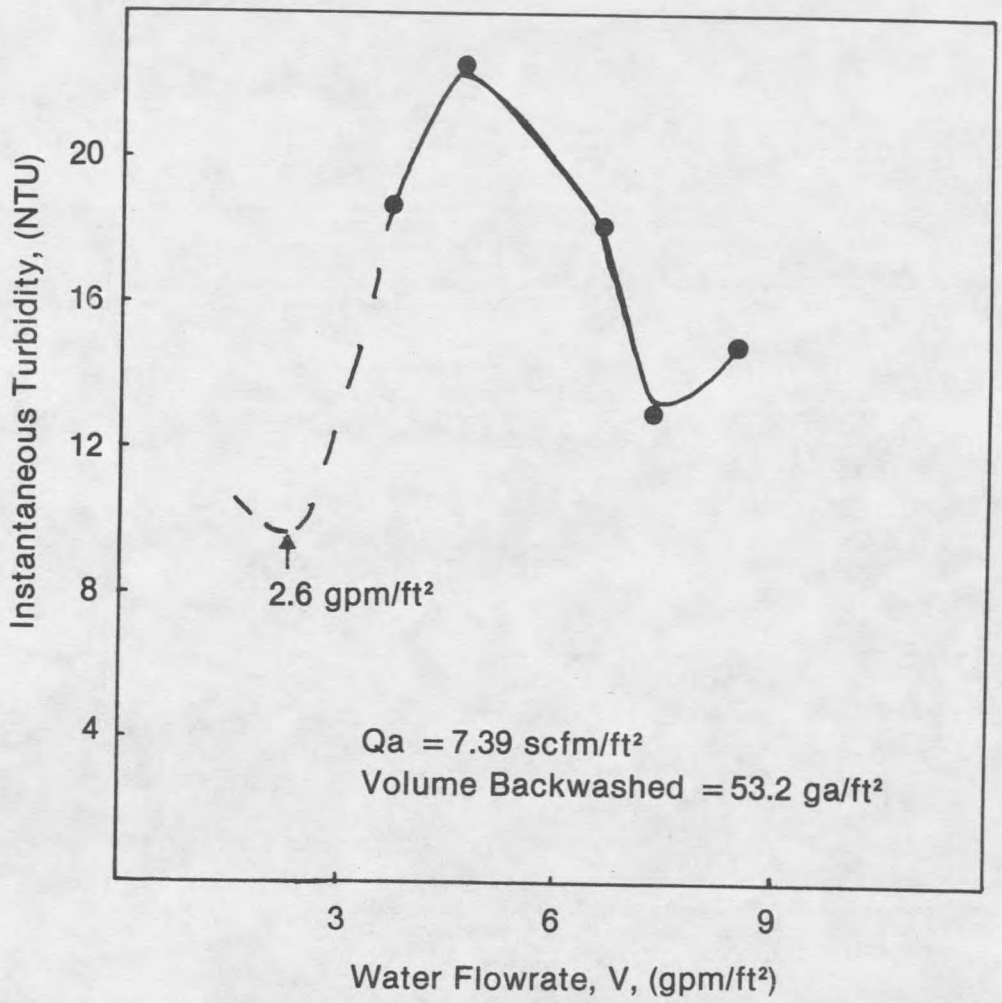

Figure 38. Instantaneous water quality, 7.39 scfm/ft² at 53.2 ga/ft².

Q_a equal 6.40 scfm/ft²

Unlike the test case, a true optimum could not be located in any of the average water quality graphs at an air flowrate equal to 6.40 scfm/ft². Of Figures 39-41 only Figure 40 can be singled out to show a trend toward an optimum at 3.6 gpm/ft². Rather than simply call this flow combination the optimum particle detachment combination, it is necessary to examine the instantaneous water quality graphs which will eliminate the dilution effect present in the average water quality graphs. The set of graphs plotted in Figures 42 and 43 now show a trend in data which is similar to the test case. It has already been established that this set of graphs provides final, and overriding, proof in choosing an air/water flow combination for optimum particle detachment. Accordingly, the water flowrate at V equal to 3.0 gpm/ft² corresponding to a sharp peak in Figure 42 and a valley in Figure 43 was chosen as the flowrate necessary to provide optimum particle detachment at an air flowrate, Q_a equal to 6.40 scfm/ft².

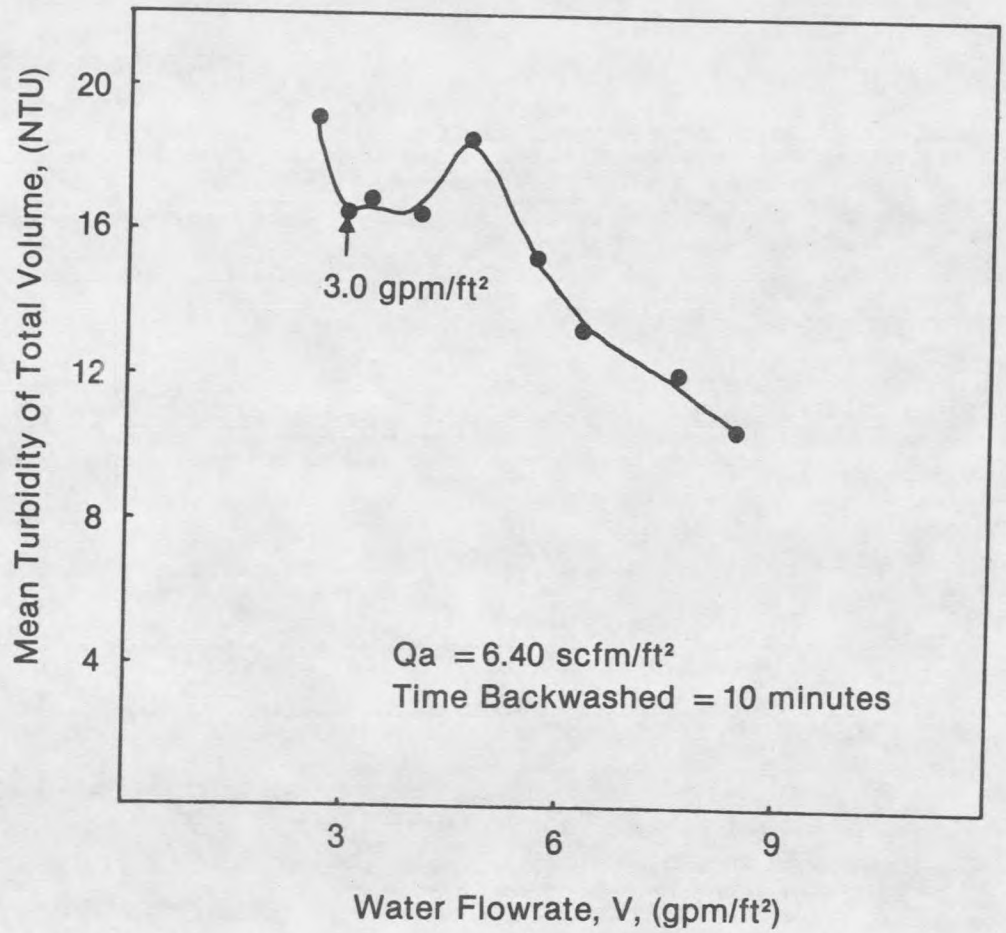

Figure 39. Average water quality, 6.40 scfm/ft² in 10 minutes.

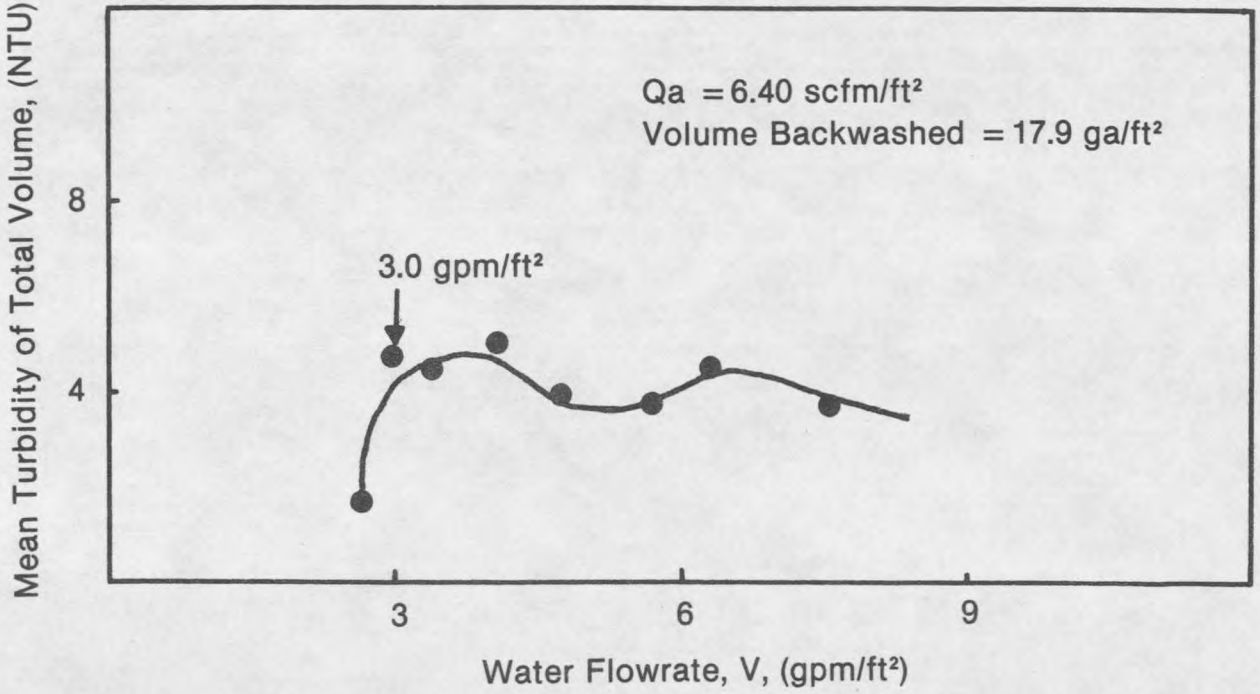

Figure 40. Average water quality, 6.40 scfm/ft² in 17.9 ga/ft².

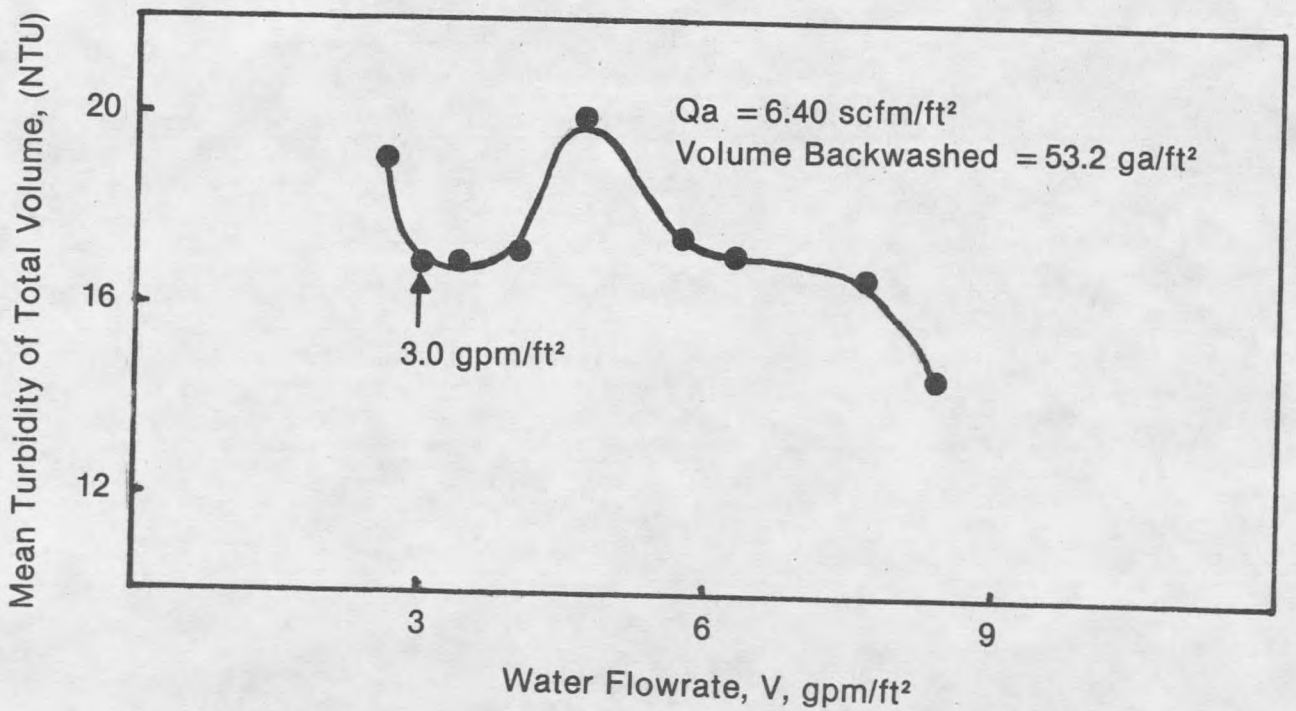

Figure 41. Average water quality, 6.40 scfm/ft² in 53.2 ga/ft².

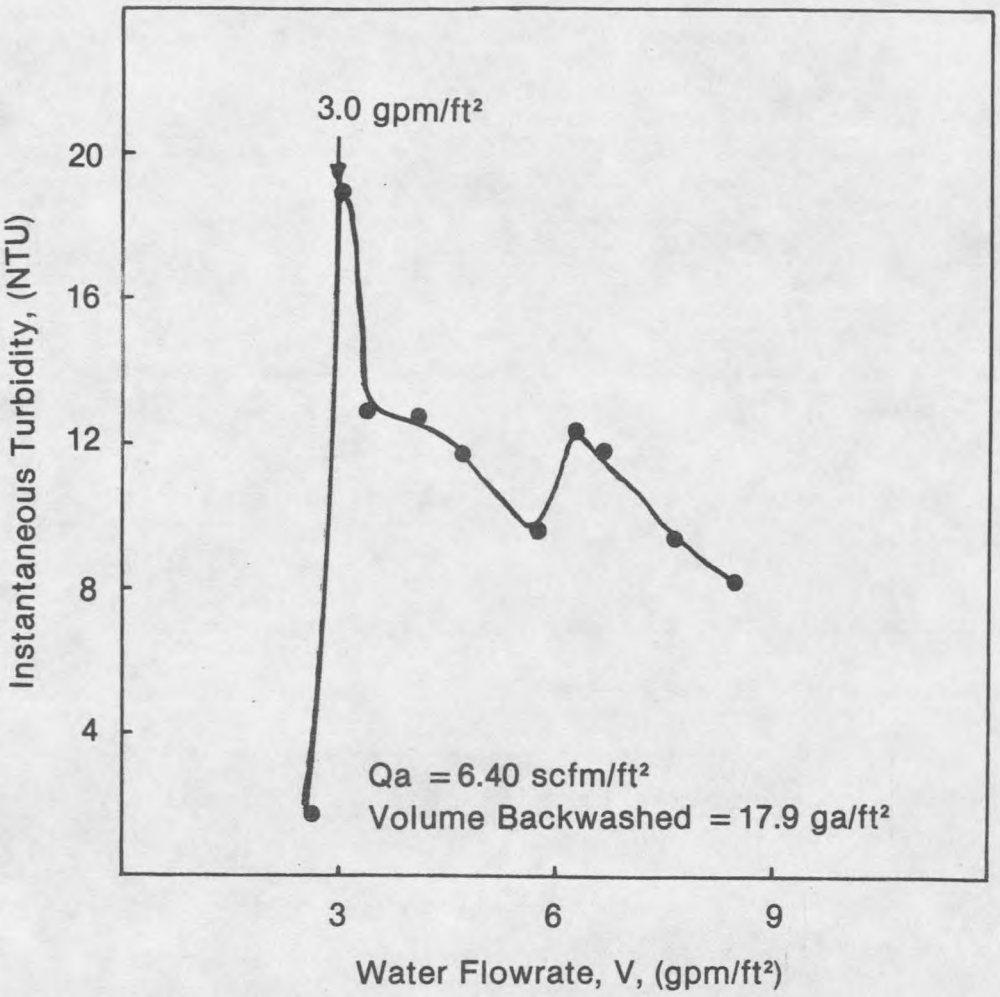

Figure 42. Instantaneous water quality, 6.40 scfm/ft² at 17.9 ga/ft².

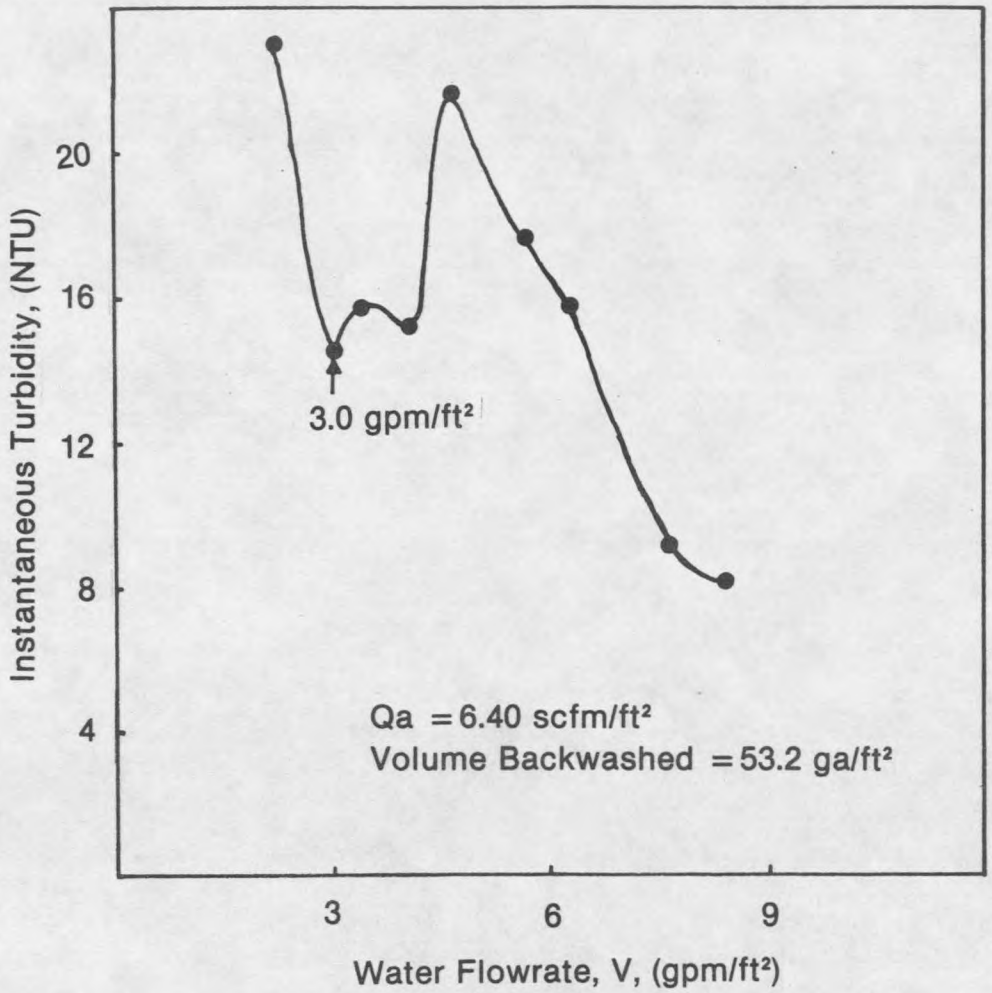

Figure 43. Instantaneous water quality, 6.40 scfm/ft² at 53.2 ga/ft².

Q_a equal 4.43 scfm/ft²

Similar to the test case, the water flowrate combined with an air flowrate, Q_a equal 4.43 scfm/ft², which provided optimum particle detachment in both the constant time graph, Figure 44, as well as the constant volume equal to 17.9 ga/ft² graph, Figure 45, was equal to 3.5 gpm/ft². This optimum was masked by dilution in the average water quality plot shown in Figure 46 at a 53.2 ga/ft² volume. The companion instantaneous water quality graphs in Figures 47 and 48, are again the deciding factor. The peak-valley correspondence indicating optimum particle detachment is evident at the applied water flowrate, V equal to 3.5 gpm/ft², where Q_a equal to 4.43 scfm/ft².

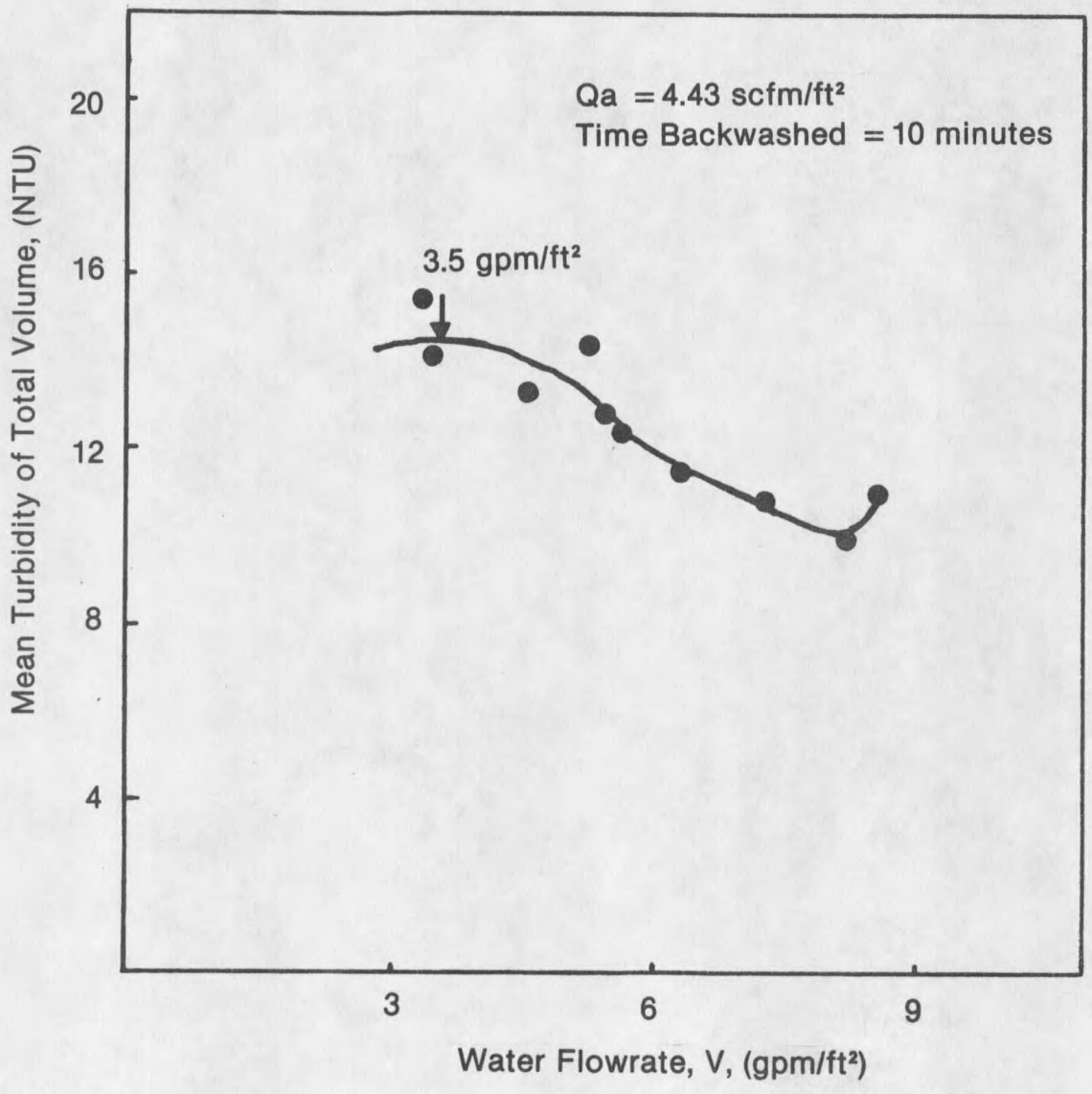

Figure 44. Average water quality, 4.43 scfm/ft² in 10 minutes.

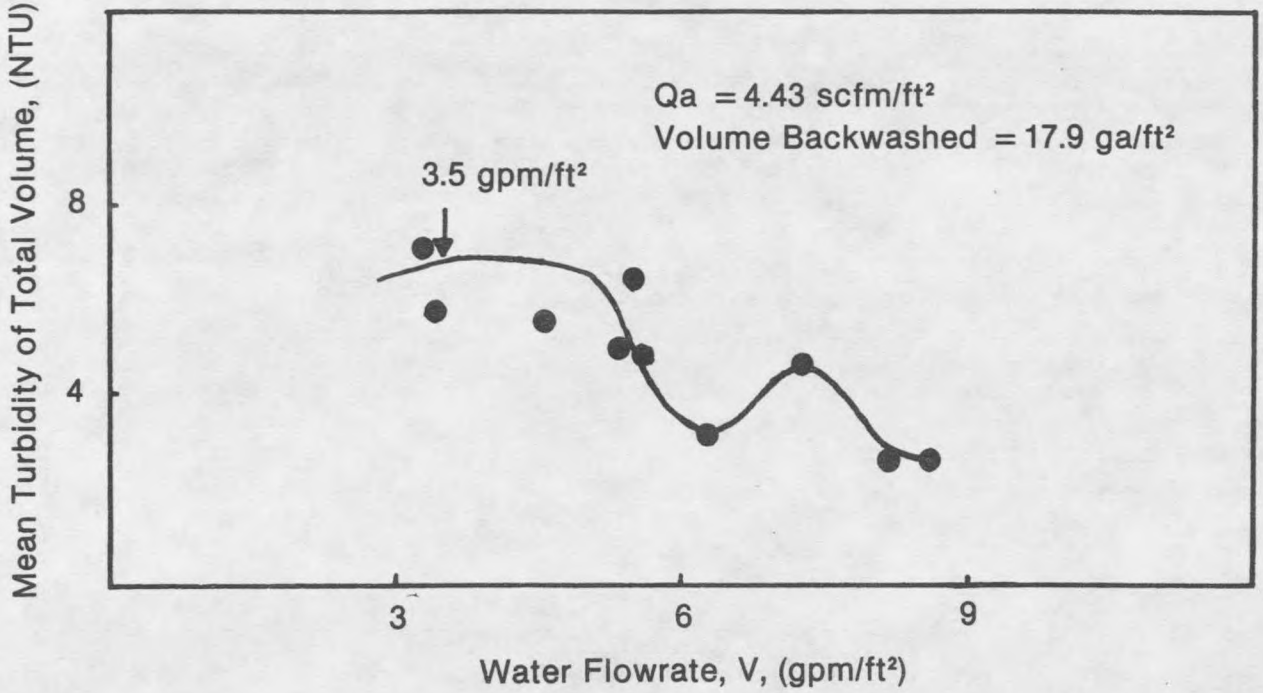

Figure 45. Average water quality, 4.43 scfm/ft² in 17.9 ga/ft².

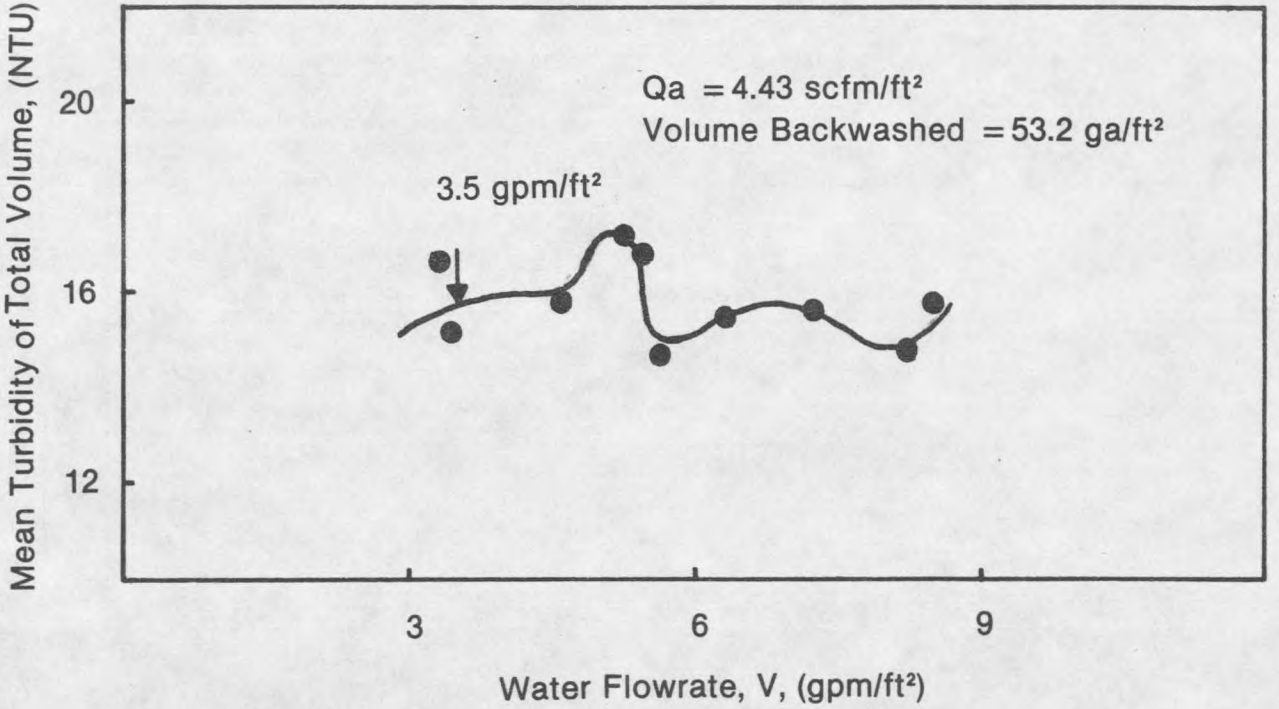

Figure 46. Average water quality, 4.43 scfm/ft² in 53.2 ga/ft².

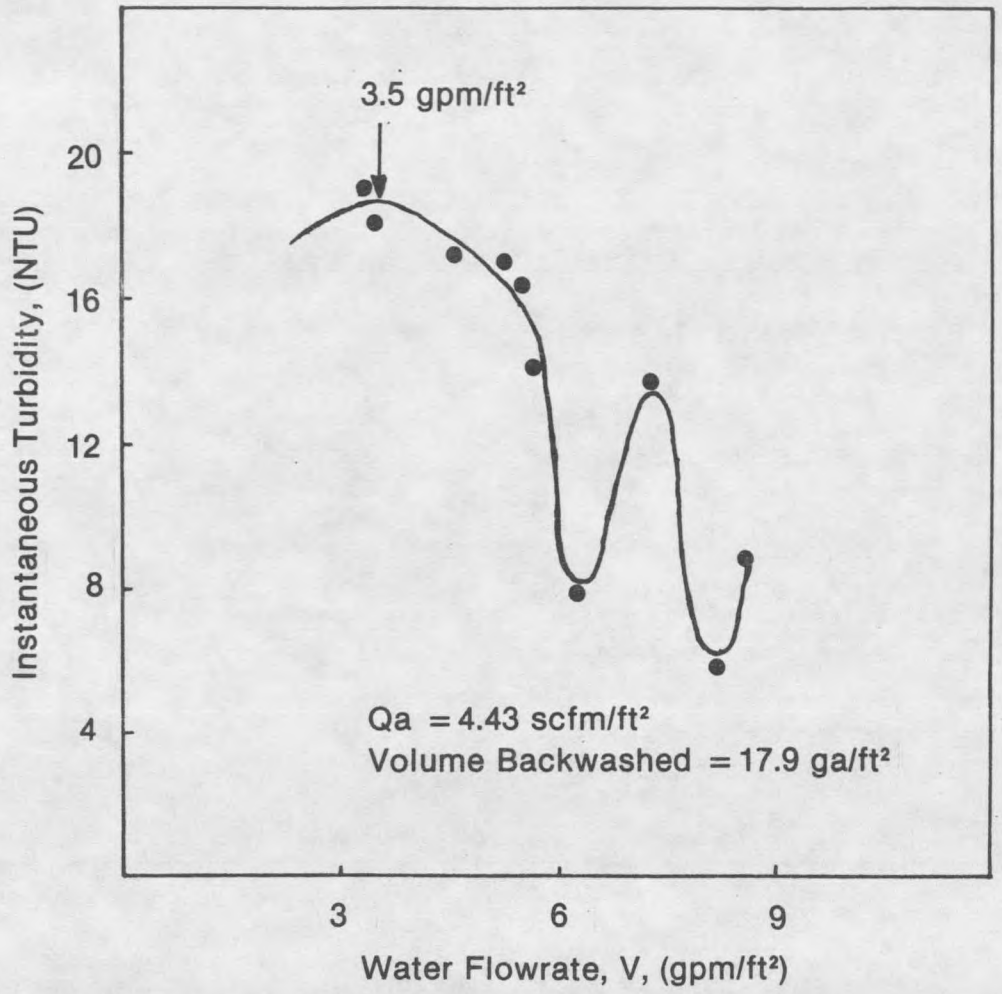

Figure 47. Instantaneous water quality, 4.43 scfm/ft² at 17.9 ga/ft².

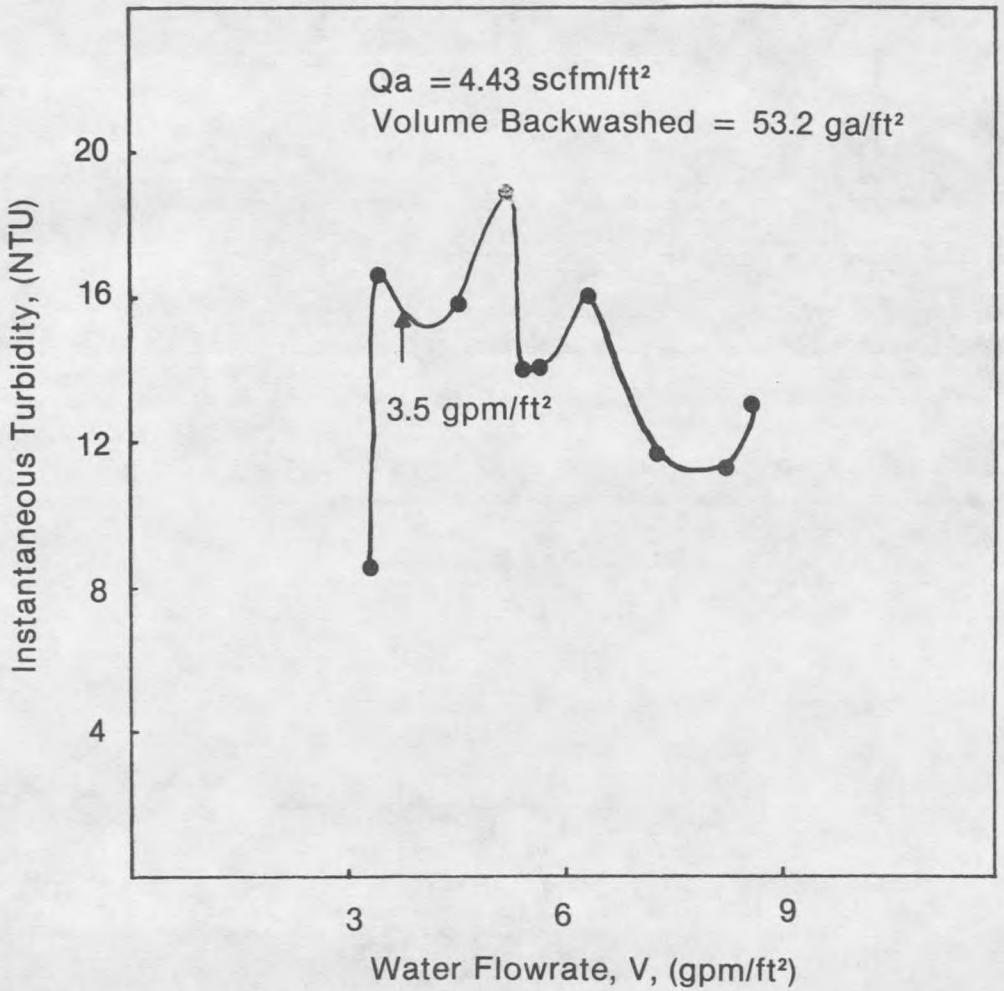

Figure 48. Instantaneous water quality, 4.43 scfm/ft² at 53.2 ga/ft².

Q_a equal 3.44 scfm/ft²

No distinct optima were noted in Figures 49-51, the average water quality plots for the air flowrate equal to 3.44 scfm/ft². Ideally, the water flowrate should have been extended well below the minimum, 3.83 gpm/ft², shown. By the outlined experimental method, however, it was not possible to obtain sufficient sample volume for analysis at reduced flows. The set of companion graphs shown in Figures 52 and 53 representing instantaneous water quality at two points during backwash show similarity to the test case. The water flowrate which provides optimum particle detachment was chosen as 4.75 gpm/ft² at an air flowrate of 3.44 scfm/ft². Although this flowrate represents the peak in Figure 52, it is not actually at a valley in Figure 53. The trend, however, is toward a minimum at this water flowrate. Alternately, it could be argued that the optimum was actually present at V equal to 3.83 gpm/ft². The absence of data below this flowrate casts some doubt upon the choice. Experimental evidence, however, will be presented to support the chosen optimum.

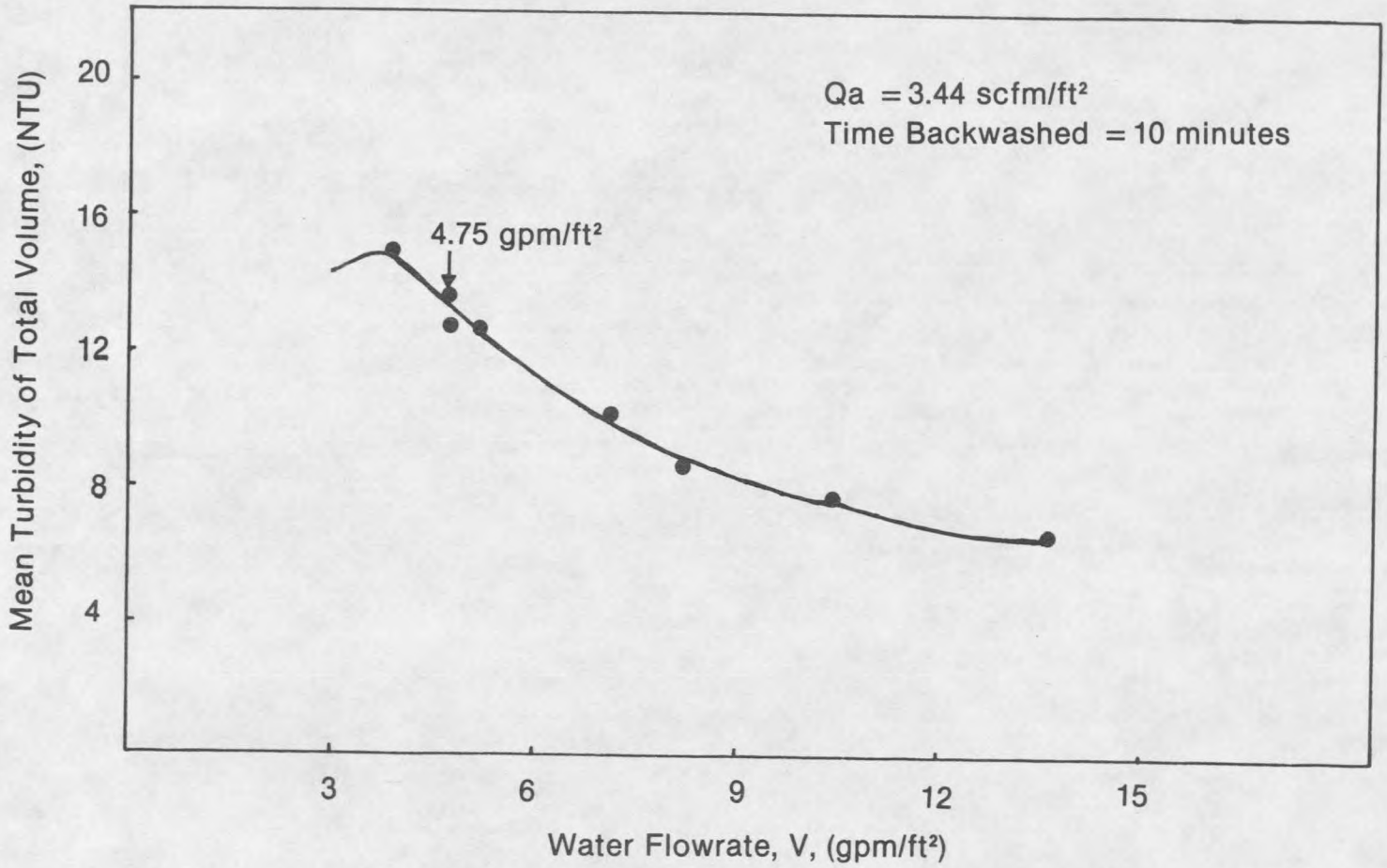

Figure 49. Average water quality, 3.44 scfm/ft² in 10 minutes.

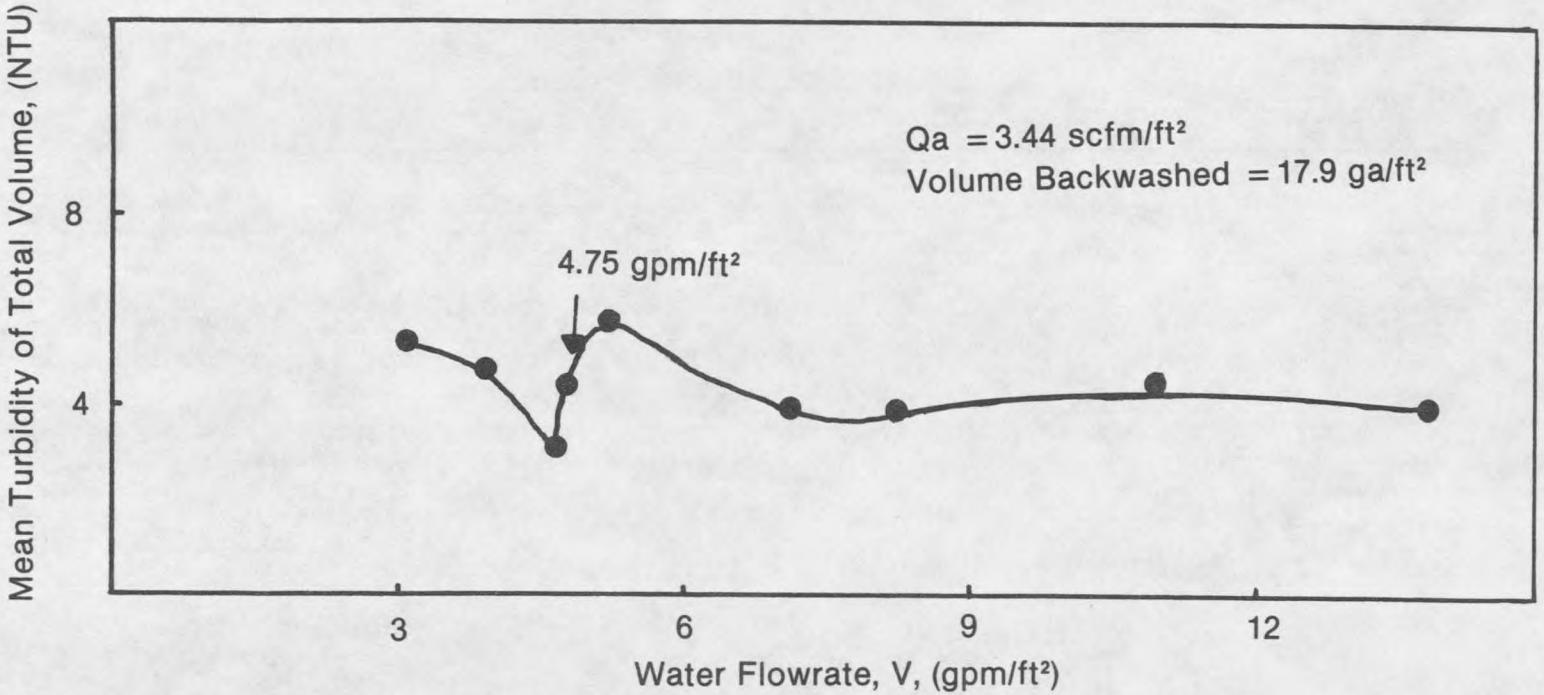

Figure 50. Average water quality, 3.44 scfm/ft² in 17.9 ga/ft².

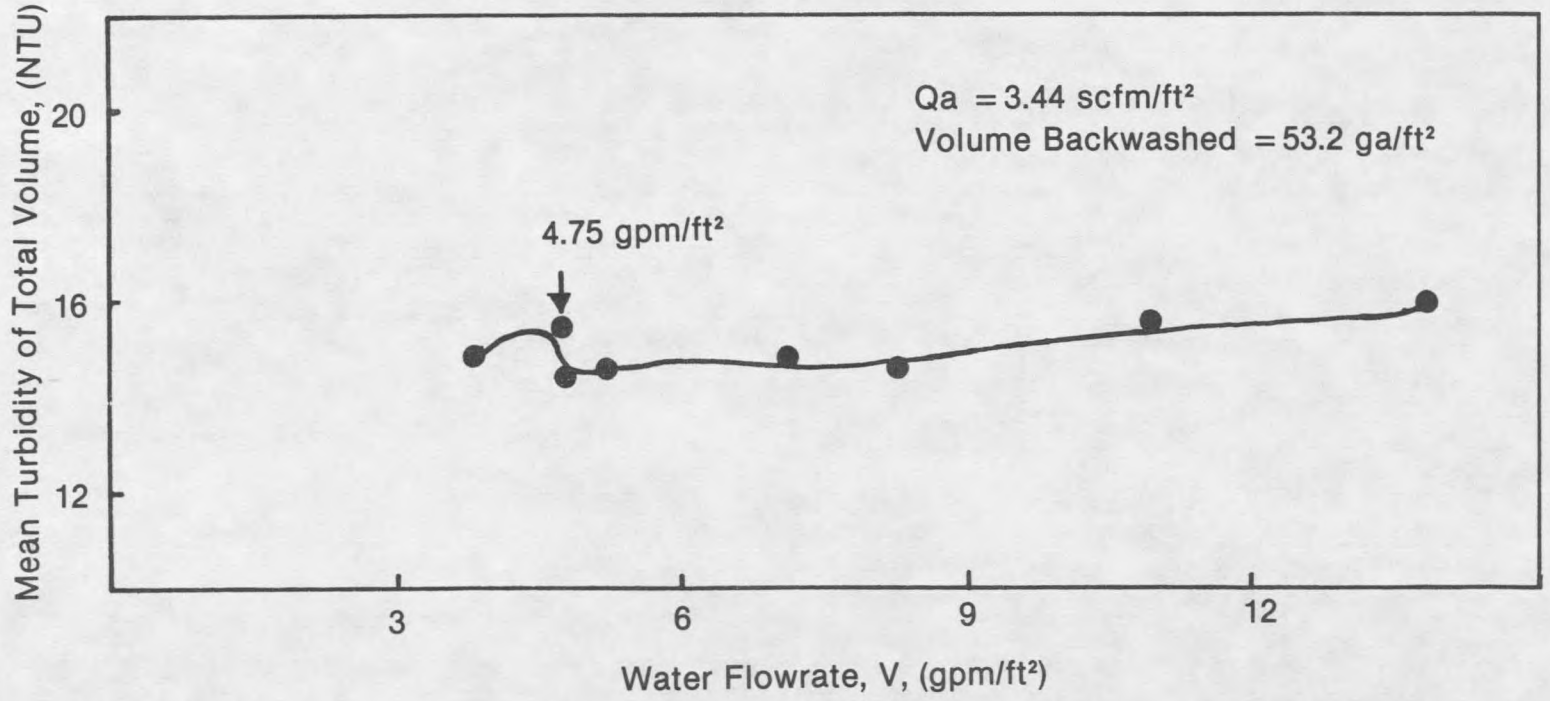

Figure 51. Average water quality, 3.44 scfm/ft² in 53.2 ga/ft².

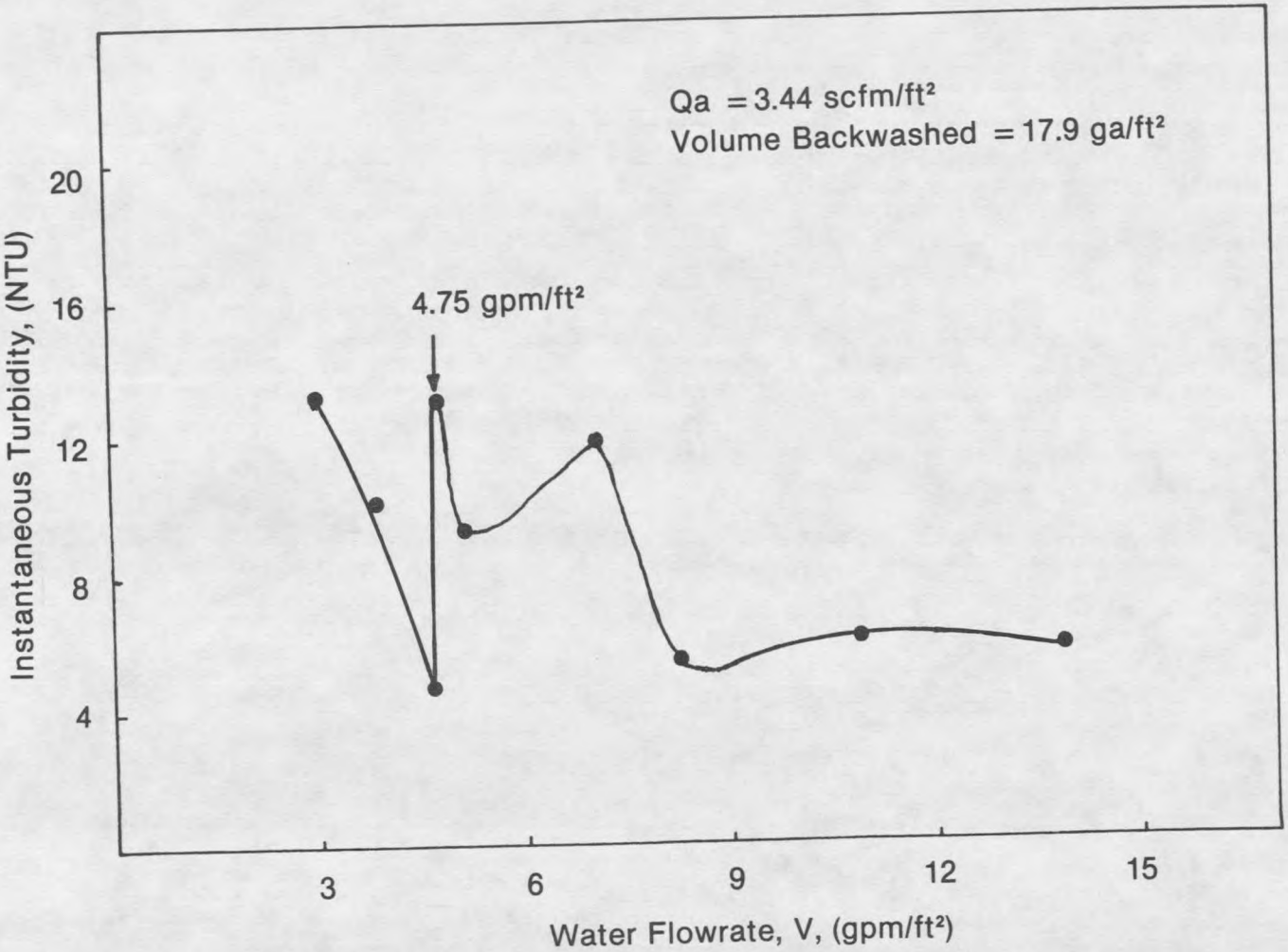

Figure 52. Instantaneous water quality, 3.44 scfm/ft² at 17.9 ga/ft².

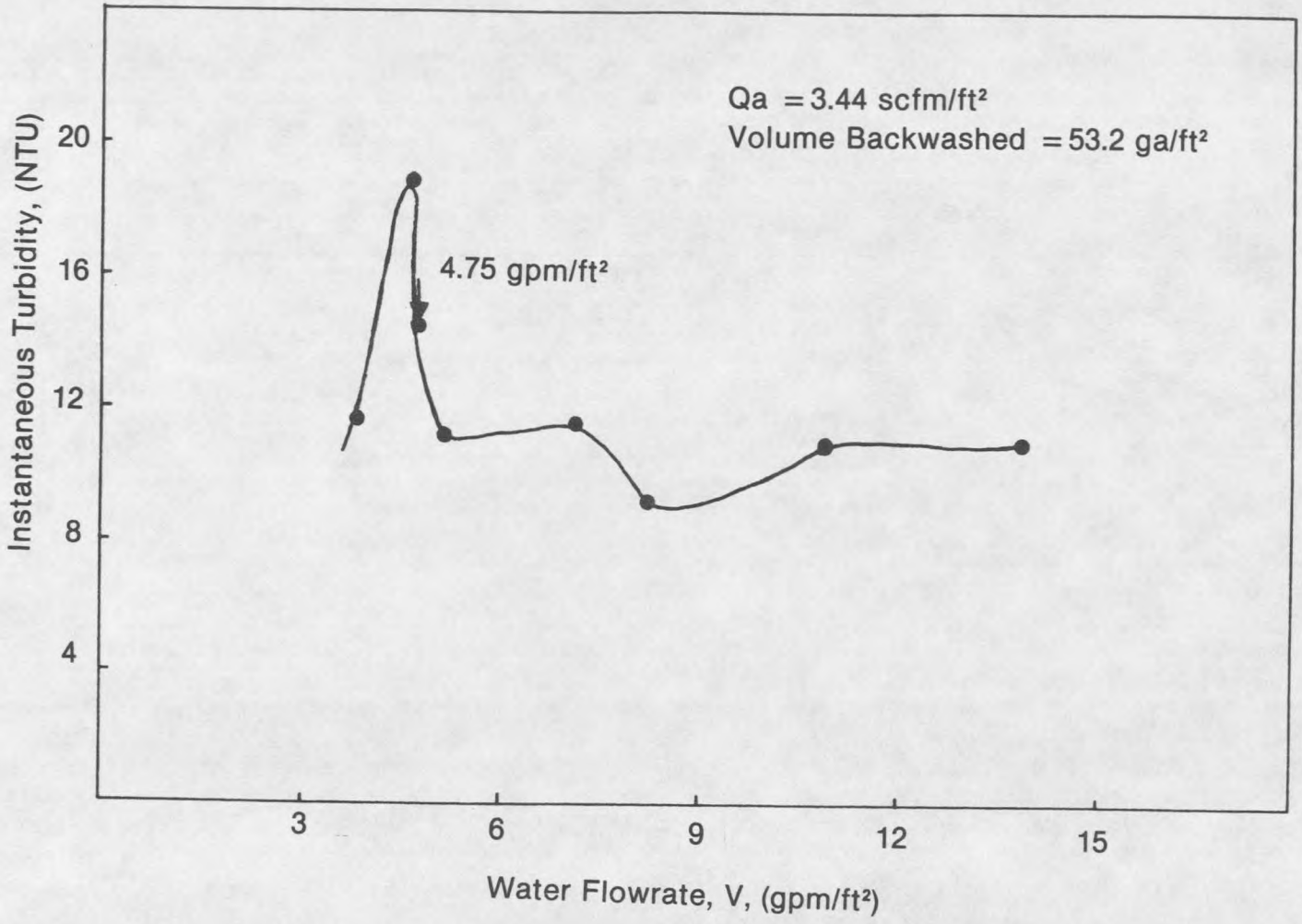

Figure 53. Instantaneous water quality, 3.44 scfm/ft² at 53.2 ga/ft².

Theoretical Applicability

Each air flowrate, Q_a, combined with the simultaneous water flowrate, V, chosen by the above optimum selection method provides the greatest particle removal per unit volume of backwash water flowing through the system. To summarize, the air/water flow combinations obtained were: given an air flowrate, Q_a, equal to 3.44, 4.43, 5.42. 6.40, and 7.39 scfm/ft^2 the water flowrate, V, required was equal to 4.75, 3.5, 3.3, 3.0, and 2.6 gpm/ft^2, respectively.

In a separate series of experimental observations, the air/media motion was observed in a range of water flows from zero water flow to 100 percent of the minimum fluidization velocity for each air flowrate. The combinations of simultaneous air scour and subfluidization water flows which provided optimum particle detachment were also observed to display collapse-pulsing behavior throughout the depth of the bed. These experimental factors, observed air/media motion, and particle detachment optima selection, support the ability of the proposed Collapse-Pulsing theory [3] to predict not only bed behavior, but optimum detachment as well.

To determine the applicability of the Collapse-Pulsing theory in predicting air/water flow combinations which optimize particle detachment the experimental results are compared to the theory. Equation 13 is applied to determine whether the experimentally observed optima plotted as percent V_{mf} versus Q_a^2 will correspond to the theoretical formulation [3]. The measured values of the coefficients necessary for reducing Equation 13 to the form of Equation 14 are summarized below.

Typical plots of air pressure (gage) below the inlet, P_1, versus water flowrate, V, at constant air flowrate, Q_a, are shown in Figures 20 through 24. The air pressures at collapse-pulse flows are shown in Figure 25. The slope of this graph, -4.60×10^{-4}, is given as the value in psig/(scfm/ft^2)^2 for k. There is some indication that the coefficient k is related

to the air flowrate in the form of a velocity head ($v^2/2g$) term. A factor of 2 relative to the inlet orifice dimension was found in this author's investigation. The measurement of the inlet orifice used previously by Hewitt [20] was made, but conclusive calculations to determine whether the factor of 2 is valid have not been performed. Preliminary calculations are shown in Appendix B.

The radius on which the surface tension acts, r, was adjusted to fit the data obtained. The values of 9.94 and 10.06 percent of grain radius are higher than that of 8.2 percent used previously [3]. These numbers are reasonable in light of the fact that the glass beads were difficult to wet, i.e., water would not fill the pore spaces without a great deal of resistance, effectively indicating a greater r value. The values used, however, are still in the range of typical pore sizes which are 7 to 10 percent of the grain size.

$P_1 = 3.23$ psig $= 465.12$ psf;

$T_{20°} = 72.75$ dyne/cm $= 4.98 \times 10^{-3}$ lbf/ft;

$r = 9.94\% \left(\frac{d_{90}}{2}\right) = 1.27 \times 10^{-4}$ ft

using $V_{mf} = 8.37$ gpm/ft^2;

$= 10.06\% \left(\frac{d_{90}}{2}\right) = 1.29 \times 10^{-4}$ ft

using $V_{mf} = 7.53$ gpm/ft^2;

$k = 4.60 \times 10^{-4} \left(\frac{\text{psig}}{\text{scfm/ft}^2}\right)^2 = 0.0662 \left(\frac{\text{psf}}{\text{scfm/ft}^2}\right)^2$;

$H_1 = 4.95$ ft; $Z = 0.783$ ft; $\epsilon_o = 0.41$;

$\phi = 25.6°$; $Sg = 2.50$; $\gamma_b = 55.2$ pcf;

$\gamma_w = 62.4$ pcf.

The final theoretical equations in the form of Equation 13 are:

$$\% \frac{V}{V_{mf}} + 0.254\, Q_a^2 = 46.57 \qquad (26)$$

using $V_{mf} = 8.37$ gpm/ft^2.

$$\% \frac{V}{V_{mf}} + 0.254\, Q_a^2 = 50.15 \qquad (27)$$

using $V_{mf} = 7.53$ gpm/ft^2.

The combination of air, Q_a, and subfluidization water flow, V, for optimum particle detachment were calculated as percent of V_{mf} versus the square of the air flow using Equations 26 and 27. V_{mf} was calculated in the Sample Calculation section of the chapter on Experimental Methodology using two methods, that of Wen and Yu [12,32] and that of Leva [21,31] with the d_{90} size equal to 0.78-mm.

The d_{90} size was chosen over the d_{60} size used in Hewitt [20,21] and Amirtharajah's [3] work for three reasons: (1) The media was basically composed of two size fractions, 49 percent retained on the 0.60-mm sieve and 47 percent retained on the 0.425-mm sieve with the balance, 4 percent, being 0.30-mm or less. When analyzed as a log-probability plot the small percentage of very small grains is disregarded. (2) The column diameter, 1.0-inch, was such that it did not allow significant mixing similar to that in Hewitt's [20,21] apparatus to warrant use of the d_{60} grain size for the collapse-pulsing analysis. This phenomenon is evidenced by the slugging behavior exhibited by the media grains during air scour. (3) Finally, when the experimental results were compared to those obtained by Hewitt and Amirtharajah [3,20,21], shown in Figure 54, the d_{90} sized V_{mf} values better fit the theory in this experimental investigation than the d_{60} sized V_{mf} values.

The theoretical equations formulated above as Equations 26 and 27 are shown in Figure 55 as dashed lines. These lines are noted as 'From Theory'. The experimental optima were also plotted in Figure 55. A linear regression was performed on the data points

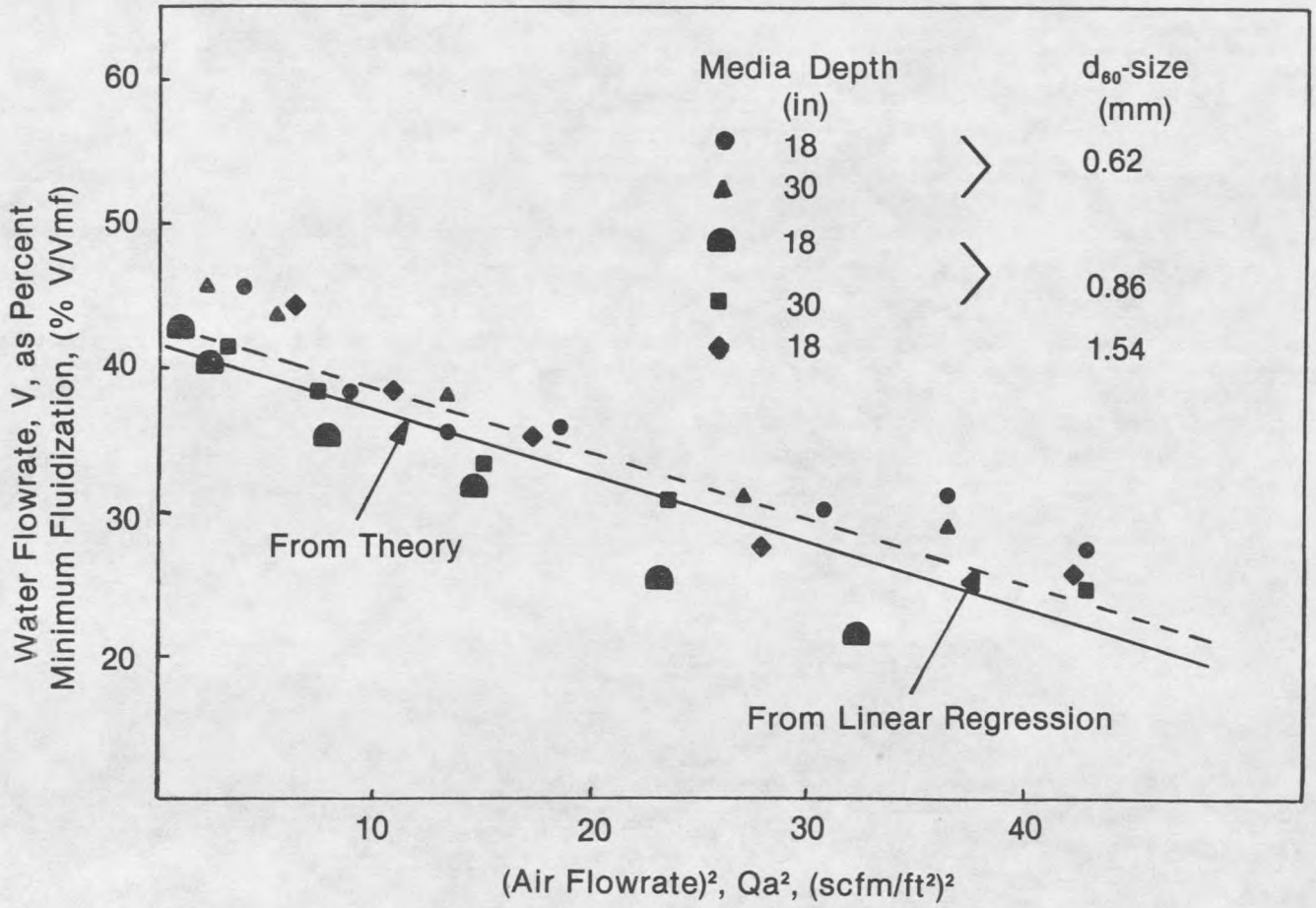

Figure 54. Hewitt and Amirtharajah's results (from 3,20,21).

at Q_a greater than or equal to 4.43 scfm/ft² where the plot appeared linear. The resulting regression equations are:

$$\% \frac{V}{V_{mf}} + 0.323\, Q_a^2 = 48.85 \qquad (28)$$

using $V_{mf} = 8.37$ gpm/ft²

$$\% \frac{V}{V_{mf}} + 0.359\, Q_a^2 = 54.30 \qquad (29)$$

using $V_{mf} = 7.53$ gpm/ft²

The lines obtained from the linear regression are shown as solid lines in Figure 55. Each regression resulted in a -0.999 correlation coefficient. The slopes of the linear regression lines have a maximum difference of 11 percent which can be attributed to the variation between the V_{mf} calculation methods.

These experimental data shown in Figure 55 display a trend similar to the results obtained by Hewitt [20,21] and interpreted by Amirtharajah [3] as shown in Figure 54. In four of the five cases studied where the air flowrates were equal to 4.43, 5.42, 6.40, and 7.39 scfm/ft² the data showed a linear trend similar to that noted in Figure 54.

The 3.44 scfm/ft² air flowrate, however, does not show the same linear trend. In fact, the data pattern obtained seems to indicate that this air flowrate lies outside the bounds of the applied theory. Short dashed lines are used to connect these points to the regression lines. The water flow required experimentally (63 or 57 $\%V_{mf}$) with this low air flow to cause collapse-pulsing is much greater than the present theory would predict (45 or 50 $\%V_{mf}$). The data given at low air flowrates in Figure 54 also show some divergence from the proposed linear theory. The fact that both sets of data show this same trend seems to indicate a lower limit for the application of the theory.

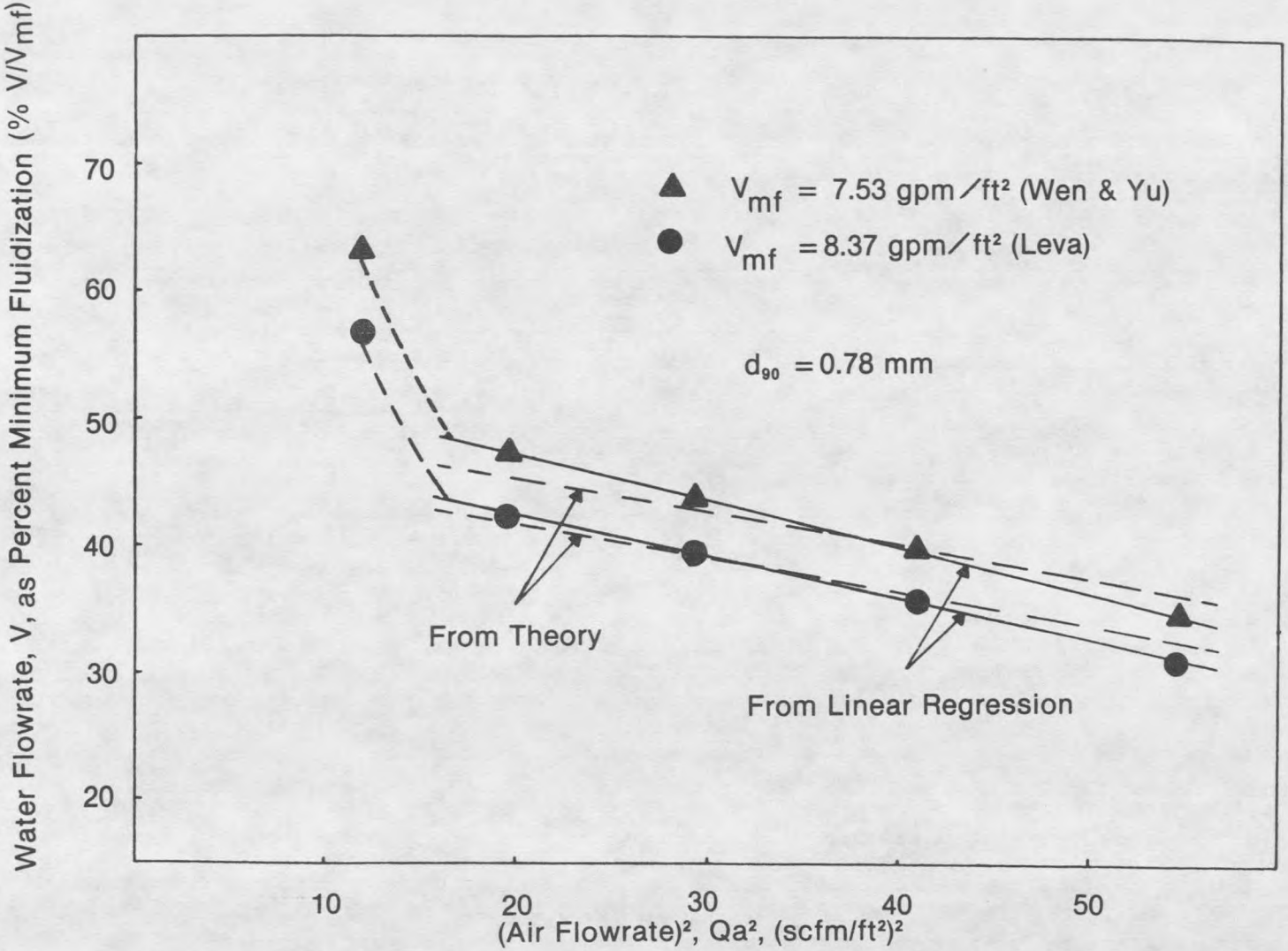

Figure 55. Optimum particle detachment as percent V/V_{mf} versus air flowrate squared.

Although it can be concluded that there is a lower limit to the bounds of the applied theory, more data are necessary to determine the exact point at which the present theory no longer applies and the reason(s) for its inapplicability. Perhaps the k term, calculated as a function of the air flow velocity and inlet orifice diameter could shed some light on an existence of a lower limit to the collapse-pulsing theory.

It is important to note that although the pilot-scale system utilized in this research was small (60-inch X 1.0-inch diameter column, 9.4-inch bed depth) and idealized (spherical glass bead media), the correspondence with Hewitt's [20,21] full scale (68-inch X 12-inch X 0.75-inch, 18 and 30-inch bed depths) sand system is excellent. The correlation between this investigation, Hewitt's work [20,21], and the theory for collapse-pulsing behavior developed by Amirtharajah [3] indicate that the theory predicting Collapse-Pulsing behavior in a granular media bed is a valid means for predicting the combination of simultaneous air and subfluidization water flows necessary for optimum particle detachment. The results of fifty pilot-plant runs indicate that the mechanics of collapse-pulsing promote collisions between the media grains resulting in significant abrasion/collisions. Abrasion/collisions are not only significant at collapse-pulsing, but optimized. Hence, best cleaning is provided to a granular media filter by simultaneous air scour and subfluidization water flows which cause Collapse-Pulsing throughout the depth of the bed.

CHAPTER 6

CONCLUSIONS

The pilot-scale investigation which was completed has succeeded in satisfying its original objectives. The air/subfluidization water flows determined to optimize particle detachment were found to combine air flowrates, Q_a equal 3.44, 4.43, 5.42, and 7.39 scfm/ft^2 with water flowrates, V equal 4.75, 3.5, 3.3, 3.0, and 2.6 gpm/ft^2, respectively. A system which employs three-phase backwash which induces Collapse-Pulsing behavior was shown experimentally to provide significant abrasion and/or collisions between individual media grains. Particle detachment is, in fact, optimized. This determination that particle detachment is optimized at Collapse-Pulsing air/water flow combinations provides immediate practical applications:

1. The effectiveness of a backwash system depends on the ability of the cycle to provide abrasion/collisions between the media grains, and thus particle detachment from the media grains. In order to provide an environment favoring particle detachment an advantageous relationship must exist between the stress and the movement in a system. Stresses are greater when the system is at rest, but movement is greater in a flowing system. The stress relationship existing during three-phase backwash of a granular media filter at a Collapse-Pulsing condition was formulated [3] to optimize the two opposing effects of stress and movement for best particle detachment. Accordingly, the individual grains were determined to slip and slide against each other at their contact points.

This investigation combined with previous work done by Hewitt [20] and Cleasby and Lorence [14] provides experimental evidence to indicate that Amirtharajah's theory developed to predict Collapse-Pulsing behavior [3] during three-phase backwash can also

be utilized to predict the air/water flow combinations which optimize particle detachment. The theory is, therefore, available for use in designing granular media filters which optimize particle detachment. The Collapse-Pulsing equation can be stated generally:

$$\% \frac{V}{V_{mf}} + mQ_a^2 = b$$

where $\%V/V_{mf}$ is the water flowrate expressed as a percentage of the minimum fluidization velocity and Q_a is the applied air flowrate in scfm/ft^2. This equation is especially convenient since the constants m and b reflect systemic coefficients relative to the column dimensions, media characteristics, and the inlet configuration which are either easily measurable or have standard values.

2. Although the present theory [3] closely predicts Collapse-Pulsing behavior in this investigation as well as in previous work [20,21], there seems to be an indication that a lower limit exists for application to granular media filter behavior. Further investigation is necessary to conclusively state the exact bounds of the theory. There is some indication that the boundary, or modification of the equation, can be provided by closely examining the air inlet orifice configuration.

3. Granular media filters which utilize the Collapse-Pulsing phenomenon for optimal cleaning conditions have the added benefit of minimized media loss. Turbulent wakes do not accompany bubble formation during collapse-pulsing.

4. Some evidence [16] exists to indicate that the use of simultaneous air and sub-fluidization water backwash can be utilized to destratify the granular media beds utilized in wastewater filtration. Perhaps Collapse-Pulsing provides sufficient destratification. Experimental evidence is necessary to state whether significant destratification occurs during collapse-pulsing, but it is this author's belief that the theory will also be applicable in this respect. The media circulation pattern observed during collapse-pulsing behavior is at least partly conclusive in this respect.

In conclusion, the original theoretical equation [3] has been experimentally validated. The Collapse-Pulsing theory has both fundamental and practical significance. Particle detachment, cleaning, is optimized at the simultaneous air and subfluidization water flows computed from the equation. The Collapse-Pulsing equation can, therefore, be confidently applied to future designs of three-phase, air/water, backwash for granular media filters.

REFERENCES CITED

REFERENCES CITED

1. Alince, B. "Deposition of Cationic Polymeric Pigments on Pulp Fibers," *Journal of Colloid and Interface Science*, 69(3): 367 (1979).

2. Amirtharajah, A. "Optimum Backwashing of Sand Filters," *Journal of the Environmental Engineering Division, ASCE*, 104(EE5): 917-932 (October 1978).

3. Amirtharajah, A. "Fundamentals and Theory of Air Scour," *Journal of the Environmental Engineering Division, ASCE*, 110: 573-590 (1984).

4. Amirtharajah, A., Morrison, R. J., and Holnbeck, S. R. "The Mechanics of Air Scour During Filter Backwash," *1981 Annual Conference Proceedings, Part 1*, American Water Works Association, 209-239 (1981).

5. Amirtharajah, A. and Trusler, S. L. "Studies on Loss of Media During Air Scour," *1982 Conference Proceedings, Part 1*, American Water Works Association, 387-404 (May 1982).

6. Amirtharajah, A. and Wetstein, D. P. "Initial Degradation of Effluent Quality During Filtration," *JAWWA*, 72(9): 518-524 (September 1980).

7. Asphalt Institute, The *Soils Manual for the Design of Asphalt Pavement Structures*, Manual Series No. 10, The Asphalt Institute, College Park, Maryland (March 1978).

8. Bowen, B. D. and Epstein, N. "Fine Particle Deposition in Smooth Parallel Plate Channels," *Journal of Colloid and Interface Science*, 72(1): 81 (1979).

9. Brace, R. and Matijevic, E. "Aluminum Hydroxide Sols—I: Spherical Particles of Narrow Size Distribution," *Journal of Inorganic and Nuclear Chemistry*, 35: 3691-3705 (1973).

10. Clayfield, E. J. and Smith, A. L. "Adhesion and Detachment of Solid Colloidal Particles in Aqueous Ionogenic Surfactant Media," *Environmental Science and Technology*, 4: 413 (1970).

11. Cleasby, J. L. and Baumann, E. R. "Backwash of Granular Filters Used in Wastewater Treatment," *Environmental Protection Technology Series, EPA-600/2-77-016*, U.S. Environmental Protection Agency, Cincinnati, Ohio (1977).

12. Cleasby, J. L. and Fan, K. "Predicting Fluidization and Expansion of Filter Media," *Journal of the Environmental Engineering Division*, ASCE, 107 (EE3): 455-471 (1981).

13. Cleasby, J. L., et al. "Backwashing of Granular Filters," *Journal of the American Water Works Association*, 69(2): 115-126 (February 1977).

14. Cleasby, J. L. and Lorence, J. C. "Effectiveness of Backwashing for Wastewater Filters," *Journal of the Environmental Engineering Division*, ASCE, 104(EE4): 749-765 (August 1978).

15. Cleasby, J. L., Stangl, E. W. and Rice, G. A. "Developments in Backwashing Granular Filters," *Journal of the Environmental Engineering Division*, ASCE, 101(EE5): 713-727 (October 1977).

16. Dahab, M. F. and Young, J. C. "Unstratified-Bed Filtration of Wastewater," *Journal of the Environmental Engineering Division*, ASCE, 103(EE1): 21-36 (February 1977).

17. Davidson, J. F. "Differences Between Large and Small Fluidized Beds," *AIChE Symposium Series*, 69(128): 16-17 (1973).

18. Davidson, J. F. and Schuler, B. O. G. "Bubble Formation at an Orifice in a Viscous Liquid," *Transactions of the Institution of Chemical Engineers*, London, 38: 144-154 (1960).

19. Elms, J. W. *Water Purification*, McGraw-Hill Book Co., Inc., New York, New York (1917).

20. Hewitt, S. R. "Air Motion Through Filter Media During Air Scour," Unpublished Master's Report, Department of Civil Engineering and Engineering Mechanics, Montana State University, Bozeman, Montana (1982).

21. Hewitt, S. R. and Amirtharajah, A. "Air Dynamics Through Filter Media During Air Scour," *Journal of the Environmental Engineering Division*, ASCE, 110: 591-606 (1984).

22. Holnbeck, S. R. "Hydrodynamics of Air Scour in Two and Three Phase Systems," Unpublished CE 575 Report, Department of Civil Engineering and Engineering Mechanics, Montana State University, Bozeman, Montana (1980).

23. Kallay, N. and Matijevic, E. "Kinetics of Detachment of Hematite Particles from Steel," *Journal of Colloid and Interface Science*, 83(1): 289-300 (September 1981).

24. Kehoe, P. W. K. and Davidson, J. F. "Pressure Fluctuations in Slugging Fluidized Beds," *AIChE Symposium Series*, 69(128): 34-40 (1973).

25. Kuo, R. J. and Matijevic, E. "Particle Adhesion and Removal in Model Systems," *Journal of Colloid and Interface Science*, 78(2): 407-421 (December 1980).

26. Leva, M. *Fluidization*, McGraw-Hill Book Co., Inc., New York, New York (1959).

27. Matijevic, E., Kuo, R. J. and Kolny, H. "Stability and Deposition Pheomena of Monodispersed Hematite Sols," *Journal of Colloid and Interface Science*, 80(1): 94 (1981).

28. Morrison, R. J. "The Hydrodynamics of Air Scour During the Backwash of Granular Filters," Unpublished Master's Report, Department of Civil Engineering and Engineering Mechanics, Montana State University, Bozeman, Montana (1978).

29. Ramaswami, D. "A Model System for the Study of Particle Detachment Kinetics in Fluidized Beds," Unpublished CE 575 Report, Department of Civil Engineering and Engineering Mechanics, Montana State University, Bozeman, Montana (1982).

30. Sanks, R. L., ed. *Water Treatment Plant Design*, Ann Arbor Science Publishers, Inc., Ann Arbor, Michigan (1980).

31. Weber, W. J., Jr. *Physiochemical Processes for Water Quality Control*, Wiley-Interscience, New York, New York (1972).

32. Wen, C. Y. and Yu, Y. H. "Mechanics of Fluidization," *Chemical Engineering Progress Symposium Series 62*, 62: 100-111, New York, New York (1966).

APPENDICES

APPENDIX A

COMPUTER PROGRAMS

```
10    REM    PROGRAM TO CALCULATE MEAN TURBIDITY
20    REM    CUMULATIVE GA/FT**2 BACKWASHED, AND SUBSEQUENTLY,
30    REM    PLOT TURBIDITY-V-CUMULATIVE BACKWASH VOLUME.
40    DIM    A(30)
50    REM    WHERE A IS TIME FOR SAMPLE I
60    B=0
70    REM    WHERE B IS TOTAL TIME
80    C=0
90    REM    WHERE C IS VOLTOT
100   D=0
110   REM    WHERE D IS A TEMPORARY ASSIGNMENT
120   F=0
130   REM    WHERE F IS THE AIR FLOW IN SCFM/FT**2
140   G=0
150   REM    WHERE G IS A TEMPORARY ASSIGNMENT
160   I=0
170   REM    WHERE I INDICATES AN ARRAY POSITION
180   J=0
190   REM    WHERE J IS A TEMPORARY ASSIGNMENT
200   K=0
210   REM    WHERE K IS CONSTANT VOLUME IN MLS
220   L=0
230   REM    WHERE L IS THE INFLUENT TURBIDITY, NTU
240   REAL   M
250   REM    WHERE M IS MEAN TURB
260   N=0
270   REM    WHERE N IS THE EXPERIMENTAL BACKWASH FLOW IN
GPM/FT**2
280   P=0
290   REM    WHERE P IS VOL*TURB
300   DIM    Q(30)
310   REM    WHERE Q IS THE VOLTOT TO I
320   R=0
330   REM    WHERE R IS THE RUN NUMBER
340   S=0
350   REM    WHERE S IS THE SUM OF VOL*TURB
360   DIM    T(30)
370   REM    WHERE T IS TURB, NTU
380   DIM    V(30)
390   REM    WHERE V IS VOL, ML
400   DIM    W(30)
410   REM    WHERE W IS GA/FT**2
420   Y=1
430   REM    WHERE Y IS A PRINT FLAG
440   Z=0
450   REM    WHERE Z IS A COUNTER
460   PRINTER IS 701
470   INPUT  "ENTER RUN #",R
480   PRINT  "RUN #";R
490   PRINT
500   INPUT  "ENTER INFLUENT TURBIDITY IN NTU's",L
```

```
510     PRINT    USING "2D.DD,2X,3A,X,8A,X,9A";L,,,NTU","INFLUENT",
"TURBIDITY"
520     PRINT
530     INPUT    "ENTER AIR FLOW IN SCFM/FT**2.",F
540     PRINT    USING "2D.3D,2X,9A,D,2X,3A";F,"SCFM/FT**",2,"AIR"
550     PRINT
560     INPUT    "DO YOU WANT DATA OUTPUT TO PRINTER (Y=1/N=0)?",Y
570     IF Y=0   THEN PRINTER IS 1
580     PRINT    USING "13X,5A,14X,10A";"TOTAL","CUMULATIVE"
590     PRINT    USING 600
600     IMAGE    X,"I",3X,"TIME",4X,"TIME",5X,"VOL",10X,"VOLUME",13X,
"TURBIDITY"
610     PRINT    USING 620
620     IMAGE    5X,"SECS",4X,"SECS",5X,"MLS",7X,"MLS",5X,"GA/FT**2",6X,
"NTU"
630     PRINT
640     INPUT    "IF THIS IS A CONSTANT V CALCULATION, ENTER VOLUME IN
MLS. IF NOT, ENTER 0.",K
650     FOR I=1 to 30
660     INPUT    "ENTER SAMPLE TIME IN SECS. ENTER 0 TO STOP.",A(I)
670     IF A(I)=0 THEN 1010
680     INPUT    "ENTER VOLUME IN MLS.",V(I)
690     INPUT    "ENTER TURBIDITY IN NTU.",T(I)
700     C=C+V(I)
710     Q(I)=C
720     IF K>0 THEN
730             IF Q(I)>=K THEN
740                 C=K
750                 F=Q(I)-K
760                 D=F*(A(I)/V(I))
770                 J=A(I)
780                 A(I)=J-D
790                 G=V(I)
800                 V(I)=G-F
810                 Q(I)=K
820             ELSE
830                 GOTO 860
840             END IF
850     END IF
860     B=B+A(I)
870     REM      CALCULATE CUMULATIVE GA/FT**2
880     W(I)=Q(I)/(.0055*3785)
890     REM      AREA=.0055 FT**2
900     REM      3785 ML/GA
910     PRINT    USING 920;I,A(I),B,V(I),Q(I),W(I),T(I)
920     IMAGE    X,DD,X,4D,4X,4D,3X,4D.DD,2X,4D.DD,2X,4D.DD,2X,6D.DD,25X,
DD.DD
930     P=V(I)*T(I)
940     S=S+P
950     IF Q(I)=K THEN 970
960     NEXT I
```

```
970   IF Y=0 THEN PRINTER IS 701
980   PRINT
990   PRINT   USING 1000;W(I)
1000  IMAGE   "AT CONSTANT VOLUME",6X,6D.DD,2X,"GA/FT**2"
1010  Z=I-1
1020  IF Y=0  THEN PRINTER IS 701
1030  PRINT   USING 1040;S
1040  IMAGE   "THE PARTSUM IS",10X,6D.DD,2X,"MLS*NTU"
1050  PRINT   USING 1060;C
1060  IMAGE   "THE VOLTOT IS",11X,6D.DD,2X,"MLS"
1070  IF Y=0  THEN GOTO 1120
1080  REM     CALCULATE GPM/FT**2 FOR THE RUN
1090  N=C*60*144/(B*3.14*.5^2*3785)
1100  PRINT   USING 1110;N
1110  IMAGE   "EXPERIMENTAL BW FLOW IS",X,6D.DD,2X,"GPM/FT**2"
1120  M=S/C
1130  PRINT   USING 1140;M
1140  IMAGE   "THE MEAN TURB IS",8X,6D.DD,2X,"NTU"
1150  PRINT
1160  PRINT
1170  PRINT
1180  PRINT
1190  PRINT
1200  INPUT   "DO YOU WANT THE DATA PLOTTED (Y=1/N=0)?",Y
1210  IF Y=0  THEN 1820
1220  REM     SUBPROGRAM TO PLOT DATA
1230  GCLEAR
1240  GRAPHICS ON
1250  PRINT   CHR$(12);
1260  WINDOW -30,190,-15,95
1270  AXES    10,5,0,0,2,2
1280  REM     LABEL X
1290  LORG 4
1300  FOR I=20 to 190 STEP 20
1310  MOVE I,-5
1320  LABEL I
1330  NEXT I
1340  MOVE 70,-10
1350  LABEL   "CUMULATIVE VOLUME, GA/FT**2"
1360  REM     LABEL Y
1370  LORG 2
1380  FOR I=10 TO 90 STEP 10
1390  MOVE    -20,I
1400  LABEL I
1410  NEXT I
1420  MOVE    -30,80
1430  LABEL   "T"
1440  MOVE    -30,80
1440  LABEL I
1450  LABEL   "U"
1460  MOVE    -30,70
```

```
1470   LABEL   "R"
1480   MOVE    -30,65
1490   LABEL   "B"
1500   MOVE    -30,60
1510   LABEL "I"
1520   MOVE    -30,55
1530   LABEL   "D"
1540   MOVE    -30,50
1550   LABEL   "I"
1560   MOVE    -30,45
1570   LABEL   "T"
1580   MOVE    -30,40
1590   LABEL   "Y"
1600   MOVE    -30,30
1610   LABEL   "N"
1620   MOVE    -30,25
1630   LABEL   "T"
1640   MOVE    -30,20
1650   LABEL   "U"
1660   REM     LABEL PLOT
1670   LDIR    0
1680   LORG    5
1690   MOVE    50,90
1700   LABEL   "TURB-V-CUMULATIVE"
1710   MOVE    80,85
1720   LABEL   "BACKWASH"
1730   MOVE    110,80
1740   LABEL   "VOLUME"
1750   LORG    5
1760   FOR I=1 TO Z
1770   MOVE    W(I),T(I)
1780   CSIZE   4,1
1790   LABEL   "o"
1800   NEXT I
1810   CALL Graphics_dump(701)
1820   GCLEAR
1830   END
1840   SUB Graphics_dump(INTEGER Device_selector)
1950!  (FILE "82905DUMP") Dumps Graphics to HP82905B printer
1860*
1870*
1880*
1890*
1900*
1910*
1920*
1930*
1940*
1950*
1960*
1970*
```

1980*
1990*
2000*
2010*
2020*
2030*
2040*
2050*
2060*
2070*
2080*
2090*
2100*
2110*
2120*
2130*
2140*
2150*
2160*
2170*
2180*
2190*
2200*
2210*
2220*
2230*
2240*

```
10    REM    PROGRAM TO CALCULATE PARTICLE FRACTION REMOVED
DURING BACKWASH
20    C=0
30    DIM F(3)
40    REAL M
50    DIM P(30)
60    DIM Q(30)
70    INTEGER R
80    DIM T(3)
90    DIM V(3)
100   DIM W(30)
110   DIM X(30)
120   DIM Y(30)
130   INPUT "ENTER RUN #",R
140   PRINTER IS 701
150   PRINT "RUN #";R
160   PRINT
170   INPUT "ENTER FLOW VALUE AS GPM/FT**2",E
180   PRINT USING "2D.2D,2X,20A";E,"GPM/FT**2"
190   PRINT
191   INPUT "ENTER AIR FLOW IN SCFM/FT**2",A
192   PRINT USING "2D.3D,2X,10A";A,"SCFM/FT**2"
193   PRINT
200   REM    SLOPE OF [PART]-V-TURB PLOT EQUALS M
201   M=7.80E+6
210   REM    Y-INTCPT OF [PART]-V-TURB PLOT EQUALS B
220   INPUT  "ENTER INITIAL TURBIDITY OF SOL.",T(1)
230   INPUT  "ENTER VOL FILTERED IN MLS.",V(1)
240   INPUT  "ENTER TURBIDITY REMAINING AFTER RUN.",T(2)
250   INPUT  "ENTER VOL MEASURED IN MLS.",V(2)
260   INPUT  "ENTER TURBIDITY WASHED FROM SCREEN.",T(3)
270   INPUT  "ENTER VOL WATER USED TO WASH SCREEN, MLS.",V(3)
280   FOR J=1 TO 3
290   F(J)=V(J)*(M*T(J)+B)
300   NEXT J
310   Z=F(1)-F(2)-F(3)
320   REM    WHERE Z IS THE # PARTICLES DEPOSITED DURING FILTRATION
330   PRINT  USING "2X,30A,2X,D.DDE";"TOTAL PARTICLES COLLECTED",Z
340   PRINT
350   PRINT  USING 360
360   IMAGE  2X,"I",12X,"# PARTICLES",18X,"X",10X,"1-X"
370   PRINT  USING 380
380   IMAGE  7X,"REMOVED IN I",7X,"TOT TO I"
390   PRINT
400   FOR I=1 TO 30
410   INPUT  "ENTER SAMPLE VOLUME IN MLS. ENTER 0 TO STOP.",W(I)
420   IF W(I)=0 THEN 570
430   INPUT  "ENTER TURBIDITY IN NTU.",P(I)
440   Y(I)=W(I)*(M*-(I)+B)
450   REM    WHERE Y IS THE # PARTICLES REMOVED IN SAMPLE I
460   C=C+Y(I)
```

```
470     REM     WHERE C IS THE TOTAL # PARTICLES REMOVED TO I
480     X(I)=C/Z
490     REM     WHERE X(I) IS THE FRACTION OF PARTICLES REMOVED
500     REM     DURING BACKWASH TO I
510     Q(1)=1-X(I)
520     REM     WHERE 1-X(I) IS THE FRACTION OF PARTICLES STILL
530     REM     ATTACHED TO THE GRAINS
540     PRINT   USING 550;I,Y(I),C,X(I),Q(I)
550     IMAGE   X,DD,6X,D.DDE,8X,D.DDE,8X,2D.4D,6X,2D.4D
560     NEXT I
570     PRINT   "EOR"
580     END
```

APPENDIX B

PRELIMINARY CALCULATIONS TO DETERMINE k's RELATIONSHIP TO INLET CONFIGURATION

The value of Q_a is based on column diameter

D = 1.0-inch

Given the relationship

$$A_1 v_1 = A_2 v_2$$

rearranging:

$$v_2 = \frac{A_1 v_1}{A_2}$$

the air flowrate can be converted to air inlet orifice dimensions

inlet orifice = 1.0-mm

$$v_1 = Q_a$$

therefore,

$$v_2^2 = \left(\frac{A_1}{A_2}\right)^2 Q_a^2$$

The velocity head is given by:

$$\frac{v^2}{2g} \cdot \gamma = \text{velocity head}$$

then

$$\frac{v^2}{2g} = \frac{\left(\frac{A_1}{A_2}\right)^2 Q_a^2}{2g}$$

therefore:

$$k = \left(\frac{A_1}{A_2}\right)^2 \cdot \frac{\gamma}{2g}$$

In this instance k can be calculated:

$$\left(\frac{A_1}{A_2}\right)^2 /2g = \frac{[\pi\ (0.5\ \text{in})^2 \times (\text{ft}/12\ \text{in})^2]^2}{[\pi\ (0.5\ \text{mm})^2 \times (\text{in}/25.4\ \text{mm})^2 \times (\text{ft}/12\ \text{in})^2]^2\ 2\ (32.2\ \text{ft/sec}^2)}$$

$$\frac{A_1^2}{A_2^2 \cdot 2g} = 14.36\ \text{min}^2/\text{ft}$$

$$k = 14.36 \times 0.075$$

$$= 1.08 \frac{\text{min}^2 \cdot \text{lbf}}{\text{ft}^2}$$

theoretically

$$k = 0.254 \frac{\text{min}^2 \cdot \text{lbf}}{\text{ft}^2}$$

similarly for Hewitt's work [20,21]

Column 12-inch X 0.75-inch

Inlet 6.0-mm circular orifice

$$k = 2619.4 \times 0.075$$

$$k = 196.5 \frac{\text{min}^2 \cdot \text{lbf}}{\text{ft}^4}$$

theoretically [21]

$$k = 0.45$$